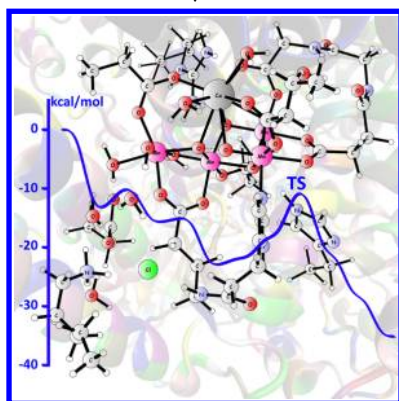# Quantum Chemical Studies of Mechanisms for Metalloenzymes

Margareta R. A. Blomberg,[†] Tomasz Borowski,[‡] Fahmi Himo,[†] Rong-Zhen Liao,[†] and Per E. M. Siegbahn*,[†]

[†]Department of Organic Chemistry, Arrhenius Laboratory, Stockholm University, SE-106 91 Stockholm, Sweden
[‡]Jerzy Haber Institute of Catalysis and Surface Chemistry, Polish Academy of Sciences, ul. Niezapominajek 8, 30-239 Kraków, Poland

CONTENTS

1. INTRODUCTION

Two decades ago, theoretical model calculations played a truly minor role in understanding mechanisms of redox-active metalloenzymes. The methods available to treat transition metals were either not accurate enough or much too slow for meaningful applications. The chemical models for the treatment of enzymes were also underdeveloped. This situation changed due both to developments of methods and to insights from applications. First, fast density functional theory (DFT) methods were developed to a stage where the accuracy was not far from that of the most accurate, but much slower, ab initio methods for molecules containing first-row atoms. The introduction of density gradient terms for the exchange part and of fractions of exact exchange were major improvements.[1] During the first years of applying these methods it was soon realized that the accuracy was often quite reasonable also for transition-metal complexes.[2,3] The second important reason for the progress in this area came from a decade of experience using small models for treating

transition-metal complexes. Among other things, it was surprisingly found that many aspects of the mechanisms of large organometallic complexes could be understood, at least qualitatively, using quite small models. Individual reaction steps including transition-state structures turned out to be quite insensitive to the size of the model.

Two, originally quite different, approaches have been developed and used to study mechanisms of redox-active metalloenzymes. In one approach, the cluster model, the experience is used that even small quantum mechanical models can capture the main features of a mechanism. The first DFT application using this model for a mechanism of a redox-active enzyme was made in 1997 for methane monooxygenase (MMO).[4] In the other approach, the entire enzyme is treated with a small core described quantum mechanically, while the rest is described by molecular mechanics, the quantum mechanics/molecular mechanics (QM/MM) model.[5] The first application using QM/MM for a redox-active enzyme mechanism was made in 2000 for galactose oxidase.[6] Over the years, both approaches have been developed from their original form. Nowadays, QM cluster models are often quite big, with more than 200 atoms, and larger and larger QM parts are used in the QM/MM approach. In this way the results using these approaches have converged toward each other. Results from both types of modelings will be described in this review. As shown below, the QM cluster approach has so far been the by far most commonly used way to treat mechanisms of redox-active metalloenzymes.

At the present stage, theoretical model calculations must be regarded at least of equal importance in determining mechanisms for metalloenzymes compared to traditional spectroscopic techniques. The latter have the obvious advantage that they are applied on the actual system, but they have the disadvantage that interpretations are quite often extremely difficult. In both approaches, the accuracy of the results obtained has to be guaranteed. In theoretical modeling, not only the method but also the modeling of the real system has to be accurate. After nearly two decades of experience, the understanding of the limitations and applicability of different models has grown and reached a mature stage. This may even be claimed to be the most important development in this area.

The present review has its main focus on the mechanisms of redox-active metalloenzymes. Therefore, computational results on structural and spectroscopic issues which are not directly related to the mechanisms are only rarely treated. There are also some results for metalloenzymes that are not redox-active, such as the section on zinc-containing enzymes, since the modeling aspects are similar. It should finally be mentioned that all results present in the literature cannot be discussed, and some selection has been made. For example, there are many rather recent reviews on more specialized issues, which summarize the results obtained at that stage. In those cases only the more recent results and the main earlier findings are discussed. Furthermore, the sections on the different topics are more or less extensive, reflecting the expertise of the authors.

2. METHODS AND MODELS

As described in the Introduction, the cluster approach for modeling enzyme reactions uses a limited number of atoms taken out of the enzyme to represent the active site. All atoms in the chosen cluster are then treated quantum mechanically at the highest possible level, which so far has mainly meant hybrid DFT. For enzymes containing transition metals, this model has been in use for about 15 years,[4] with gradually larger clusters being

employed. Even though more and more of the main effects are taken care of by models with a size of 200 atoms, it is not unlikely that there exist situations where groups outside the model can make significant contributions. How the surroundings of the active site are treated in different approaches will be described below.

In the early stages of modeling enzyme reaction energetics, it was considered necessary to include a large part of the enzyme for a realistic description. In the beginning of the 1990s it was normally concluded that small cluster models are not very useful since they neglect the effects of the surrounding protein and solvent.[7] A natural way out of this problem was to treat the rest of the enzyme using a simpler, normally classical, description, which was done in the QM/MM method.[5] For a recent comprehensive review on QM/MM methods for biological systems see ref 8.

An even simpler way to treat the surrounding enzyme than to use the QM/MM method is to use a continuum representation. In its simplest variant (not used anymore) the quantum chemical cluster is placed in a spherical cavity surrounded by a polarizable continuum with dielectric constant ε. With a cavity of radius R and point charge q, the interaction energy between the cluster and the continuum has the analytical solution

$$E_q = [(\varepsilon - 1)/2\varepsilon]q^2/R$$

This is the so-called Born model from 1920. An extension to the case of point dipole μ leads to the Onsager model with the analytical solution

$$E_\mu = [(\varepsilon - 1)/(2\varepsilon + 1)]\mu^2/R^3$$

Interaction energies for more elaborate charge distributions and cavity forms can today be easily obtained, although not analytically. Normally, the cavity is defined by an interlocked superposition of atomic spheres with radii near the van der Waals values. In most of the applications discussed here, the interaction energy is obtained by solving the Poisson equation self-consistently using a charge distribution from the cluster in a quantum mechanical description. This is termed the self-consistent reaction field (SCRF) method. There are a large number of different variants of these methods in use; see, for example, reviews in refs 9 and 10. In our experience, relative effects on the potential energy surfaces are not sensitive to the method used, at least in cases where the effects are rather small. If charges in the continuum part outside the cluster model are being considered, the Poisson–Boltzmann equation has to be solved instead, using an electrolyte with a certain ionic strength. For applications on enzymes with transition metals, see, for example, ref 11.

During the first years of using the DFT-cluster model for metalloenzyme reactions, experience was gathered for rather small cluster models of 30−50 atoms using the simple dielectric cavity method with a dielectric constant of 4.0 for the surrounding enzyme.[12] It was concluded that when there are no long-range charge separations involved in the reaction studied, the effects of the surrounding medium on the reaction energetics are generally small, on the order of 1−3 kcal/mol. This was shown in detail in a model study on manganese catalase.[13] This was a quite surprising finding at the time, since the effects of the surrounding enzyme were usually considered extremely important; see above.[7] For applications on more demanding reactions involving large charge separations, see further below in the context of cluster size convergence.

The most difficult situations to describe with the cluster model are undoubtedly the cases where the model changes its charge, such as in the calculations of redox potentials and pK_a values. Somewhat ironically, these values would otherwise be the most natural points of comparison to experiments, since there is a wealth of experimental information available. It is easy to see that a change of charge gives rise to a very long-range response from the surrounding medium. If the simple Born formula above is used with a dielectric constant of 4.0 and a model with a radius as large as 5 Å, the contribution from outside the model to the redox potential would still be around 20 kcal/mol. This is a too large effect to be accurately described by a simple dielectric cavity model. Even more importantly, these models assume homogeneous surroundings. It is well-known that enzymes use inhomogeneously positioned charges to optimize redox potentials and pK_a values for their purposes.[14] Even if dielectric effects are included, the errors can therefore still be 5−10 kcal/mol. For transition-metal complexes in solvents such as water and acetonitrile, Friesner et al. have obtained good agreement with experimental redox potentials with errors of 0.1−0.2 V, using a seven-parameter model.[15]

For the calculation of redox potentials of metalloenzyme systems, the group of Noodleman had the largest experience during the early years of DFT-cluster modeling.[11] They used Poisson−Boltzmann-based methods, where the model was partitioned into three regions. The cluster region used $\varepsilon = 1.0$ and the outermost bulk region $\varepsilon = 80.0$. The intermediate protein region used $\varepsilon = 4.0$ and a partial charge representation of the protein. Not counting the inherent error of the DFT method, they claim an accuracy for redox potentials normally within 0.2 V. Different versions of the QM/MM method, where no dielectric constant is used for the protein region, have also been used by several groups to calculate redox potentials; see, for example, ref 16. They use their QTCP (QM/MM thermodynamic cycle perturbation) approach and claim an accuracy almost entirely limited by the DFT method used. Worth mentioning among other methods is the protein dipoles Langevin dipoles (PDLD) model, which has been used to calculate relative redox potentials of transition-metal redox couples in enzymes but with a classical description of the active site; see, for example, ref 17. None of these methods have been used for obtaining the energetics of entire catalytic cycles.

For many of the studies discussed in this review, an entirely different method was used for obtaining the energetics when protons and (or) electrons leave (enter) the active site.[18−23] In contrast to the other methods mentioned above, this method is built on the fact that entire catalytic cycles are calculated. In the systems where this method is applicable, the electron donor (acceptor) to (from) the active site is the same for all steps in the cycle. The same requirement holds also for the proton donor (acceptor). This is not as severe a restriction as it may seem, but is rather the most common situation for metalloenzymes. The method has, for example, been successfully applied to important enzymes such as photosystem II (PSII) in photosynthesis and cytochrome c oxidase (CcO) in the respiratory chain. A key point of the method is that the total driving force for the catalytic cycle is taken from experimental redox potentials. These values can in most cases be obtained from standard textbooks. The calculation starts by the evaluation of the relative gas-phase energies for removing (adding) a proton/electron couple from (to) the active site. In PSII and CcO this means four and in hydrogenase two relative energies. Since the charge of the active site remains the same in all these processes, the effects of the surrounding enzyme

should be small, typically only a few kilocalories per mole, and can be added to the relative values using a simple solvation model. With this information, there is only one way to fit the calculated values to the experimental driving force. Together with the chemical steps, this defines the major part of the potential surface. As a corollary to this insight, it can be concluded that the surrounding enzyme cannot significantly modify these energy levels of the potential surface by using charged amino acids around the active site. However, it is often of interest to also obtain individual redox and pK_a values during the reaction. This requires the use of one, but only one, additional experimental value. Any energy value related to the potential surface can be used. For example, in PSII the details obtained accurately from experiments for the beginning of a single S transition were enough to determine all absolute redox potentials and pK_a values during the entire cycle.[24] Three major advantages with the method are that a detailed knowledge of the surrounding enzyme is not necessary, the calculations are guaranteed to give the right driving force, and the donors (acceptors) involved do not have to be considered at all. Unlike the other methods discussed above, the method will also partly correct errors of the DFT method, since it uses an experimental driving force.

The quantum chemical cluster approach for modeling enzymatic reactions has been described in detail in recent reviews.[25,26] It is, however, important here to recapitulate some of the most important features of the approach, to illustrate its strengths and limitations and some of the recent developments.

As mentioned above, in the cluster approach a relatively small part of the enzyme around the active site is carved out and treated with relatively accurate electronic structure methods (typically hybrid DFT). Very early studies on metalloenzymes, for example, the one on MMO,[4] gave quite promising results in spite of the use of very small cluster models (20−30 atoms), showing that it was indeed possible to answer some meaningful chemical questions regarding local geometry, electronic structure, and reactivity. With the increasing computer power, cluster models have become gradually larger, and more elaborate questions can be addressed. It should be emphasized that, even with the possibility to use larger models, small clusters continue to have a significant advantage at the early stages of the mechanistic investigations. First, they can be used to investigate a larger number of different mechanisms. Second, it is significantly easier to avoid artifacts and therefore obtain computationally correct results. It is the rule rather than the exception that when the results significantly differ between a small and a large model, the result for the small model is more likely to be correct. The difficulty in obtaining computationally correct results remains a significant problem using large models, in particular for QM/MM, even for experienced users.

The neglected enzyme surroundings can influence the results in two major respects, sterically and electrostatically. The sterics, i.e., the restrictions provided by the protein matrix on the movements of the various groups of the active site, can be taken into account by simply fixing some suitable coordinates at the periphery of the model, typically where the truncation is made.[27] In this way, one can avoid artificial movements of the active site groups, which sometimes can be caused by quite small energetic driving forces, but which can render the model entirely unreliable. This coordinate-locking scheme might sound like a drastic approximation, but it has been carefully tested in a large number of cases, among them a case where the backbone positions have been moved more than 1 Å.[28] An even more drastic case is discussed below for photosynthetic water

oxidation, where different X-ray structures differ by up to 3 Å at some places.[24] Furthermore, it should be remembered that, with an increasing model size (i.e., when the locking is further away from the reacting parts), the error becomes smaller as the model is less rigid and the various groups have more flexibility. In addition, metalloenzymes have an advantage in that the metal ions function as anchors in the model, keeping at least the first-shell residues in reasonable positions and orientations even without locking. A special case has recently been pointed out,[29] in which an aspartate (with its short side chain) moved dramatically in a critical step. In such a case, the locking of coordinates should be made further away than the α-carbon. Whenever there is reason to suspect problems, the procedure is easily checked by releasing the constraints.

The electrostatic contribution of the missing enzyme surroundings can be modeled using the above-mentioned SCRF methodology, with some assumed dielectric constant, typically ε = 4.0. Also, here, it is easy to realize that the approximation will work better and better as the model size increases and a larger portion of the enzyme is treated quantum mechanically. In recent years, careful systematic studies using increasing model sizes of the active sites have shown that the solvation effects of the surrounding enzyme environment decrease surprisingly rapidly and, for most cases tested, almost vanish at a size of around 200 atoms.[30−33] This has been demonstrated for some electrostatically challenging cases, such as the formation of an ion pair in the reaction of 4-oxalocrotonate tautomerase,[30] the release of a chloride ion in the reaction of haloalcohol dehalogenase,[31] the transfer of a methyl cation group in the reaction of histone lysine methyltransferase,[32] and the decarboxylation reaction of aspartate decarboxylase.[33] Table 1 illustrates this convergence for the case of haloalcohol dehalogenase HheC.[31]

Table 1. Calculated Barriers and Reaction Energies (kcal/mol) Using Various Models of the Haloalcohol Dehalogenase HheC Active Site[31]

	model I, 83 atoms		model II, 112 atoms		model III, 161 atoms	
	$\Delta E^{\ddagger}$	ΔE	$\Delta E^{\ddagger}$	ΔE	$\Delta E^{\ddagger}$	ΔE
ε = 1	+23.0	+17.5	+17.9	+14.1	+18.2	+5.5
ε = 2	+17.8	+8.2	+15.8	+8.3	+17.7	+4.9
ε = 4	+15.0	+3.4	+14.6	+5.2	+17.4	+4.5
ε = 8	+13.5	+1.0	+14.0	+3.6	+17.1	+4.3
ε = 16	+12.8	−0.3	+13.7	+2.8	+17.0	+4.2
ε = 80	+12.2	−1.2	+13.5	+2.2	+17.0	+4.2

Another aspect of a model, sometimes critical, concerns the protonation states of the different groups. Normally, for large models, the residues should take their normal charge state at the investigated pH. In small models, and for residues close to the surface of the model, it will sometimes be better energetically to go away from the natural protonation state. One illustrative case is glycine N-methyltransferase (GNMT), in which a methyl cation is transferred from an S-adenosyl-L-methionine (SAM) cofactor to a glycine substrate.[34] The carboxylate moiety of the glycine hydrogen bonds to a positively charged arginine residue in the active site. If a minimal model is constructed consisting only of the substrate in the anionic form and a heavily truncated model of SAM, where only one carbon is kept on each side of the sulfur (see Figure 1), the methyl transfer takes place spontaneously during the geometry optimization and no
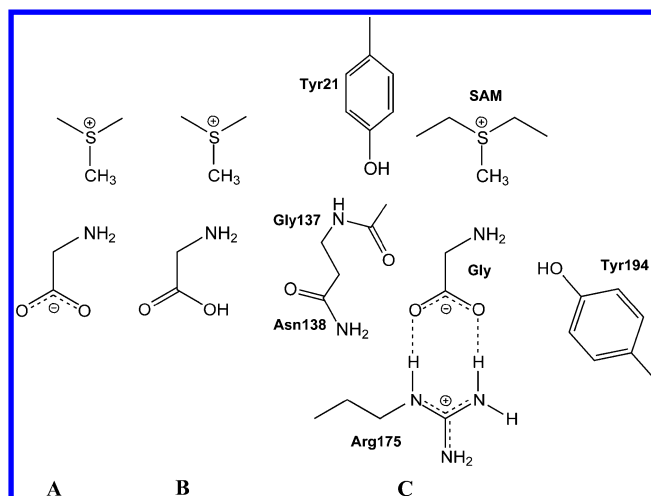

Figure 1. Different models for the methyl transfer reaction in GNMT: (A) minimal model with anionic substrate, (B) minimal model with protonated substrate, (C) large model with several surrounding groups.

transition state (TS) can be located. This is not surprising considering that SAM is positively charged and the substrate is negatively charged. However, if the substrate is modeled in a neutral form, i.e., with a protonated carboxylate, one can locate a transition state. The calculated barrier is 16.6 kcal/mol assuming a dielectric constant of 4. It is interesting to note that when a much larger model (98 atoms) is used that includes the arginine, an extended model of SAM, and several other groups at the active site, the barrier is calculated to be 15.0 kcal/mol, which is quite close to the result of the minimal model with the substrate in its neutral form.[34] This is not a coincidence, but is quite generally found in situations like this. Another quite common situation occurs for carboxylates close to the surface of the model, which tend to artificially obtain spin if they are not protonated.

The DFT functional by far most used in metalloenzyme applications is the B3LYP functional by Becke.[1] It is a hybrid functional, which means that it contains a fraction of exact exchange, in addition to the normal exchange-correlation part. In more recent applications, the fraction of exact exchange, originally set to 20%, has been decreased to 15%,[35] which often improves redox energies. Recent theoretical work[36] has made it possible to include also dispersion effects in a simple way for the energies. These effects have been studied for some of the systems discussed in the present review. It was found that they are generally small for different reaction steps occurring within a model, but can be substantial when a molecule from the outside becomes bound to a metal, or correspondingly when it is released.[37] This occurs, for example, when a water molecule or dioxygen becomes bound or released. Striking examples are also the binding of methyl or adenosyl to cobalamin, where the contribution from dispersion can be larger than 10 kcal/mol.

3. PHOTOSYSTEM II

Water oxidation in PSII is one of the largest projects undertaken so far using DFT and the cluster model. Model studies have been performed constantly since the beginning of this approach in 1997.[38a] Therefore, the description of this mechanism will be given more space in the review.

The reaction catalyzed is

$$2H_2O + 4h\nu \Leftrightarrow O_2 + 4H^+ + 4e^-$$
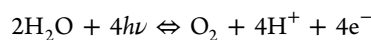
From saturating flash experiments, water oxidation is known to occur in four steps.[39] The intermediates of these steps are denoted S_0 through S_4. The actual catalyst for the O−O bond formation step is the oxygen-evolving complex (OEC), which has long been assumed to contain four manganese centers and most likely calcium. Suggestions of two manganese dimers and a calcium somewhat outside the OEC have also been made. Following each photon flash, one electron is removed from the OEC between the S states, and O_2 is released in the S_4 to S_0 transition. Protons are removed to keep the charge as constant as possible. O_2 formation occurs at S_4.

During the first five years after 1997, the modeling of water oxidation in PSII was quite rough, since no X-ray structure of the enzyme was yet available. General questions were addressed such as the electronic structure requirement for forming an O−O bond. It was, for example, found that an oxygen radical is necessary for a low-barrier mechanism,[38b] a requirement that still applies. A mechanism where the oxyl radical is attacked by an outside water was suggested. In the next couple of years, the model was refined[38c] on the basis of suggestions from spectroscopy, mainly from EXAFS (extended X-ray absorption fine structure).[40] In 2004, there was an experimental break-through when the first X-ray structure with detailed information about the OEC appeared, although at a low resolution of 3.5 Å.[41] A cubane form of the OEC was suggested, with the cube formed by three manganese atoms and one calcium atom linked by oxo bridges. The fourth manganese was linked to the cube at one of the cubane oxo corners. In the coming years, new structures of gradually higher resolution were produced, still not higher than 2.9 Å.[42] A more accurate X-ray structure with an atomic resolution of 1.9 Å was finally presented in 2011[43] (see Figure 2),
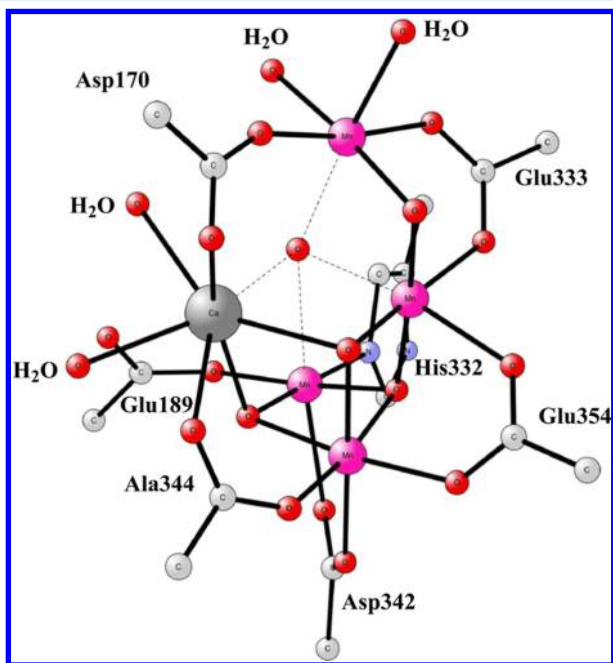

Figure 2. Oxygen-evolving complex of PSII.

but at that stage an accurate structure of the OEC had already been produced by DFT modeling calculations in 2008,[22] including a detailed water oxidation mechanism,[38d] which still holds today; see further below.

The ligand structure of the OEC is shown in Figure 2. The amino acids are the same as those in the original structure,[41] but

the connections to the metal atoms are significantly different, actually quite similar to those of the 2.9 Å structure.[42] An important aspect of the ligation is that the rather limited number of amino acids are able to produce fully octahedral coordinations for three of the manganese atoms, without requiring ligating water-derived ligands. The outermost (dangling) manganese is the only exception. A low number of easily available protons is important for the mechanism; see further below. There is essentially only one difference from the previous DFT structure, and this concerns Asp170, which is bridging between Mn and Ca in the high-resolution structure, but end-on-bound to manganese in the DFT structure.

A comparison of the core parts of the different structures is shown in Figure 3. The orientation of the structures was made
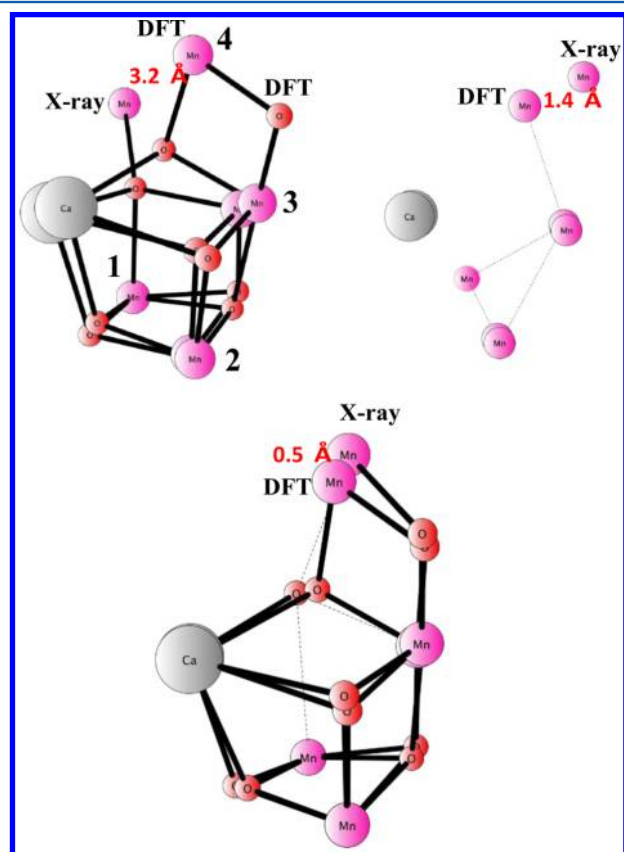

Figure 3. Comparison of the DFT structure[22] with the 3.5 Å X-ray structure[41] (upper left), the 2.9 Å structure[42] (upper right), and the 1.9 Å structure (bottom).[43] For the comparison to the 2.9 Å structure no oxygens are given since they were not suggested in that structure. To clarify which atoms belong to which structure, the atoms are labeled "DFT" and "X-ray" when the positions are significantly different.

such that one Mn atom of the structures compared is placed at the same position and the other two in the cube are placed as close as possible to each other. This avoids bringing in an irrelevant rotation between the complexes. The most striking difference between the DFT structure and the 3.5 Å structure is the positioning of the outer manganese, which differs by 3.2 Å. In the DFT structure the outer manganese is connected to the cube by two μ-oxo bridges, while in the 3.5 Å structure it is only connected to one of the bridging oxo ligands in the cube. There is also an additional oxo bridge between the Mn atoms in the theoretical structure. A similar, significant but smaller, difference is seen in the comparison to the 2.9 Å structure, where the

positioning of the outer manganese differs by 1.4 Å. The positions of the oxo bridges were not suggested in that structure due to the low resolution, but a single oxo bridge to the outer manganese can be assumed on the basis of the Mn–Mn distance of 3.3 Å (according to EXAFS, there should be one longer Mn–Mn distance of 3.3 Å). In the DFT structure, this distance of 3.3 Å is instead within the cube. As will be seen below, the region between the outer manganese and the cube is the region where O–O bond formation most likely takes place according to the present DFT studies. In particular, a sufficiently open space in this region is necessary for a low-barrier mechanism. This is precisely the region where the low-resolution structures are incorrect, and these structures have therefore mainly led to suggested water oxidation mechanisms that according to DFT comparisons are significantly wrong.[38d] The mechanism that has been suggested on the basis of the X-ray structures is an attack on an oxo group by an external water or a water bound to calcium. On the other hand, the positionings of the outer manganese and the oxo bridges between the manganese atoms in the recent 1.9 Å structure are very similar to those in the DFT structure. The additional oxo ligand is there, and the 3.3 Å distance is within the cube in both structures. Still, the outer manganese position differs by 0.5 Å, mostly due to X-ray reduction but also due to the above-mentioned misplacement of Asp170 in the theoretical structure.

The central oxygen position is a surprising feature of the 1.9 Å structure; see Figure 2, where all distances between this oxygen and manganese are quite long. It has been shown by calculations that this type of bonding cannot occur unless all three surrounding manganese atoms are in the Mn(III) state.[24] This rules out the possibility that the X-ray structure is in the resting S_1 state as claimed. Reduction to at least the S_0 state is required, but even a further reduction is likely.[44−46]

The initial mechanism obtained for O–O bond formation was one where an oxyl radical is attacked by an outside water.[38b] This mechanism continued to be the best one found for several years, even after the appearance of the first X-ray structures. However, the barrier obtained as the model was improved was too high, about 25 kcal/mol compared to an experimental barrier of 10–15 kcal/mol. This size of error is much larger than what can be expected from the present modeling, and in 2006 it was decided that the mechanism had to be abandoned.[38d] At that stage, quite large modifications of the low-resolution X-ray structure had already been found necessary. For example, it had been found that the dangling manganese was too close to the cube in the 3.5 Å structure and had to be moved further out. A reasonable S_4 state was eventually reached with an optimal position of the oxyl radical, which was still found to be required for the bond formation. From this structure all possibilities to form an O–O bond were tried, and one mechanism had a much lower barrier than the other ones. Quite surprisingly, this mechanism involved bond formation in the center of the OEC between the oxyl radical and a bridging oxo ligand, a mechanism that had not been suggested before. An important feature of the mechanism was also that the spins on the atoms involved were alternating, which was necessary for a smooth bond formation between the reactant oxyl radical state and the peroxide product. This condition also led to a requirement for two directly involved manganese centers with antiferromagnetic (AF) coupling. AF (rather than ferromagnetic) coupling had previously been shown to be almost unimportant for the thermodynamics of water oxidation, and the large importance for the kinetics was quite surprising. The requirement for two directly involved manganese centers

with the right orientation furthermore gave an explanation for key aspects of the structure of the OEC. It also explained why mechanisms with only one manganese directly involved, such as in the water attack mechanism and the mechanisms for biomimetic complexes, failed (and still fail) to give a low barrier for O–O bond formation. The same idea applied to cobalt complexes actually suggests that they do not have the same possibility as manganese complexes to form a low-enery barrier, since cobalt is low-spin-coupled at the relevant oxidation states.[47]

On the basis of previous modeling experience, the mechanism described above is quite convincing compared to other suggested mechanisms. It has, so far, not happened that a mechanism with a barrier more than 10 kcal/mol higher than another one has turned out to be the correct mechanism. If the barriers for different mechanisms would have been more similar, the situation would have been different. It should be emphasized that none of the X-ray structures available were compatible with the mechanism found. The dangling manganese is too close to the cube in the 3.5 Å structure, and in the 2.9 Å structure, the dangling manganese is too far away with only a single oxo bond to the cube (according to its position in the structure), while the optimal mechanism requires two bridging oxo bonds.

The conclusion that the right mechanism was found was used to try to find a better structure of the OEC than those available in 2008. To do this, the optimized transition state was fitted into the 3.5 Å X-ray structure by fixing the backbone positions of the atoms in the model. The fitting turned out to be easily accomplished. To reach the resting structure, electrons and protons were added at optimal positions, and the geometries were reoptimized. When this was done, a structure came out which was significantly different from the low-resolution structures. A comparison of the core structures is given in Figure 3. The optimized core furthermore fitted the X-ray density; see Figure 4. For the comparison to the recent 1.9 Å high-resolution structure from 2011, see above.

In the past two years there has been remarkable progress on the experimental side. On the basis of the new X-ray structure and old DFT structure, using electron paramagnetic resonance (EPR), electron–nuclear double resonance (ENDOR), and DFT, a detailed structure of the OEC in the S_2 state was
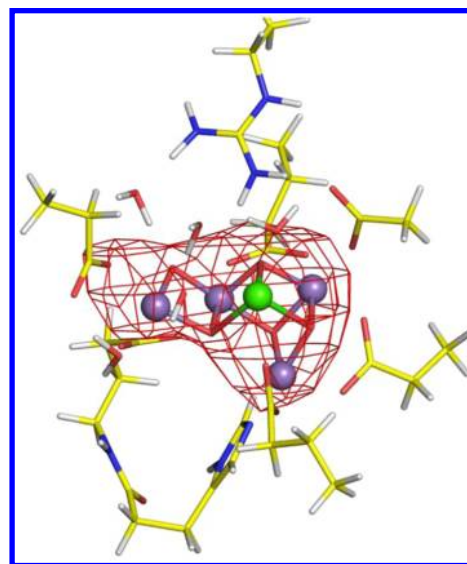

Figure 4. DFT-optimized S_1 resting structure placed into the X-ray density from the 3.5 Å structure.

reached[44a] that agrees almost perfectly with a structure obtained independently by energy minimization.[38e] Even more importantly, using W-band ^{17}O electron−electron double resonance (ELDOR)-detected NMR spectroscopy, information about the substrate positions was obtained,[48] strongly suggesting the oxo position given by the DFT mechanism described above as being one of the substrate positions. The other substrate position is still not completely clear, but the one given by DFT remains a valid possibility. Another important result in these studies was that the two previously observed spectroscopic states in S_2 were identified. The energies of these states were found to be quite close, in agreement with earlier studies.[23]

In the meantime, other theoretical work was performed, most of which has led to other suggestions. Cluster models and mechanisms have been studied by Pace et al.[49] They suggest lower oxidation states than those suggested here and in most other studies. They base their conclusions on a computational analysis of NEXAFS (near-edge X-ray absorption fine structure) spectra using a TDDFT (time-dependent DFT) approach. In a recent study it has been questioned whether the TDDFT method is accurate enough for the analysis, and also whether NEXAFS, also termed XANES (X-ray absorption near-edge structure), is a reliable technique for determining oxidation states.[38f] Given the close contact between the Mn atoms in the OEC, it would be extremely surprising if the low oxidation suggestion could produce a reactive state in S_4, since an oxygen radical has to be close to a Mn(III) center. In 2007, Kusunoki[50a] suggested a structure for the S_0 state based on the 2.9 Å structure,[42] with the same correct and incorrect aspects as that structure. The ligands are at essentially the correct place, but the dangling manganese is too far out, connected to the cube by only one oxo ligand and having three water ligands, two of which were suggested to be the substrates on the basis of water exchange considerations. In 2011, after the high-resolution structure, the model was refined. The originally suggested mechanism was kept, now supported by EXAFS calculations. To explain the unusual position of the central oxo ligand, it was suggested that there are two different structures for the S_1 state with equal energy.[50b] In contrast to the cluster approach, the QM/MM method has been used by Batista et al.[51] They restricted the structures investigated to be similar to the 3.5 Å structure.[41] For the best structure obtained, they also did an analysis of EXAFS spectra and found that their suggested structure would match the experimental spectrum if it was only slightly modified. They took this information to be a confirmation of the correctness of their suggested structure. After the new X-ray structure by Shen et al. appeared, it became clear that their suggested structure was quite different from the real structure. Later on it was shown that, using their type of analysis, other quite different structures also match the EXAFS spectra well. Furthermore, Batista et al. suggested an O−O bond formation mechanism that is different from the preferred one discussed above. A nucleophilic attack from an external water (or water bound to calcium) was suggested to form the bond with an oxygen radical bound to manganese. Their mechanism is the same as that suggested earlier in several studies starting in 1999,[38b,c] but which was demonstrated to lead to too high barriers in a study in 2006.[38d] Neese et al.[44b] used a spectroscopic DFT approach to investigate several types of clusters. They suggested that three of these structures, including the previous theoretical structure,[22] which were found to match the EPR spectra best, would be most similar to the real structure. In a later study,[38g] but before the 1.9 Å structure appeared, it was shown using an energy minimization approach that the structure

suggested by Batista et al., and all the new structures studied by Neese et al., were energetically quite far above the DFT structure discussed above and therefore had to be mechanistically different from the real structure. Actually, the same conclusion could be made for all four structures suggested by polarized EXAFS,[52] which were concluded to be significantly wrong energetically.[23] On the other hand, the structure suggested by Dau et al., also based on EXAFS, is quite similar to the DFT structure.[45b] At that point Neese et al.[44c] did a new more extended DFT analysis and concluded that the previous DFT structure[22] matched the experimental multifrequency EPR and ^{55}Mn ENDOR spectra best. Simultaneously, and independently, Kaupp et al.[38h] reached the same conclusion. With the appearance of the high-resolution structure, this conclusion was definitely confirmed. More recently, Batista et al. have analyzed the protonation state of the S_1 state of the Shen structure.[51e] They concluded that the Shen X-ray structure is a mixture of oxidation states. A similar conclusion was also reached in other recent studies.[38,44−46] In another study,[51f] Batista et al. analyzed the role of chloride by deleting it and concluded that one role might be to prevent salt bridges which would hinder proton transfer. Other more direct effects on the redox potentials and pK_a values were not considered.

The optimal water oxidation mechanism described above is consistent with a vast, and growing, amount of experimental information;[44,48] see above. One of the most surprising features of the mechanism is that it requires that one substrate oxygen is bound as a bridging oxo group in the center of the OEC. This becomes even more surprising in light of water exchange experiments that show that this oxygen can be exchanged with oxygen from solvent water faster than seconds, in both the S_2 and S_3 states. This is very unusual for a metal-bridging oxo group and has therefore been the feature of the DFT mechanism that is hardest to accept.[45,53,54] In a recent DFT study,[38i] agreement with experiments was found for a rather complicated water exchange mechanism. The interpretation is consistent with the above DFT mechanism for O−O bond formation. A key to the exchange is that a central Mn has to be reduced to a Mn(III) state to release the bond to the substrate oxygen. This can explain the quite unexpected result that the exchange is slower for S_1 than for S_2. It is directly seen from the mechanism why water exchange results for smaller models containing fewer Mn atoms are not representative of the OEC.

Results from NEXAFS measurements are other cases which have been difficult to interpret and have led to quite different suggestions for the O−O bond formation mechanism. From very similar spectra, one interpretation has been that all Mn centers in the S_3 state have Mn(IV) oxidation states,[45d] in agreement with the DFT mechanism, while, in another interpretation, one of the Mn centers has been suggested to have oxidation state Mn(III) and an oxygen is instead oxidized to a radical.[55] In a DFT study it was shown that the spectrum for an OEC model with all Mn(IV) centers can be incorrectly interpreted as if one of the Mn centers is only Mn(III), if the edge is determined by a second-derivative method. A half-height method was instead recommended for similar systems, but this is not a certain method either.[38f]

To fully understand water oxidation, not only the O−O bond formation mechanism and the structure but also the energetics of all redox steps, including different deprotonations and the required proton motion on the complex, need to be found. To construct an energy diagram with all this information, the method described in the Methods and Models above has been used. With experimental redox potentials of 1.25 V for P_{680},[56,57]

the oxidant in PSII, and a potential for water oxidation at pH 7 of 0.8 V, the driving force in the OEC water oxidation becomes 41.5 kcal/mol. In a recent study,[24] it was suggested that the driving force could actually be increased to 51.5 kcal/mol through an interaction between P_{680}^+ and the OEC in the later transitions. As discussed above, the driving force combined with calculated *relative* energies is enough to uniquely determine the energies for redox steps where H^+-e^- couples are removed from the OEC. This determines the major part of the diagram and does not require knowledge of the enzyme surrounding the OEC. However, to also determine the steps where only an electron (or a proton) is removed, one additional experimental value is needed; which one is arbitrary. For the OEC it was decided to take the parameter that would match experimental observations for the S_3 to S_4 transition.[45e] The energetic results without a membrane gradient are collected in the diagram shown in black in Figure 5. O−O bond formation is rate limiting with a barrier
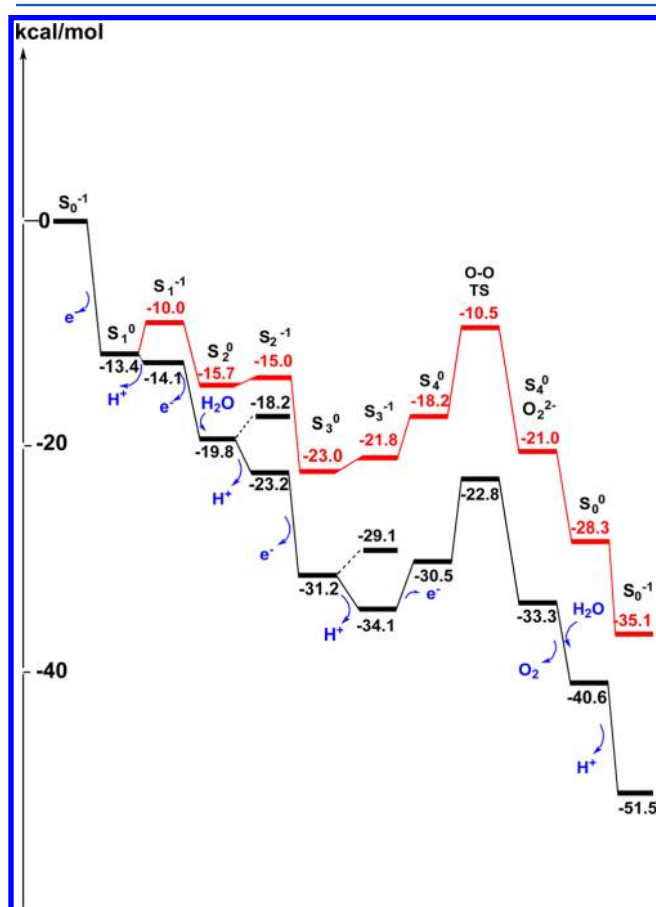

Figure 5. Full-energy diagram for water oxidation from S_0 back to S_0. The black curve is without and the red curve with a full membrane gradient.

from the resting S_3^{-1} state of 11.3 kcal/mol (34.1 − 22.8). An important point about the mechanism is that protons and electrons are removed in an alternating fashion, which preserves the charge of the catalyst as much as possible. The mechanism in the figure is in agreement with experiments as to when the protons and electrons are released from the OEC and when the two substrate water molecules enter it, one in S_0 and one in S_2. It agrees also with the fact that only an electron is released in the S_1 to S_2 transition. Also shown in the figure in red are the results when a full pH gradient of 3 pH units is applied. This means that

4.1 kcal/mol is added every time a proton is released. Remarkably, the membrane gradient only increases the barrier for the rate-limiting step from 11.3 to 12.5 kcal/mol, even though the driving force is reduced from 51.5 to 35.1 kcal/mol. A schematic figure of the mechanism obtained is shown in Figure 6.

4. HEME ENZYMES

Many proteins contain a heme cofactor, i.e., a porphyrin ring with an iron ion in the center. The main roles of the heme cofactors can be divided into three categories: electron transfer, transport and storage of molecular oxygen, and catalysis. The heme group can alternate between the Fe(II) and Fe(III) oxidation states, which makes it suitable as an electron transfer cofactor, either in specific electron transfer proteins, called cytochromes, or as cofactors inside an enzyme, transporting electrons to an active site in the same enzyme. This role of the heme group has not been extensively studied using density functional theory and therefore will not be further discussed here. Hemoglobin and myoglobin are involved in storage and transport of molecular oxygen in mammals. In these proteins the oxygen molecule binds to the reduced iron center (Fe(II)), and apart from molecular oxygen, these enzymes can also bind other small molecules, such as CO and nitric oxide (NO). The properties of the heme group binding to different small molecules have been studied by several authors, and these studies will be briefly discussed in one of the sections below. The main target of this section of the present review is the catalytic role of the heme group, which has been studied extensively using quantum chemical methods, mainly density functional theory. Thus, in many enzymes, a heme group is part of the active site where different types of chemical transformations occur. A large family of such enzymes is the cytochrome P450 superfamily, which contains many different enzymes (isoforms), all with the heme group as the main part of the active site. Many different aspects of these enzymes have been studied computationally, and the most important or most recent of those studies will be discussed in the first subsection below. Another family of enzymes where the heme cofactor plays a catalytic role is the heme−copper oxidase superfamily, which contains different types of cytochrome *c* oxidase and also nitric oxide reductase. These enzymes have a binuclear active site, which apart from the heme group contains a non-heme metal, either copper or iron. The heme−copper oxidases are membrane enzymes, and in particular the cytochrome *c* oxidases are of special interest since they are involved in the important process of pumping protons across the membrane. They have been studied extensively, both experimentally and computationally, and some of those studies will be discussed in the second subsection below. Finally, in the third subsection below, a few studies of other heme-containing enzymes will be briefly discussed.

To model biochemical reaction mechanisms in heme enzymes is quite demanding, since already an unsubstituted iron−porphine group has almost 40 atoms. In very early QM studies aimed at investigating reaction mechanisms of cytochrome *c* oxidase and cytochrome *c* peroxidase, which implies a large number of calculations, even smaller models were used for the porphyrin.[58,59] In more recent studies the most commonly used heme model is a full iron−porphine, but without side chains, in particular in studies of cytochrome P450.[60,61] However, since some of the side chains affect the redox properties of the iron center, it might be important to include them in the model. An example is the formyl substituent in heme *a*, present, e.g., in some forms of cytochrome *c* oxidase, which is found to affect the
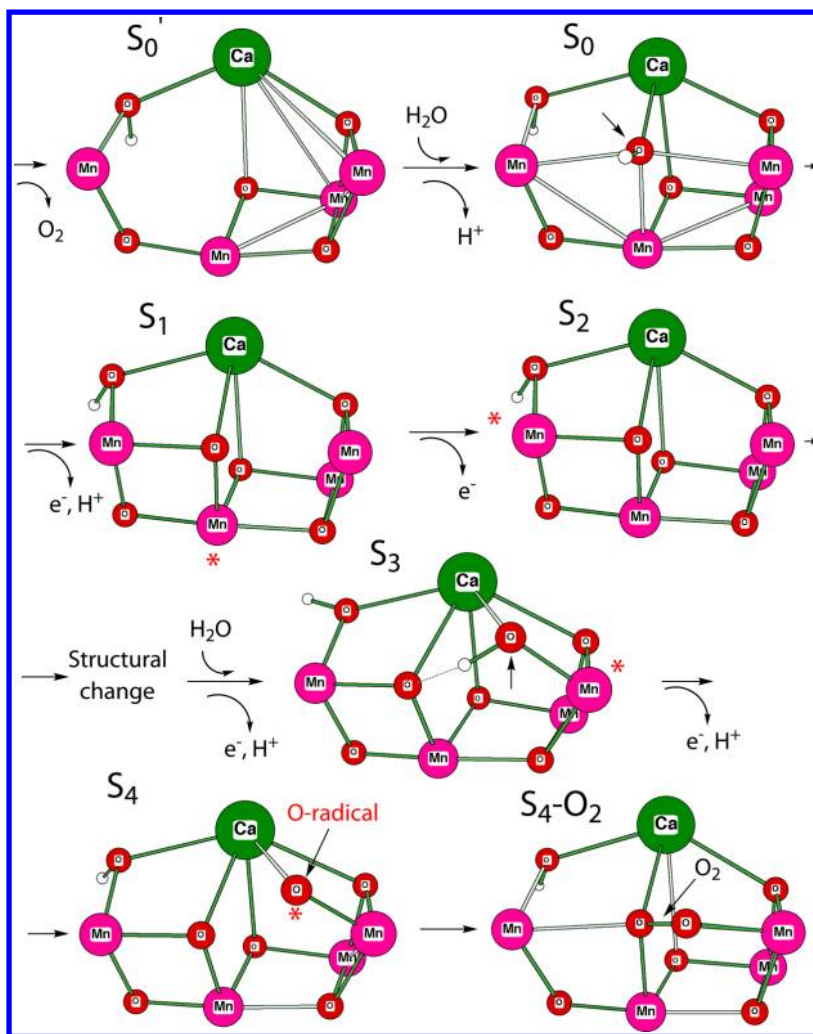
Figure 6. Schematic picture of the different S transitions. The structures have been optimized, but only the most important atoms are shown. An asterisk marks the atom that has been oxidized in that transition.

ionization potential of ferrous heme by 4 kcal/mol in DFT calculations.[62] Inclusion of the propionate side chains (labeled A and D in Figure 8 below) is connected with special difficulties, which are common to all modeling of charged groups. In an early QM study of cytochrome c oxidase, the heme a_3 propionate side chains were included in a model of the binuclear center, and one of them was protonated to simulate the salt bridge to a positively charged arginine (similar to propionate A–Arg299 in Figure 8), while the other one was left unprotonated, since its hydrogen-bonding partner is neutral (similar to propionate D in Figure 8 with Arg112 replaced by a protonated Asp).[21] This type of model easily leads to artificial spin population on the unscreened negatively charged carboxylate group, which in this case was handled by optimizing the structure with a dielectric medium present.[21] However, as was shown later this type of model still leads to a too large proton affinity of the negatively charged group, and a reliable model must include hydrogen-bonding partners (in this case a protonated Asp) to the negatively charged group (in this case the unprotonated propionate side chain).[19] A similar problem occurred in a QM/MM model of cytochrome P450, in which case it was argued that the spin population occurring on a heme propionate should be of chemical significance;[63] see further below.

4.1. Cytochrome P450

Cytochrome P450 (CYP) is a large superfamily of enzymes, present in many different organisms from all forms of life. These enzymes are involved in a large variety of reactions, including breakdown of exogenous compounds (detoxification) as well as synthesis of, e.g., signaling substances. The enzyme is mainly a monooxygenase, and the active site has a heme group, which is activated by the reaction with molecular oxygen. The active species in catalysis is believed to be an Fe^{IV}=O complex with a porphyrin radical, referred to as compound I (Cpd I), and which has two close-lying spin states, quartet and doublet, with the triplet coupled electrons on Fe(IV)=O coupled ferromagnetically or antiferromagnetically to the porphyrin radical. Due to its great importance, this family of enzymes has been studied extensively, both experimentally and computationally. Many reviews have been written; at least three reviews focusing on theoretical studies of P450 have fairly recently been published in *Chemical Reviews*.[60,61,64] Since the present review aims at giving a broad overview of what can be achieved regarding bioinorganic reaction mechanisms using a quantum chemical approach, some of the most important results from the previously published reviews on P450 will be repeated here, while the less common reactions and more detailed questions will not be discussed.
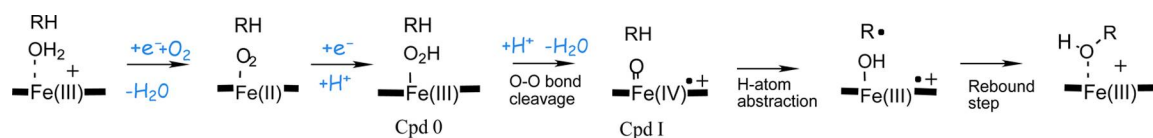
Figure 7. Catalytic cycle of P450 starting from the water-ligated ferric state, including formation of compound I and alkane (RH) hydroxylation via the rebound mechanism.
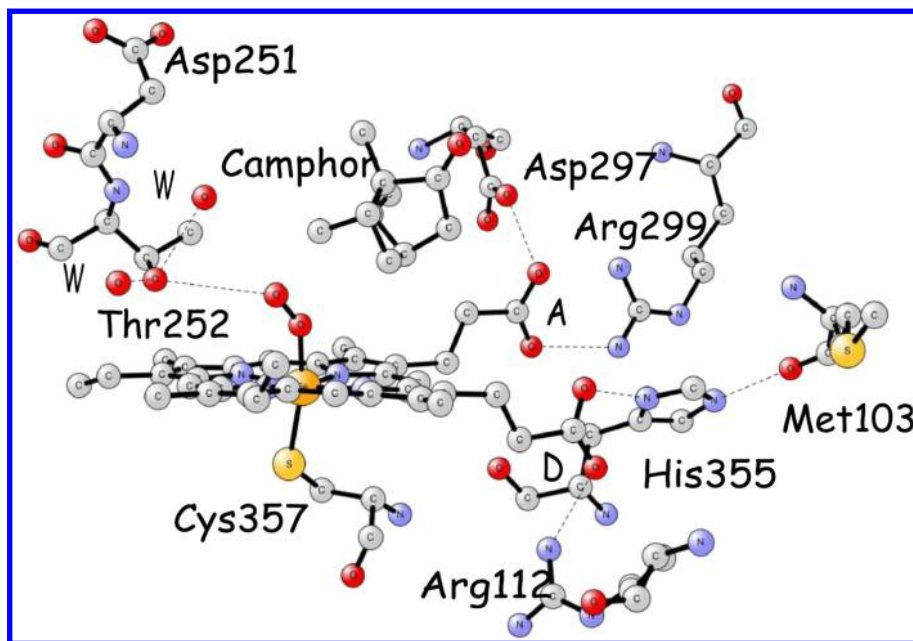

Figure 8. X-ray structure of the active site of P450$_{cam}$ (CYP101) with molecular oxygen and the camphor substrate[66] (PDB 1DZ8).

4.1.1. Catalytic Cycle: Compound I Formation. As mentioned above, the active site of the P450 enzymes contains a heme group, which is built from a protoporphyrin IX, an iron ion, and a conserved cysteine as the proximal iron ligand. The resting state is ferric (Fe(III)) with a distal water ligand on iron. The enzyme is activated by the reaction with molecular oxygen and reduction by two electrons. The source of the electrons depends on the species; in, e.g., mitochondrial P450, it is NADPH (reduced nicotinamide adenine dinucleotide phosphate). Coupled to the reduction, proton uptake from the bulk occurs, yielding Cpd I and a water molecule, as follows:

$$Porf-Fe(III)^+-OH_2 + O_2 + 2e^- + 2H^+ - H_2O$$
$$\rightarrow Porf^+-Fe(IV)=O \; (Cpd\,I) + H_2O$$
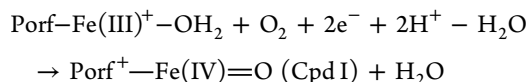
Cpd I has not been isolated as an intermediate in the oxidation reactions in P450, and until recently its properties could mainly be inferred from comparisons to other systems performing similar reactions (e.g., chloroperoxidase) and from theory.[61,65] However, in 2010 Rittle and Green managed to prepare high yields of Cpd I from a reaction between P450 (CYP119) and chloroperbenzoic acid, and it could be spectroscopically and kinetically characterized,[65] essentially confirming the expected electronic properties.

The Cpd I formation reaction described in the equation above is initiated by the entrance of the substrate, i.e., the organic molecule to be oxidized, into the active site of the enzyme; see the reaction scheme in Figure 7. Before molecular oxygen can bind to the heme, iron needs to be reduced to Fe(II) and the water molecule has to be released. It has been suggested that the water molecule has to leave its coordination to iron before the

reduction occurs, thereby acting as a "gate" for the entire reaction.[61] In agreement with such a function of the water molecule, DFT calculations have shown that the electron affinity of the pentacoordinated Fe(III) complex is about 10 kcal/mol higher than that of the hexacoordinated Fe(III) complex.[61] This result shows that the binding energy of water is 10 kcal/mol lower for the Fe(II) complex than for the Fe(III) complex, which can indicate that the water molecule leaves in concert with the reduction. Molecular oxygen binds to the reduced heme, forming the oxy–ferrous intermediate, for which the crystal structure was determined in 2000;[66] see Figure 8. This complex can also be described as a ferric–superoxide complex; according to the calculated electronic structure,[61] it has a singlet ground state, with antiferromagnetic coupling between the low-spin heme iron and the superoxide, very similar to that of many other oxy–ferrous heme complexes.

Thus, the first steps of the reaction in Figure 7, the one-electron reduction and the replacement of the distal water with molecular oxygen, are well established. The general picture of the catalytic cycle is that the next step is the second reduction, forming a ferric–peroxo complex, followed by uptake of a proton to form the ferric–hydroperoxide referred to as compound 0, Cpd 0 (see Figure 7).[61,67] This part of the reaction, the formation of Cpd 0, is probably the least understood, and it has not been well studied computationally. Experimentally, this second reduction step is described to be the rate-limiting step in many P450 oxidation reactions, and the ferric–peroxo intermediate is claimed to be observed only under very extreme conditions.[67] Clearly, the reduction potential of the already reduced oxy–ferrous state is very low, if it is not preceded by a charge-compensating proton uptake. If such an unstable intermediate as

the ferric–peroxo state is at all formed, it will be immediately protonated into the hydroperoxide complex, which indeed seems to be better characterized experimentally,[67] and Cpd 0 is therefore generally accepted as an intermediate in the P450 reaction.[68] Computationally (using DFT(B3LYP)/MM) the formation of Cpd 0 has only been studied starting from the two-electron-reduced state, investigating the proton transfer step without taking into account the energy cost of the second reduction step, most likely leading to a too low calculated barrier and a too exergonic reaction.[61,69]

As mentioned above, Cpd I was recently characterized experimentally, and it was shown to be competent to perform substrate oxidation,[65] which supports its involvement as an intermediate in the P450 reaction scheme. The addition of a proton to Cpd 0 and cleavage of the O–O bond should lead to the formation of Cpd I (see Figure 7), and this part of the reaction has been studied using both pure QM(DFT) and QM(DFT)/MM models. In the early studies the proton was added to the distal oxygen in Cpd 0, without any energy cost, and it was concluded that the O–O bond was cleaved without any barrier in a very exergonic process, leading to Cpd I and a water molecule.[70,71] Later computational studies, both pure QM and QM/MM, using more realistic models, have pointed out different problems with the original type of mechanism, where a proton is added to the distal oxygen in the Cpd 0 hydroperoxide, one being that the O–O bond cleavage barrier is too high when a more realistic cost of the proton is taken into account.[68,72,73] On the basis of QM calculations, a different type of O–O bond cleavage mechanism was suggested, which is referred to as a somersault mechanism, in which the O–O bond is homolytically cleaved in the peroxide, leading to an O–H radical that is rearranged and forms a hydrogen bond to the proximal oxygen.[68] The so-formed metastable radical intermediate was proposed to act as an oxidant in P450 hydroxylation reactions.[68] In a more recent QM study, the somersault O–O bond cleavage reaction was investigated with and without the substrate to be oxidized present, and the barrier height was found to depend on the substrate.[74] The somersault O–O bond cleavage mechanism has been adopted as a first step in Cpd I formation, and the barrier was found to be 15.4 kcal/mol in a QM/MM study.[73] A subsequent exergonic protonation of the metastable intermediate yields Cpd I, with Cpd 0 and Cpd I estimated to be of similar energy.[73] In that study of Cpd I formation, the proton donor is an aspartic acid (Asp251; see Figure 8), assumed to be protonated at the start of the reaction, and the proton path involves a few water molecules and a threonine (Thr252; see Figure 8).

To summarize, significant knowledge about the early parts of the catalytic cycle of P450, leading to the formation of Cpd I, has been gained from computational studies. However, a comprehensive computational study of Cpd I formation, starting from the resting ferric water-bound active site and including realistic estimates of the cost of electron and proton transfer from outside the enzyme, is still missing. It should be possible to do this using an approach similar to that described elsewhere in this review for other enzymes where electrons and protons enter or leave the active site, such as the heme–copper oxidases and PSII.

4.1.2. Alkane C–H Activation: Rebound Mechanism. An important property of the cytochrome P450 enzymes is their ability to catalyze the oxidation of aliphatic carbon–hydrogen bonds, a most difficult task. The generally accepted mechanism for the hydroxylation of C–H bonds is the so-called rebound mechanism, suggested by Groves and McClusky.[75] In this mechanism the first step is a H atom abstraction from the substrate by Cpd I, leading to an alkyl radical and an iron–hydroxo intermediate, followed by a rebound step where the substrate radical binds to the oxygen of the hydroxyl group, forming a ferric–alcohol complex; see the last two steps in Figure 7. A large number of computational studies, both QM and QM/MM, have been performed on this reaction for a number of different substrates, confirming the general features of the rebound mechanism and showing that the first hydrogen abstraction step is rate-limiting for this part of the reaction. A specific purpose of the early calculations on alkane C–H oxidation by P450 was to explain the radical clock experiments, which indicated that the lifetime of a substrate radical was too short to be compatible with the rebound mechanism. This controversy was suggested to be solved by the two-state reactivity (TSR) scenario found in the calculations, showing that the low-spin state reacts without a barrier for the second rebound step, leading to conserved stereochemistry, while the high-spin state has a barrier for the second step, allowing stereochemical scrambling to take place.[76] It can be noted that in recent QM/MM calculations on the hydroxylation of small alkanes by P450$_{BM3}$ it was found that in these cases also the high-spin state reacts without any barrier.[77]

One of the computationally most investigated substrates is camphor, which is the natural substrate of the bacterial P450$_{cam}$ enzyme; see Figure 8. Experimental rate observations indicate that the barrier for substrate hydroxylation should be ≤13 kcal/mol; see ref 78 and references therein. Early calculations, both QM and QM/MM, gave too high barriers of about 20 kcal/mol,[61] and another controversy occurred when it was claimed that the propionate substituents on the heme group (see Figure 8) participated in the hydroxylating reaction, decreasing the barrier significantly.[63] The involvement of the carboxylate groups in catalysis was suggested to originate from differential electrostatic stabilization, which could be observed in the calculations as a changing spin population on carboxylate oxygen atoms. However, it was later shown that both the occurrence of the unpaired spin on the propionate groups and the effects on the barrier height were artifacts due to inappropriate computational procedures, such as leaving Asp297 (see Figure 8) unprotonated.[79,80] The most recent computational results for the 5-exohydroxylation of camphor are in quite good agreement with the experimental rate estimate, in particular when dispersion effects[36] are added for the QM parts. QM(B3LYP) calculations give a barrier of 15.6 kcal/mol relative to the weakly bound encounter complex, which decreases to 11.9 kcal/mol when dispersion effects are included.[78] The corresponding values obtained at the QM(B3LYP)/MM level are 13.1 and 8.3 kcal/mol, respectively.[81] All these recent results for the hydroxylation barrier in camphor include zero-point effects, which decrease the barrier by 5.0 kcal/mol. Recently it was proposed that the accuracy of calculated energetics of redox reactions involving transition metals can be improved if an extended so-called localized orbital correction is introduced into the B3LYP functional, and it was shown that such a correction would significantly lower the barrier for alkane hydroxylation in P450.[15] It can also be noted that calculations on a series of different alkanes have shown that it is possible to correlate the barrier height for the hydrogen atom abstraction step with the calculated C–H bond strength, and further insights into the hydroxylation reaction can be gained from valence bond analysis of the computed trends and the reaction patterns.[61]

4.1.3. Alkene Oxidation: Competition between Epoxidation and Allylic Hydroxylation. The presence of C=C double bonds in unsaturated substrates opens up the possibility of oxidation reactions other than the C−H oxidation discussed above, the most important one being epoxidation of the substrate by Cpd I; see the scheme in Figure 9. The epoxidation reaction in
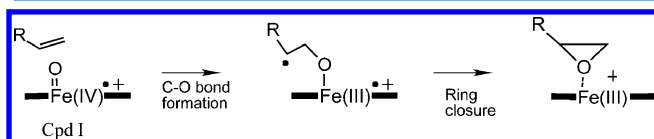

Figure 9. Scheme showing the main steps in alkene epoxidation by Cpd I in P450.

P450 has been studied for several different substrates, e.g., propene and cyclohexene, and the calculated energy profiles show large similarities with the hydroxylation reaction discussed above.[60] The reaction between Cpd I and the C=C double bond occurs in two steps: in the first, rate-limiting C=C activation step, a C−O bond is formed, together with a substrate radical, and in the second, ring closure step, the second C−O bond is formed (see Figure 9).[60] There are different electronic states possible for the intermediate formed after the first step, which means that products other than the epoxide can also be formed. It was furthermore found that, much like those for the hydroxylation reaction, the low-spin intermediates form epoxide without any barrier and with conserved stereochemistry, while the high-spin intermediates can give different products and also have a barrier for epoxide formation, allowing scrambled stereochemistry.[61]

An interesting selectivity issue arises for the oxidation of alkenes, where a competition between epoxidation and hydoxylation of an allylic C−H bond can occur. Experimentally it has been found that for cyclohexene a number of different P450 isoforms give approximately equal amounts of epoxide and allylic hydroxide, while propene, at least for one P450 isoform, P450$_{LM2}$, only gives rise to epoxide.[60,61] Early QM calculations on propene gave almost identical barriers for epoxidation and allylic hydroxylation, in contradiction to the experimental observation. In an attempt to improve the QM model of Cpd I, hydrogen-bonding partners to the proximal cysteine sulfur were introduced, and they were claimed to have an important differential effect on the two barriers under investigation, making the epoxidation barrier significantly higher than the hydroxylation barrier for propene.[60,82] In contrast, later QM studies gave no effect from cysteine hydrogen bonds on P450 hydroxylation reactions,[28] a result which is in line with the very long hydrogen bond distances obtained in the original investigation.[60,82] For cyclohexene the results from QM calculations show a preference for allylic hydroxylation, in disagreement with the experimental observations that equal amounts of the two products are produced.[61] QM/MM

calculations on both substrates, propene and cyclohexene, did not improve the agreement with experiment, since in both cases the hydroxylation reaction was clearly preferred before epoxidation.[61,83] In recent QM calculations on both substrates it was found that dispersion effects modify the barrier heights in the right direction, such that for cyclohexene the two barriers are actually quite similar, in good agreement with the experimental observations that both products are observed.[78] For propene the epoxidation barrier decreases more than the hydroxylation barrier from the dispersion effects, but the results still do not agree with the experimental observation that only epoxidation is observed.[78] The effects of adding dispersion to the QM part in QM/MM calculations were also investigated for the same systems.[81] However, those results are more difficult to interpret, since the calculated barrier heights vary among the different energy profiles investigated for each reaction. The different energy profiles correspond to different starting structures, i.e., different possible binding modes of the substrate. This illustrates a general difficulty when studying reactions by cytochrome P450 computationally: it is not always obvious which is the preferred substrate-binding mode. Therefore, it is a common procedure in QM/MM studies to perform initial docking and/or MD simulations to obtain likely modes of substrate binding.

Recently a systematic QM study of epoxidation by P450 Cpd I and similar oxidants was performed. Several different alkene substrates were studied, and the gas-phase energy differences between the separated reactants and the transition state for C−O bond formation were plotted against various variables. On the basis of those diagrams, the study was claimed to show that the rate constant for substrate epoxidation correlates with the ionization potential of the substrate, as well as with the electronic properties of the oxidant.[84] The regioselectivity between substrate epoxidation and hydroxylation was also investigated, and it was claimed to be purely substrate dependent.[84]

4.1.4. Aromatic Oxidation: Side-On and Face-On Orientation. Oxidation of aromatic compounds by P450 can lead to different products, most importantly epoxides and phenolic products. Several computational studies, at both the QM and QM/MM levels, have been performed for the simplest aromatic compound, benzene, which is a substrate of some P450 isoforms.[61] The computational studies show that different final products can be formed from a common intermediate, a σ-complex with a C−O bond, formed between the approaching benzene substrate and the Cpd I oxygen; see Figure 10. QM/MM calculations on this step gave barriers close to the value corresponding to the experimental rate for hydroxylation of benzene in one P450 isoform (2E1),[85] and it was concluded that this is the rate-limiting step.[81] However, in the more recent QM/MM study it was found that dispersion effects in the QM part significantly lower this barrier,[81] indicating that the step involving addition of compound I to the aromatic ring is not rate-limiting. The intermediate σ-complex is found to exist in different forms, with respect to both the electronic and geometric structures. The
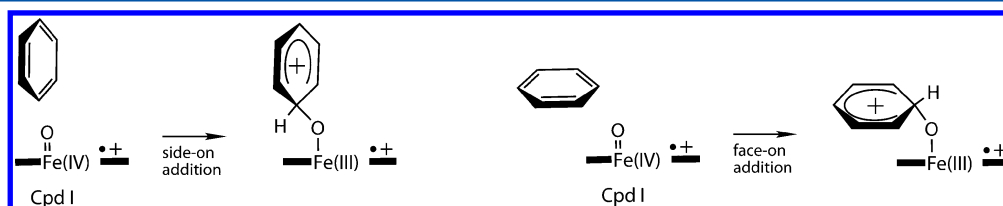

Figure 10. Scheme showing the first step of the side-on and face-on mechanisms for addition of benzene to Cpd I in P450.
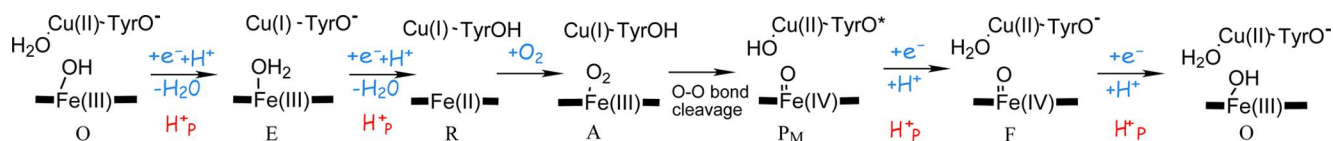
Figure 11. Catalytic cycle of CcO starting from the oxidized state **O**. The notation H_P^+ corresponds to pumped protons.

intermediate can have a substrate radical or a carbocation or different mixtures of the two. Furthermore, the substrate can be in a side-on position, with the benzene ring more or less perpendicular to the heme plane, or in a face-on position, with the benzene plane more or less parallel to the heme plane; see Figure 10.[61] The QM/MM study showed that the two geometrical forms have similar barrier heights for formation of the first C−O bond, which is still the case when dispersion effects are taken into account, indicating that both reaction paths are possible.[81,85] Both the side-on and face-on reaction paths can form both epoxide and ketone, both of which can rearrange to phenol.[85] The side-on approach can also form phenol via a shuttle mechanism, which has a N-protonated porphyrin as an intermediate.[61,85]

For more complicated aromatic substrates, there are other factors contributing to the reactivity patterns, such as interactions (attractive or repulsive) between the substrate and either the heme cofactor or amino acid residues in the active site. Recently the oxidation of the substrate dextromethorpan in one specific P450 isoform (2D6) was studied using a QM/MM approach.[86] This substrate can be oxidized in two different ways, either aromatic hydroxylation or O-demethylation, and it was found in the QM/MM calculation that only the O-demethylation pathway is possible, in accordance with experimental observations. In contrast, QM calculations on a small model including only the Cpd I cofactor and an anisole substrate give similar barriers for the two oxidation modes. It was concluded that the QM/MM calculations demonstrate the crucial role of the protein in determining the reactivity of this substrate, in contrast to QM model calculations.[86] It can be noted that an alternative way of investigating the same issue would be to perform QM calculations on a larger model including the amino acids in the active site, which would also make it possible to determine the specific roles of the individual residues.

4.1.5. Other Reactions. The cytochrome P450 enzymes are capable of performing many other types of reactions in addition to those discussed above, and many of them have been studied computationally, such as dealkylation, sulfur and nitrogen oxidation, ethanol oxidation, and C−C bond formation. For a description of those and other computational studies on P450 reactions, see the previous reviews.[60,61]

4.2. Heme−Copper Oxidases

The heme−copper oxidases constitute a large family of membrane-bound enzymes involved in aerobic respiration and denitrification. They have a large sequence homology, and they have a similar heme-containing active site. Common for these enzymes is also that, during the catalytic reactions, electrons and protons are taken up from outside the enzyme (membrane), which means that the energy cost of these reactions has to be estimated to obtain the energetics of the catalytic cycles. This is done using experimental reduction potentials in a way similar to that described in connection with the discussion about the O_2 formation in PSII. The heme−copper oxidase enzymes include both different variants of cytochrome c oxidases, which reduce molecular oxygen to water, and nitric oxide reductase, which

reduces nitric oxide to nitrous oxide. The cytochrome c oxidases are discussed in the first subsection below, and nitric oxide reductase is discussed in the second subsection below.

4.2.1. Cytochrome c Oxidase. Cytochrome c oxidase is the terminal enzyme in the respiratory chain, located in the mitochondrial or bacterial membrane. The active site is a binuclear center (BNC) consisting of a heme group (here labeled heme a_3; see further below) and a histidine-ligated copper (labeled Cu_B). One of the histidine ligands has a cross-linked tyrosine, which takes part in the redox chemistry involved in the process of reducing molecular oxygen to water; see the scheme in Figure 11. The four electrons needed to reduce one oxygen molecule to two water molecules are delivered from cytochrome c, located on the P-side of the membrane. The electrons are delivered to the BNC via two cofactors, one dinuclear copper complex (labeled Cu_A) and another heme group (here labeled heme a; see further below) located near the binuclear center. The protons needed for charge compensation and water formation are taken up from the opposite side of the membrane, the N-side. Because the electrons and protons are taken up from opposite sides of the membrane, this reaction is referred to as an electrogenic reaction. This means that each proton−electron pair taken up by the BNC corresponds to the transport of one positive charge from the N-side to the P-side, building up an electrochemical gradient across the membrane. When this gradient is present, the electron and proton uptake to the BNC will be more costly, since the charges have to move against the gradient. Since the reduction of molecular oxygen to water using electrons from cytochrome c is very exergonic, this process can still go on with the gradient present. In fact, this is how the energy is stored, and the stored energy, in the form of the gradient, is used by another enzyme in the membrane, adenosine 5′-triphosphate (ATP) synthase, to make the energy-rich compound ATP. Furthermore, the electrogenic chemistry is not the only way this enzyme stores the energy, but there is also another process, coupled to the electron transfer, which translocates protons all the way from the N-side to the P-side, thus enhancing the gradient buildup and making the energy storage more efficient.[87] These protons are referred to as pumped protons, and the protons going to the BNC, participating in the water formation, are referred to as chemical protons. The reduction of molecular oxygen in cytochrome c oxidase can thus be summarized:

$$O_2 + [4(1 + n)]H_N^+ + 4e_P^- \rightarrow 2H_2O + (4n)H_P^+$$
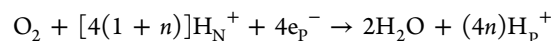
The large family of cytochrome c oxidase enzymes can be divided into subfamilies, which differ in the exact form of the heme cofactors, in the presence of different numbers of channels for proton transfer, and in the number of pumped protons per electron (the value of n in the equation above). The largest subfamily, the A-family, present in mammalians and in several bacteria, is the most studied, and the only one that will be discussed here. For the members of this family it has been shown that the value of n in the equation above is 1; i.e., there is one proton pumped per electron, meaning that for each electron

delivered to the BNC, there are two protons taken up from the N-side, one for the chemistry and one to be pumped (see Figure 11). Furthermore, the members of the A-family have two proton channels connecting the N-side with the BNC, called the D- and the K-channels. Finally, in the A-family the heme cofactors are of the heme *a* type, explaining the labeling heme *a* and heme *a₃* mentioned above.

From the description above, it should be clear that cytochrome *c* oxidase is a quite unique enzyme and is very important in bioenergetics, and it has been studied extensively, mainly experimentally, but also computationally. The most intriguing questions concern the fact that all proton motion occurs against the gradient, which means that there must be some kind of gating that prevents the protons from being taken from the thermodynamically more favorable side of the membrane. In particular, there must be special mechanisms assuring that one of the protons taken up for each electron is pumped to the opposite side of the membrane, and not used for the chemistry, which would lead to losses in energy storage. The search for proton pumping mechanisms has been one of the most active areas in bioenergetics for a long time, and in spite of this, there has still been no consensus reached about these mechanisms. Even if the proton gating and pumping mechanisms are the most interesting ones, it is also important to understand the mechanisms of the chemistry of O_2 reduction occurring in the BNC, involving the O−O bond cleavage and the four reduction steps. All these issues have been studied computationally, and the most important results obtained from density functional theory studies will be discussed below.

4.2.1.1. O−O Bond Cleavage in CcO. Molecular oxygen binds reversibly to the two-electron-reduced BNC, labeled **R**, with Fe(II) and Cu(I), forming the experimentally observed compound **A**; see the scheme in Figure 11. The next intermediate formed is labeled **P_M**, in which the O−O bond is cleaved and the cross-linked tyrosine is oxidized to a tyrosyl radical;[88−90] see Figure 11. In fact, most experiments have been performed on the so-called fully reduced form of the enzyme, which has electrons available also in the other two cofactors, Cu_A and heme *a*, and in this case the **P_M** intermediate is never observed, but instead the tyrosyl radical is reduced to a tyrosinate by the electron on heme *a*. However, the **P_M** intermediate is the one expected to be involved in the working enzyme, and it is therefore the one discussed here. Thus, the O−O bond is cleaved in the first reaction step after the O_2 molecule has bound to the BNC, with one of the oxygen atoms forming a heme—Fe(IV)=O moiety and the other oxygen atom coordinating to Cu_B, presumably as Cu(II)−OH; see Figure 11. From experimental observations it is known that there is no uptake of protons during the **R** to **P_M** reaction steps, which means that the proton in the hydroxyl group on Cu_B must be internal. It has been suggested that the proton comes from the cross-linked tyrosine, since the tyrosyl radical is most stable in its neutral form.[88−90] Investigation of the details of the O−O bond cleavage in the BNC of CcO is an excellent subject for DFT studies, in particular since neither electrons nor protons enter from outside the enzyme, and several such studies have been made using different models of the BNC, the most recent one shown in Figure 12 (built on the X-ray structure of the fully reduced CcO[91]). The first aim of DFT studies on the O−O bond cleavage step was to find out if the suggested mechanism with the formation of the tyrosyl radical was thermodynamically feasible. Using a quite small model of the BNC, it was early shown that the cleavage of the O−O bond with formation of a neutral tyrosyl radical, Cu(II)−OH, and Fe(IV)=
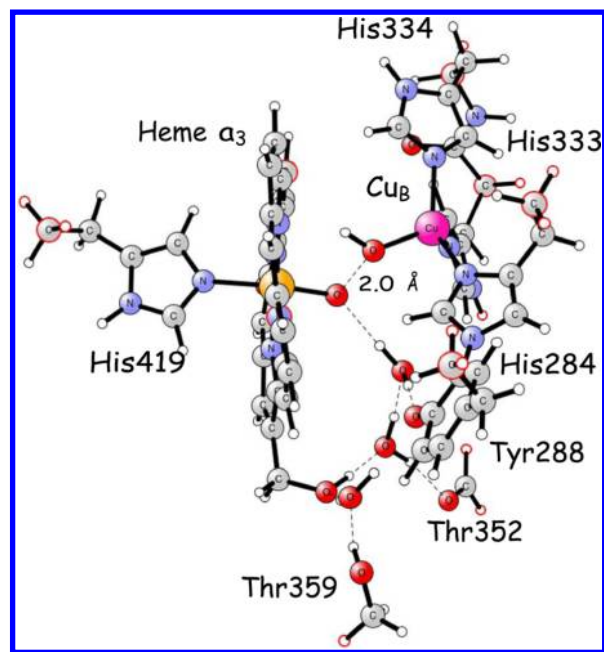

Figure 12. Optimized transition state for O−O bond cleavage in C*c*O. The atoms with red circles are fixed to the X-ray coordinates in the geometry optimizations. The model of the BNC is built on the X-ray structure of the fully reduced C*c*O[91] (PDB 3FYE).

O should be close to thermoneutral.[58] However, that very first study involved a water molecule in the O−O bond cleavage in such a way that the oxygen atom in Cu(II)−OH did not originate from molecular oxygen, which is in contradiction to experimental indications.[92] Therefore, a new study with a somewhat larger model of the BNC was performed, investigating a mechanism involving the O_2 molecule binding in a bridging mode between the two metals in the BNC,[93] and in that study the **A** to **P_M** step was estimated to be exergonic by about 4 kcal/mol. The studies mentioned so far used the B3LYP functional and included solvent effects from the surrounding protein described as a homogeneous dielectric medium. In the most recent study, using an even larger model of the BNC with about 144 atoms, see Figure 12,[94,95] using the B3LYP* functional, and including solvent, dispersion, and zero-point effects, this reaction step was found to be exergonic by 4.3 kcal/mol.[62]

Thus, quantum chemical calculations have shown that the suggested mechanism for the O−O bond cleavage, depicted as the **A** to **P_M** step in Figure 11, is thermodynamically feasible. On the other hand, the activation barrier for this step comes out too large in the calculations. From the experimental time constant for disappearance of compound **A**,[89] the free energy of activation can be estimated to be 12.4 kcal/mol using transition-state theory, and from the weak temperature dependence it is estimated that there is a large entropy effect on the barrier, resulting in an enthalpy of activation of only 6.4 kcal/mol.[89] The calculations (using several different models of the BNC) show that the reaction actually occurs in two steps. First, a proton is transferred (via one or more water molecules) from the cross-linked tyrosine to the O_2 molecule, forming an Fe(III)−OOH peroxide, with the distal oxygen coordinated to Cu(II) and with a tyrosinate. In the second step an electron is transferred from the tyrosinate to the O−O bond, which is cleaved, yielding the **P_M** product. Using the model shown in Figure 12, the actual O−O bond cleavage transition state was found 21.0 kcal/mol (with B3LYP* and solvent effects) above compound **A**, and the barrier for the
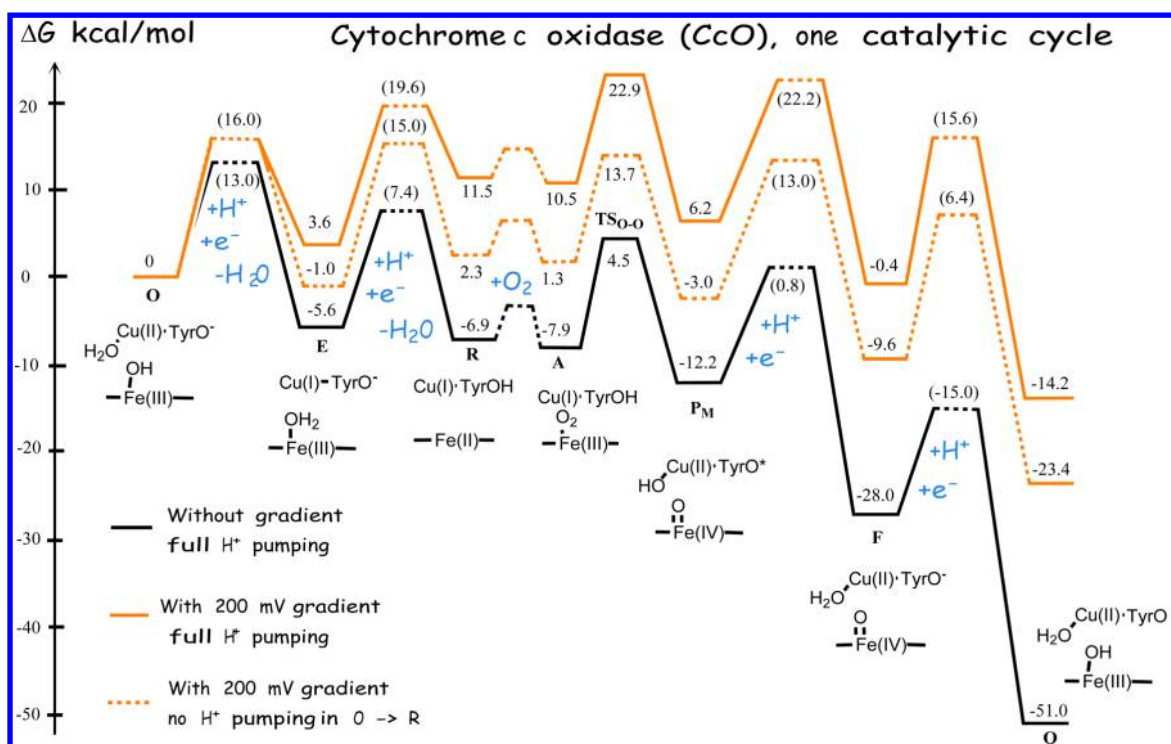
Figure 13. Calculated energy profile for one catalytic cycle of C*c*O, black curve. The relative energies without a gradient are obtained from ref 62 but with correction of the Fe(II) (rather than Fe(III)) energy by 4.6 kcal/mol to make the **R** to **A** step agree with experiment. The orange curves correspond to the situation with the gradient present; see further in the text.

preceding proton transfer step, which was more approximately investigated, was found to be about 5 kcal/mol lower.[94] The actual O−O cleavage barrier decreases to 17.6 kcal/mol when dispersion and zero-point effects are included. Compared to the free energy barrier of 12.4 kcal/mol, the calculated value of 17.6 kcal/mol is almost within the error bars (3−5 kcal/mol), but compared to the estimated enthalpy barrier of 6.4 kcal/mol, the error is still very large. The calculations show that a large part of the high O−O cleavage barrier comes from the endothermicity of the first proton transfer step, and it was found that the addition of a proton in the vicinity of the tyrosine residue stabilizes the tyrosinate intermediate and lowers the total barrier significantly.[19] A possible source of the extra proton could be a protonated lysine residue, located in the K proton path connecting the N-side of the membrane with the BNC (at the cross-linked tyrosine).[19,94] The distance between the tyrosine and the lysine is about 13 Å, which means that the lysine proton would have to move closer to the BNC to give a large enough stabilization. Another suggestion for solving the problem with the high barrier obtained for the suggested O−O bond cleavage mechanism is that the proton in the Cu(II)−OH complex actually has an origin other than the tyrosine, which means that the cost of such a proton cannot easily be estimated in the model calculations.[94,95] In summary, there is still no completely satisfactory description of the O−O bond cleavage mechanism that can explain the low experimental barrier.

*4.2.1.2. Catalytic Cycle of C*c*O.* The catalytic cycle of C*c*O, as described in Figure 11, is composed of six steps. One of the steps is the binding of molecular oxygen to the reduced BNC, the **R** to **A** step, and the next step is the O−O bond cleavage, the **A** to **P$_M$** step, described in the previous subsection. These two steps together, **R** to **P$_M$**, correspond to reducing molecular oxygen with all four electrons needed for the water formation, taking two

electrons from iron, Fe(II) → Fe(IV), one from copper, Cu(I) → Cu(II), and one from the cross-linked tyrosine, forming the tyrosyl radical. The other four steps of the catalytic cycle, **P$_M$** to **F**, **F** to **O**, **O** to **E**, and **E** to **R**, correspond to re-reducing the active site of the enzyme, with the transfer of one electron from cytochrome *c* on the P-side of the membrane to the BNC in each step. Each electron transfer is coupled to a proton transfer from the N-side of the membrane to complete the water formation. As mentioned above, and as indicated in Figure 11, each electron transfer is also coupled to a proton transfer across the entire membrane, called proton pumping and labeled H$_p^+$ in the figure. All six intermediates involved in the reaction scheme in Figure 11 have been observed experimentally and are partly characterized. However, the detailed electronic and geometric structures are not known, and to find those is one purpose of the computational studies that have been performed. The reduction level of the metal ions in the different intermediates is quite well-known from experiment, while the protonation states are more difficult to determine, as is the number of water molecules present in the BNC. The scheme presented in Figure 11, based on several DFT studies,[19,62,94] suggests that the cross-linked tyrosine remains unprotonated until the last re-reduction step, **E** to **R**, and that the two newly formed water molecules leave the BNC in the last two re-reduction steps.

The energetics of the O$_2$-binding step, **R** to **A**, can be studied computationally in the same way as the O−O bond cleavage step described above, since there are no electrons or protons entering during this step. An important aspect of the description of this step, where a small gaseous molecule becomes bound, is that there will be a significant entropy loss. Entropy effects cannot be computed using the present models, since several atoms are fixed to their X-ray coordinates, and for most of the reaction steps it can be assumed that the changes in entropy are negligible, which
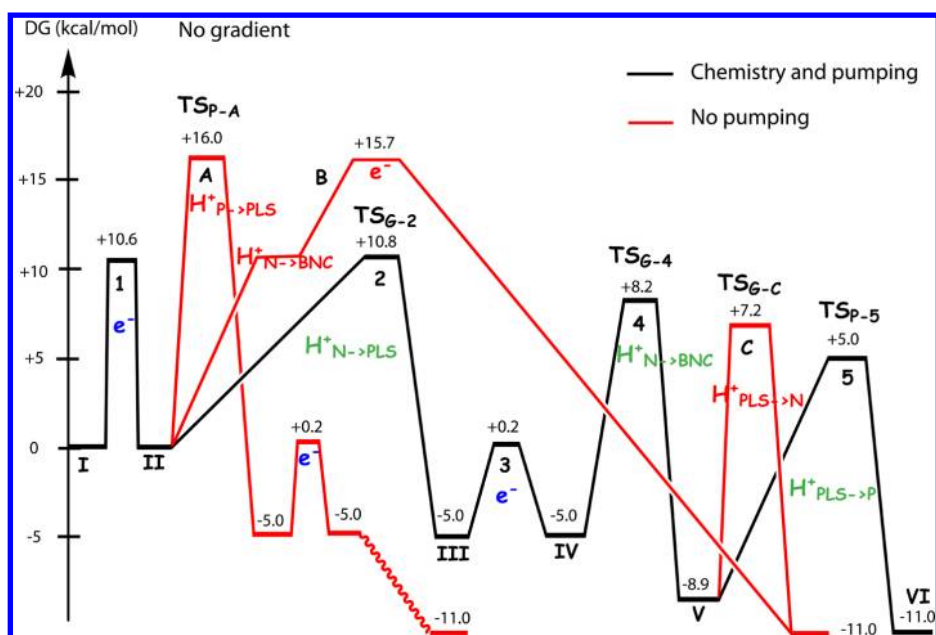
Figure 14. Energy profile for one reduction step in C*c*O. The black curve corresponds to the experimentally observed reaction, including both water formation (chemistry) and proton pumping. The red curves correspond to nonwanted reactions which would not lead to proton pumping.

is why the calculated relative energies are considered to represent changes in free energy. The exception is when a small gaseous molecule becomes bound (or released). Then the entropy change is estimated as loss (or gain) of the translational entropy of the free molecule, which is 10.8 kcal/mol in the case of O_2. The free energy of binding of O_2 relative to state **R** calculated with the model in Figure 11, using the B3LYP* functional and including solvent, dispersion, zero-point, and entropy effects, is 5.6 kcal/mol.[62] This value is a bit too large compared to experimental estimates, and it is likely due to the B3LYP* functional destabilizing the Fe(II) oxidation state relative to the Fe(III) state.[20] Introducing a stabilizing correction of 4.6 kcal/mol for the Fe(II) state gives a more reasonable binding of 1.0 kcal/mol.[62] This correction also affects the **E** to **R** transition, which involves the Fe(II) oxidation state.

To calculate the relative energies of the remaining four steps of the catalytic cycle, the re-reduction steps, the energy costs of the electrons and the protons have to be estimated. This means that the reduction potentials of the active site have to be compared to the reduction potential of the electron donor, i.e., cytochrome *c*, and the pK_a values of the active site have to be compared to the pK_a value of the proton donor, i.e., bulk water. These values cannot be calculated accurately using the present methodology. Instead experimental reduction potentials are used in a procedure described in several publications[19,62,94,95] and also in the section about PSII in the present review. The experimental reduction potentials, 0.25 V for cytochrome *c* and 0.8 for reduction of O_2 to water, give an exergonicity of one catalytic cycle of C*c*O of 51.0 kcal/mol (2.2 V).[96] In combination with the calculated free energy for the chemistry, the cost of each reduction step (transfer of one electron from the donor and one proton from the bulk) is set to reproduce the total exergonicity. Together with the calculated relative energies of the intermediates, this determines the energetics for each of the reduction steps in the catalytic cycle. Using this procedure and the model in Figure 12, the energy profile shown as the black curve in Figure 13 is obtained.[62] The energies are calculated using the B3LYP* functional with the correction for the Fe(II)

state mentioned above and including solvent, dispersion, zero-point, and entropy effects. Furthermore, simplified and approximate barriers (13 kcal/mol) for the combined electron and proton transfer reactions in each reduction step are introduced, on the basis of the fact that the reduction steps occur on a microsecond time scale.[62] Finally, in the energy profile, the experimental value for the O−O bond cleavage is used and a small entropy barrier is introduced for the binding of the O_2 molecule.

The energy profile in Figure 13 shows that all reduction steps are exergonic, but the two reduction steps occurring directly before the O−O bond cleavage are only weakly exergonic, much less exergonic than the other two reduction steps occurring directly after the O−O bond cleavage. This result is in agreement with experimental values for the reduction potentials involved in the different reaction steps.[97] It should be noted that all the C*c*O energetics discussed so far refer to the situation with no electrochemical gradient present across the membrane, and in this situation there is no cost for pumping protons from one side of the membrane to the other, affecting the thermodynamics. For the working enzyme there is always a gradient present, and to understand the mechanisms of the enzyme, the effects of the gradient on the energetics have to be estimated. The maximum gradient is known to be 200 mV, 4.6 kcal/mol,[96] which means that moving one charge against the gradient across the entire membrane adds an extra cost of 4.6 kcal/mol to the energy profile. For the energy profile in Figure 13, all points, except the approximate electron/proton barriers, correspond to moving full charges across the entire membrane, and therefore, the effects of the gradient can easily be estimated; see the full orange curve in Figure 13, in which it is assumed that the enzyme pumps one proton per electron also with a full gradient. As can be seen from the full orange energy profile, with the gradient present, two of the reduction steps become endergonic, which in turn also raises the barriers in such a way that the rate of the catalytic reaction would decrease significantly. The electron/proton transfer barriers are assumed to increase to 16 kcal/mol when the full gradient is present, while the intrinsic O−O bond cleavage

barrier is not affected. However, since the endergonicity of preceding steps adds to the total barrier heights, several barriers become around 20 kcal/mol or more, which corresponds to a too slow rate, not in accordance with experimental observations. The main reason for the high barriers is the original low exergonicity in two of the reduction steps, and if the total exergonicity was more evenly spread over the reduction steps, there would be no endergonic steps, even with a full gradient and full proton pumping. This uneven distribution of the reaction exergonicity over the reduction steps is a major problem in understanding this enzyme, discussed by several authors,[96−98] and it has been suggested that the enzyme somehow can store energy between the reduction steps.[96] Another suggestion, based on the computed energy profile, is that even if the enzyme pumps one proton per electron without and with a low gradient, with a full gradient it is possible that only the two most exergonic reduction steps are coupled to proton pumping, and in the other two reduction steps the pumping mechanism allows for leakage of the protons expected to be pumped.[94,95] Such a scenario is shown as the dotted orange curve in Figure 13, and as can be seen, in this situation there are no very high barriers.

Apart from the studies discussed above, only a few density functional studies have addressed the entire catalytic cycle of C*c*O,[99,100] and the results of those studies were discussed already in a previous review.[95] One of those studies adopts an approach similar to that discussed above, and although some results differ significantly, the main results are rather similar.[99] The difference is most likely due to convergence to an excited state for one of the intermediates in ref 99, as described in the previous review.[95] The other study[100] is concerned with a different subfamily of C*c*O (the B-family), and a very different approach is used. Among other things, more attention is paid to a detailed description of the proton and electron shifts in the BNC, resulting in a rather complicated energy diagram for a 14-step cycle.[100] Therefore, the energy diagram in ref 100 is not directly comparable to the energy diagram presented above.

4.2.1.3. Proton Pumping in CcO. The most fascinating property of the cytochrome *c* oxidase enzyme is the ability to pump protons against the electrochemical gradient. A working mechanism for proton pumping must contain two main ingredients. The first one is a mechanism for coupling electron and proton transfer, which makes it possible to transfer two protons per electron, one for the chemistry and one for pumping. The second ingredient is a gating mechanism, which at different stages governs the protons to move to the right place and against the gradient. Both these ingredients can most easily be described by an energy diagram for one reduction step in C*c*O, showing the energetics for the elementary electron and proton transfer steps; see Figure 14. The figure shows the only realistic energy profile for one reduction step, published so far, that includes the most important gating situations.[101−103] The black curve in the energy diagram is constructed using kinetic information from an experiment on one reduction step (**O** to **E**[104]), generalized to a situation where all reduction steps have the same exergonicity. The black curve corresponds to the actual reaction taking place, including both chemistry and proton pumping, and it contains the coupling mechanism to be described below. The red curves in Figure 14 correspond to nonallowed processes that would not lead to proton pumping, and they have been constructed on the basis of assumptions for possible gating mechanisms, also discussed below.

To describe the pumping and gating mechanisms, two facts, apart from the fact that the chemistry takes place in the BNC

(one electron and one proton per reduction step), have to be known. One fact is that there exists a place in the vicinity of the BNC where the protons to be pumped are temporarily stored during the process, which is referred to as the pump-loading site (PLS). The PLS is often assumed to be one of the propionate groups of the heme cofactors. The other fact is that the BNC, the PLS, and the electron transfer cofactor heme *a* are all close enough to each other for significant (several kilocalories per mole) electrostatic interaction. The basic coupling mechanism for proton pumping is more or less generally accepted, and it can be described as follows, referring to Figure 14. In step 1 an electron from cytochrome *c* arrives at heme *a*, which triggers the uptake of a proton from the N-side to the PLS in step 2. This proton transfer occurs via a transition state labeled TS$_G$, assumed to be near a protonated glutamic acid in the D-channel for proton transfer, and which also interacts significantly electrostatically with heme *a* and the BNC. The proton in the PLS triggers the electron transfer from heme *a* to the BNC, step 3, which in turn leads to uptake of a proton from the N-side to the BNC for the chemistry, step 4. At this stage there is no longer any uncompensated negative charge that can stabilize the proton in the PLS, and the proton is therefore expelled to the P-side in step 5. For this mechanism to work, there are several gating situations, where the wrong process, not leading to proton pumping, must have a higher barrier than the allowed process. Some of the gating situations are shown in Figure 14, where the red curves, representing the nonallowed processes, have higher barriers than the black curve, representing the wanted process. The gating mechanisms are quite complicated, and there is no consensus about the details. Here, only one suggested gating mechanism connected to the role of the transition state TS$_G$ will be briefly described.[101−103] In this mechanism the TS$_G$ is suggested to be positively charged, which is achieved by an extra proton moving in the D-channel toward the PLS, rather than taking the proton from the protonated glutamic acid and making it fully deprotonated. The positive charge on the TS$_G$ makes this transition state stabilized by the electron arriving in heme *a*, in the same way as a proton in the PLS is stabilized by this electron. Thus, from state II in Figure 14, TS$_{G−2}$ is lower than TS$_{P−A}$, which prevents proton uptake from the P-side. For a later state of the reaction, labeled V in the diagram, the proton in the PLS must be prevented from moving back to the N-side, and rather be pumped to the P-side. In this situation, V, there is no uncompensated negative charge to stabilize the positive TS$_{G−C}$, which is therefore raised in energy and gives a higher barrier for back-leakage to the N-side than for pumping the proton to the P-side via TS$_{P−5}$.

The mechanisms discussed above have been suggested on the basis of experimental kinetic information, the X-ray structure, electrostatic considerations, and careful analysis. A few DFT calculations have been performed to evaluate certain aspects of the suggested mechanisms. One DFT study used a model of about 250 atoms, including the heme *a* cofactor, the region around the suggested PLS, the region around the suggested TS$_G$, and a very simplified description of the BNC (essentially only the Cu$_B$ ion).[105] Using this model, it could be shown that the Coulombic effect from an electron in heme *a* is very similar at the PLS and TS$_G$, which is the basic ingredient in the suggested gating mechanism. Using the same model, a value of 15.3 kcal/mol was obtained for the back-leakage barrier, TS$_{G−C}$, which was estimated to be 16.1 kcal/mol (8.9 + 7.2) in Figure 14, using simple electrostatics and the X-ray structure. DFT calculations
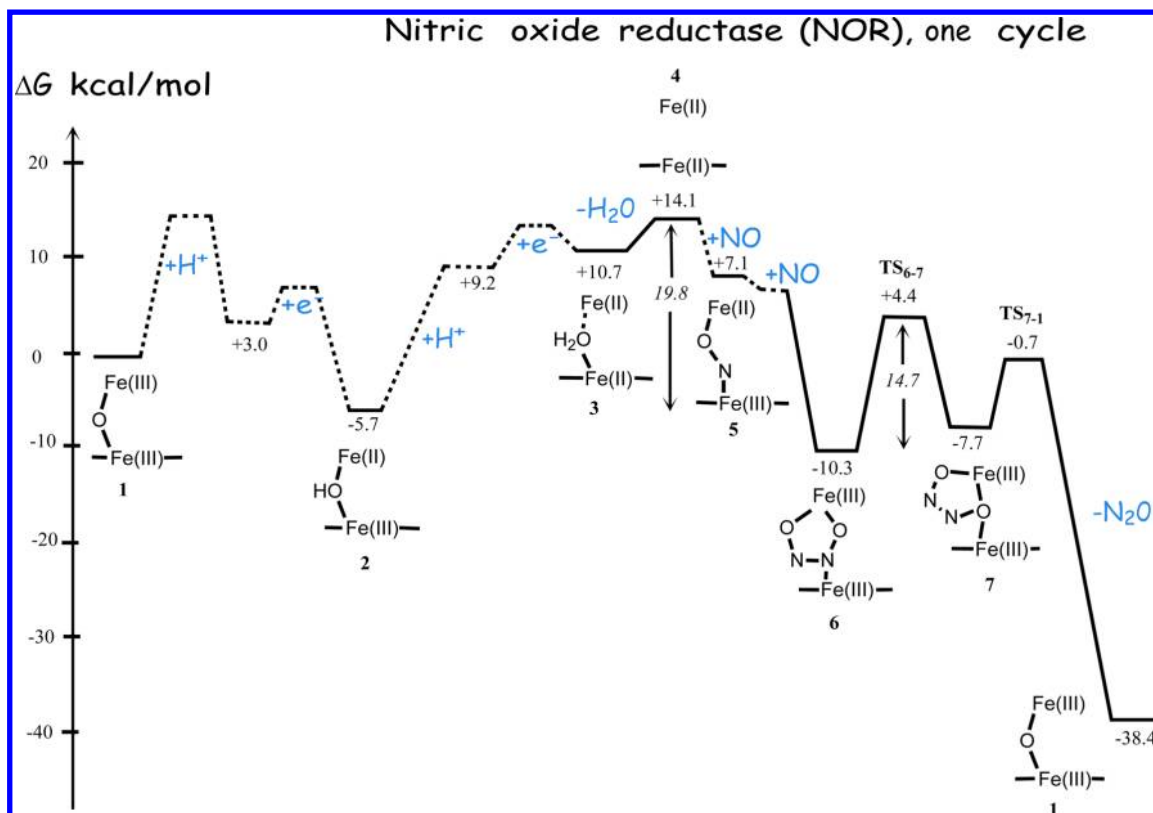
Figure 15. Calculated energy profile for the catalytic reaction in NOR starting from the oxidized binuclear center. The barriers for proton and electron uptake (dotted curve) are estimated using a combination of computational and experimental results.[108]
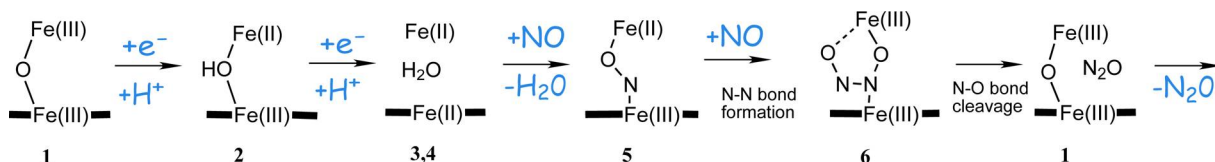

Figure 16. Suggested mechanisms for the catalytic reaction in NOR starting from the oxidized binuclear center.[108]

on a much larger model with about 390 atoms gave a very similar value of 15.4 kcal/mol for the same barrier.[101]

4.2.2. Nitric Oxide Reductase. Nitric oxide reductase (NOR) catalyzes the two-electron reduction of nitric oxide to nitrous oxide and water as one of the steps in the denitrification pathway. As mentioned above, NOR has an active site very similar to that of C*c*O, with the Cu$_B$ ion replaced by a non-heme Fe$_B$. The cross-linked tyrosine is missing, and Fe$_B$ has a glutamate ligand, apart from the three histidines. Also for the NOR enzymes there are subfamilies, and the most well-characterized one is the cytochrome *c* oxidizing NOR, cNOR, which like C*c*O has cytochrome *c* as an electron donor, and which is the only type of NOR discussed here. An interesting difference between C*c*O and cNOR is that it has been found that the chemical reaction in cNOR is nonelectrogenic; i.e., the electrons and protons are transferred to the BNC from the same side of the membrane, the P-side, and there is no proton pumping in cNOR.[106] This result is even more surprising since, counted per electron, the reduction of nitric oxide to nitrous oxide and water by electrons from cytochrome *c* is more exergonic than the corresponding reduction of molecular oxygen to water in C*c*O. Much less is known about the NOR reaction as compared to the C*c*O reaction, and since the reaction of two NO molecules to form N$_2$O and water is a bit more complicated with regard to bond

formation and bond cleavage, there are more possibilities available. The suggested mechanisms have been classified according to the type of coordination of the two NO molecules to the Fe ions in the BNC, and they are therefore labeled cis:b$_3$, cis:Fe$_B$, and trans mechanisms, respectively.[107,108] It is furthermore not known from experiment at what stage of the reaction the electrons or protons enter.

Using a model of the BNC based on the first, recently determined X-ray structure of cNOR,[107] a DFT study of the catalytic NO reduction has been performed. A procedure similar to that described above for C*c*O was used to determine the overall reaction energy for one catalytic cycle, and an energy profile could be calculated which agrees on the most important points with experimental information; see Figure 15.[108] The mechanism suggested on the basis of the calculations is summarized in the scheme in Figure 16, and it is a cis:b$_3$ type of mechanism. The calculations also showed that the suggested trans type of mechanism, where one NO molecule coordinates in a trans manner to each of the metal ions in the BNC, is energetically quite unfavorable. In the mechanism suggested, the two NO molecules coordinate to the reduced BNC with two Fe(II) ions (labeled **4** in the scheme), and nitrous oxide is formed and released (**4** to **1**) before the re-reduction of the active site occurs (**1** to **4**). An interesting result from the calculations is that

the energy profile obtained explains the nonelectrogenicity of the NO reduction reaction.[62] As discussed above, in the reduction of molecular oxygen in CcO, all reaction steps where the enzyme is re-reduced by the electrons from cytochrome *c* are exergonic, and when the gradient starts to build up, they become less exergonic due to both the electrogenicity of the chemistry and the proton pumping. In contrast, as can be seen from the energy profile in Figure 15, the re-reduction of the enzyme in cNOR is endergonic and is actually involved in the rate limitation of the entire catalytic reaction. The endergonicity of the two-electron reduction is 14.1 kcal/mol, from **1** to **4** in the energy profile, and the rate-limiting barrier is as high as 19.8 kcal/mol, from **2** to **4**, which means that if the reaction were electrogenic, the rate-limiting step would be even higher, and the reaction would become too slow when there is a gradient present.[62] Therefore, the reaction in cNOR has to be nonelectrogenic, in particular since the enzyme is located in a membrane where a gradient is actually present from other enzymes.

4.3. Other Heme-Containing Enzymes

In this section a few heme-containing enzymes that have been studied computationally using density functional theory will be briefly discussed. Included enzymes are myoglobin, nitric oxide synthase, cytochrome cd_1 nitrite reductase, and cytochrome *c* nitrite reductase.

The binding of molecular oxygen to a ferrous heme group is important in many enzymes, e.g., hemoglobin, myoglobin, cytochrome *c* oxidase, and cytochrome P450. Other small molecules, such as NO and CO, can bind to the same Fe(II) position, either as a reaction step in itself in some enzymes, such as in nitric oxide reductase, or as a competitor inhibiting the binding of molecular oxygen. Estimating the binding energies of these small molecules to the ferrous heme complex in different surroundings is therefore an important ingredient in the elucidation of many enzymatic reaction mechanisms. Comparisons to experimentally determined dissociation barriers show that the calculated binding energies using the B3LYP functional for these small molecules are significantly too small, at the same time as, e.g., CASPT2 calculations give good agreement with experiment.[109−111] An important finding is that the addition of dispersion effects, using the empirical formula by Grimme,[36] to the B3LYP results significantly improves the agreement with experiment.[37] In a recent combined QM and QM/MM study, geometries and EPR parameters were calculated to gain insight into the bonding and electronic structure of NO-bound myoglobin.[112] An interesting methodological aspect of that study is that it was shown that QM-optimized structures using a truncated model involving an unsubstituted heme group, NO, a valine (Val68), the proximal and distal histidines (His93, His64), and a protonated lysine (Lys45; see Figure 17[113]) did not give structures consistent with those derived from QM/MM calculations using the same QM part. However, a larger more balanced QM model, also including the negatively charged groups located close to the positively charged lysine (Asp60 and one of the heme propionate substituents, PropD; see Figure 17), was shown to replicate the QM/MM results.[112]

Not only is NO a toxic radical molecule, but it also plays an important role in biosignaling, and it is produced by the enzyme nitric oxide synthase (NOS), which exists in several isoforms. The active site of this enzyme is similar to that of cytochrome P450, containing a heme with a cysteine residue (Cys194) as the proximal axial ligand; see Figure 18. NOS catalyzes the generation of NO from L-arginine ($RNH_2C-NH_2^+$) (Arg906
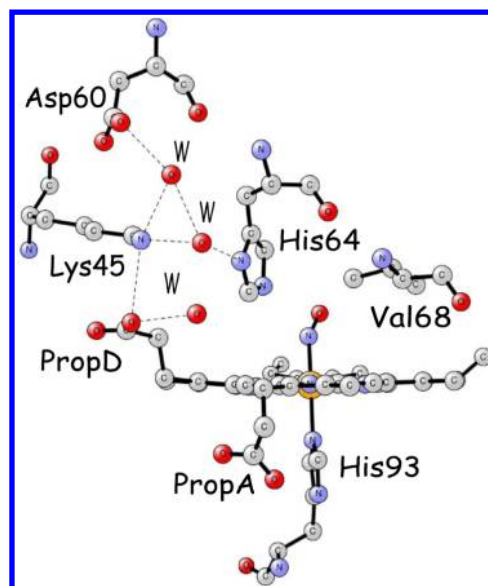

Figure 17. X-ray structure of the active site of myoglobin with bound NO[113] (PDB 2FRJ).
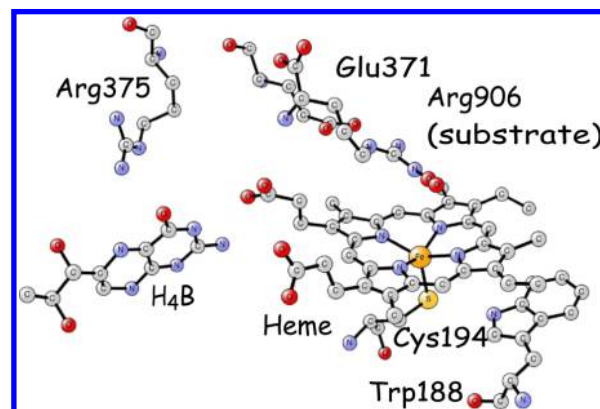

Figure 18. X-ray structure of the active site of nitric oxide synthase[114] (PDB 1NOD).

in Figure 18[114]), molecular oxygen, and external electrons ultimately delivered by NADPH in a process composed of two cycles. In the first cycle L-arginine is hydroxylated to *N*-hydroxy-L-arginine (RNH_2C-NOH, NHA), which requires one oxygen molecule and two external electrons. In the second cycle another oxygen molecule and one external electron are used to transform the NHA to NO and L-citrulline ($RNH_2C=O$). A tetrahydrobiopterin (H₄B; see Figure 18) cofactor binding near the active site has been found to play an essential role in both cycles, and an H₄B radical has been observed at certain stages of the reaction.[115] The detailed reaction mechanisms are not known for either of the two cycles, but most likely the initial steps of both cycles are similar to those of the catalytic cycle of P450, with a ferric heme receiving one electron and thereafter binding the oxygen molecule. The first cycle, which obtains a second external electron and performs a hydroxylation, might occur in the same way as hydroxylation in P450 with Cpd I as the active oxidant; see, e.g., ref 115. In contrast, computational studies on the first cycle of NOS have been interpreted to indicate that there might be significant differences compared to that of P450. On the basis of the results from a QM study, it was suggested that in the first cycle of NOS Cpd I is reduced to Cpd II before the hydroxylation

of the arginine occurs and that the arginine has to become deprotonated in a previous step.[116,117] Quite different conclusions were drawn from a QM/MM study on the first NOS cycle, which was suggested to indicate that a Porf$^+$−Fe(III)−OOH intermediate with a porphyrin radical is involved in the arginine hydroxylation reaction and the suggested mechanism also involves an H$_4$B cofactor radical.[118] For the second NOS cycle, mainly two different mechanisms for the oxidation of the arginine hydroxide, NHA, have been suggested, involving either a Cpd 0 type hydroperoxide as the active species or Cpd I as the active oxidant.[119] On the basis of a QM study on the second NOS cycle, it has been suggested that a heme-bound hydrogen peroxide intermediate is formed initially and that via a ping-pong peroxidase-type mechanism this leads to the formation of a Cpd I species, which in turn via a tetrahedral transition state results in the NO product.[120]

At least two different heme-containing nitrite reductase enzymes have been investigated computationally. Cytochrome cd_1 nitrite reductase catalyzes the one-electron reduction of nitrite (NO$_2^−$) to NO as one of the steps in the denitrification process. This enzyme contains a unique d_1-heme cofactor in the active site, and in a combined ENDOR and QM(DFT) study, it was suggested that the unique d_1-heme structure plays a role in releasing the NO product from the ferrous state of the enzyme.[121] Cytochrome c nitrite reductase, on the other hand, catalyzes the six-electron reduction of nitrite to ammonia, without any observable intermediates such as NO or hydroxylamine. This enzyme is a dimer, where each monomer holds five heme c groups, and one of the heme c groups has a lysine as an axial ligand and constitutes the active site where the nitrite binds; see Figure 19.[122] In a QM study the initial steps of nitrite
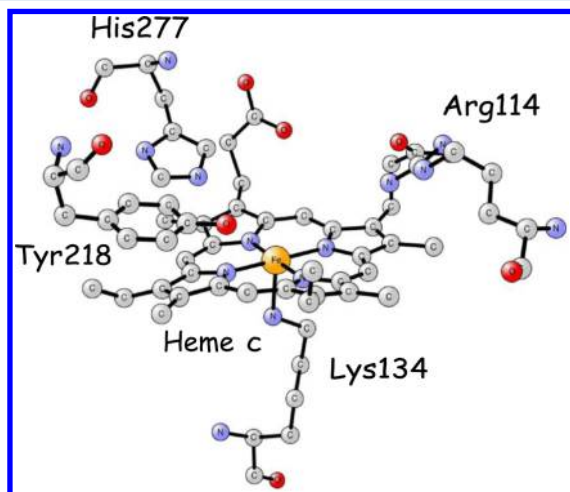

Figure 19. X-ray structure of the catalytically active site in cytochrome c nitrite reductase[122] (PDB 1FS7).

reduction were investigated using a model including the second-sphere amino acids shown in Figure 19.[123] It was concluded that the transfer of two protons to the substrate, leading to release of one water molecule, gives the most reasonable barrier if the protons are delivered via the histidine (His277) near the active site. In a second QM study, starting from the product heme−NO complex of the initial reaction, the recharging of the active site with protons and electrons, preparing for the final catalytic steps, was studied using a similar model.[124] It was concluded from kinetic simulations based on the QM-calculated energy profiles that the most likely recharging process occurs through two

consecutive proton-coupled electron transfer steps and also that the active site tyrosine (Tyr218) does not seem to play a radical transfer role, as has been suggested in the literature.[124]

5. NON-HEME IRON ENZYMES

5.1. Mononuclear Non-Heme Iron Enzymes

Iron-dependent enzymes hosting a single iron ion in their active sites and binding the metal without involvement of the porphyrin prosthetic group constitute a large superfamily of biocatalysts participating in a vast range of biological processes. The scope of chemical transformations catalyzed by this group is likewise very broad, yet in most cases these are oxidative reactions involving molecular oxygen. In the past decade our understanding of catalytic mechanisms of these enzymes has advanced considerably thanks to intense experimental and computational research. Below we provide a review of computational studies devoted to O$_2$ activation by mononuclear non-heme iron enzymes. Instead of trying to be exhaustive, the review picks representative cases and aims at showing how the computations shed new light on the mechanisms of these reactions.

5.1.1. Tetrahydrobiopterin-Dependent Hydroxylases. The family of tetrahydrobiopterin-dependent hydroxylases (PDHs) encompasses aromatic amino acid hydroxylases such as phenylalanine hydroxylase (PAH), tyrosine hydroxylase (TyrH), and tryptophan hydroxylase (TrpH), all of which catalyze hydroxylation of a respective amino acid and (6R)-L-$erythro$-5,6,7,8-tetrahydrobiopterin (BH$_4$) cofactor. A representative reaction for this enzyme family is hydroxylation of phenylalanine to tyrosine catalyzed by PAH (Figure 20).
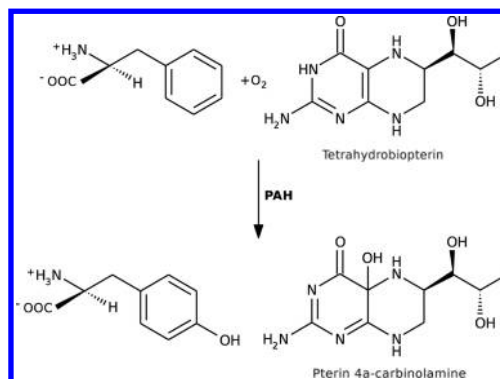

Figure 20. Catalytic reaction of phenylalanine hydroxylase-coupled hydroxylation of phenylalanine and tetrahydrobiopterin.

This is a key step in catabolism of phenylalanine, and deficiency of PAH leads to a hereditary metabolic disease—phenylketonuria. The other aromatic amino acid hydroxylases participate in similarly vital metabolic pathways. More specifically, TyrH catalyzes conversion of tyrosine to L-3,4-dihydroxyphenylalanine (L-DOPA), which is a substrate for biosynthesis of dopamine, adrenaline, and noradrenaline, i.e., neurotransmitters and hormones. TrpH introduces a OH group into the indole ring of tryptophan, and this is a rate-limiting step in biosynthesis of another neurotransmitter—serotonin.

The X-ray crystal structure of PAH (Figure 21) clearly showed that BH$_4$ binds in the second coordination shell of the active site iron; however, the distance between the Fe ion and BH$_4$ does not preclude an (indirect) bonding between the two entities. Concerning the first coordination shell, the arrangement of ligands is typical for the two-His−one-carboxylate super-
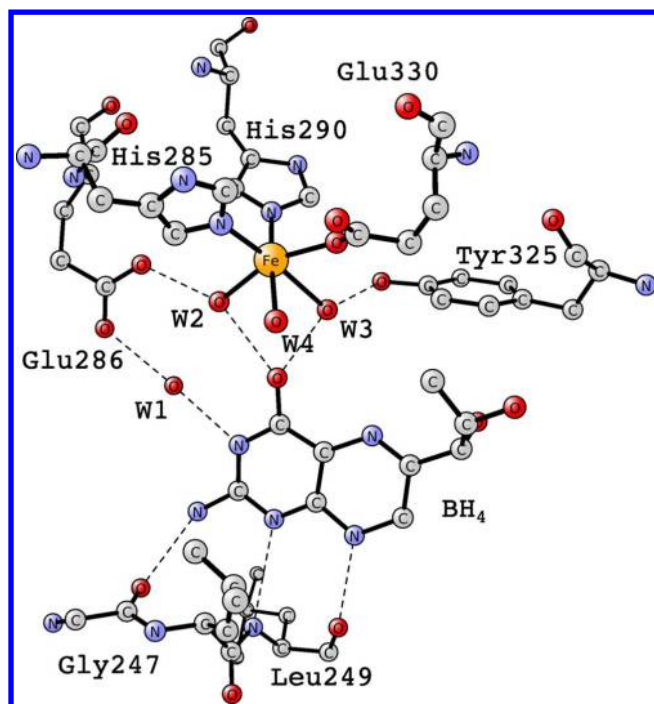
Figure 21. X-ray structure of the active site of PAH (PDB 1DMW).

family.[125,126] Accordingly, three sites on one face of the octahedron are taken by two histidines and one glutamate, whereas the remaining three apexes are occupied by water molecules.

Circular dichroism (CD) and magnetic circular dichroism (MCD) spectroscopic results indicated that when both substrate and BH_4 are bound, the metal has five ligands, and one of the water molecules is supposed to have left the coordination shell.[127,128] This vacancy was postulated to be the place of dioxygen binding.

The complete catalytic reaction of PAH has been studied with DFT-cluster modeling, with the most important conclusion that the reaction proceeds with generation of an iron–oxo reactive species that is responsible for hydroxylation of the aromatic amino acid.[129,130] Here we summarize the results pertaining to O_2 activation by PDHs, whereas a description of aromatic ring hydroxylation and other reactions elicited by iron–oxo species can be found in the previous reviews.[131,132]

The DFT study on the dioxygen activation by PDHs was conducted with the B3LYP functional applied to an active site model constructed on the basis of the X-ray crystal structure depicted in Figure 21.[129] The water molecule labeled "W4" was removed, consistent with the spectroscopy results mentioned above and the fact that this coordination site is geometrically most suitable for generation of a peroxo bridge between the

metal and BH_4. The model included the remaining first-shell ligands and, from the second shell, Glu286, W1, and BH_4.

The mechanism of dioxygen activation by PDHs that was supported by the DFT-cluster modeling study can be viewed as a prototypical mechanism of generation of iron–oxo species at a mononuclear Fe(II) site with a two-electron donor (co)-substrate. The key features of this mechanism (see Figure 22) are the following: (a) the reactive state is a spin quintet, (b) an intermediate with a peroxo bridge between high-spin Fe(II) and BH_4 forms, and (c) heterolysis of the O–O bond proceeds with protonation of the leaving (distal) oxygen. As will be seen below, analogous reaction paths are often found for other mononuclear non-heme enzymes producing ferryl species.

Concentrating a little more on the details of the reaction (Figure 22), it can be noticed that dioxygen binds to the metal at the vacant coordination site and the ground state of the resulting ternary PAH–Fe–BH_4–O_2 complex is a spin septet. The free energy computed for O_2 uptake is +10.3 kcal/mol, which is a quite typical value obtained with active site models and the B3LYP functional. It mainly accounts for entropy loss when dioxygen gets trapped in the enzyme active site. Such high endergonicity at the beginning of the reaction would increase the barrier of the following step to a level not at all compatible with enzymatic rates. However, as will be discussed in more detail below (for isopenicillin N synthase), the active site models tend to underestimate the O_2-binding energy, and the contributions missing in active site models basically cancel the entropy loss. Hence, the energy of the septet PAH–Fe–BH_4–O_2 complex was taken as a zero level, which is compliant with an accepted approach to assume the unfavorable entropy contribution is canceled by "protein" effects.

As mentioned above, the DFT results showed that the progress of the reaction requires the O_2-bound complex to be excited to a low-lying quintet state. The spin density distribution obtained for the reactive quintet species indicates its structure is best represented by Fe(III)–$O_2^{•-}$ with high-spin Fe(III) antiferromagnetically coupled to the superoxide anion. On the free energy scale the quintet lies 5.1 kcal/mol above the ground state, yet this endergonic spin crossover pays off as it enables a low-barrier attack of the superoxide on BH_4. This step, involving a barrier of 16.6 kcal/mol, leads to an intermediate with a peroxo group bridging between high-spin Fe(II) and BH_4, which means the cofactor was two-electron-oxidized. Subsequently, the catalytic reaction advances via a formally heterolytic cleavage of the O–O bond that proceeds in two one-electron steps: the more difficult first step for an electron transfer from high-spin Fe(II) to the O–O σ^* orbital (computed barrier of 4.8 kcal/mol) and the very facile and barrierless second step when the O–O half-bond is cleaved as the distal oxygen accepts a proton from one of the water ligands. The O–O bond cleavage is an exergonic reaction, and it yields a hydroxylated form of the cofactor and the reactive Fe(IV)=O species. The latter is engaged in
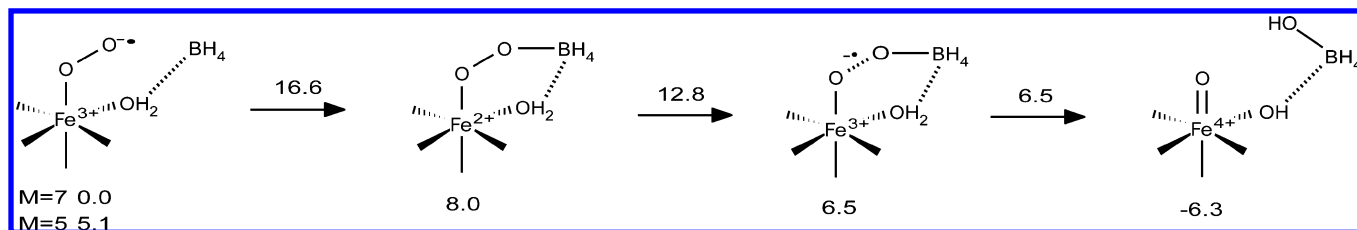

Figure 22. Suggested reaction mechanism for O_2 activation by PDHs. Free energy values are given in kilocalories per mole.[129]

3621

dx.doi.org/10.1021/cr400388t | Chem. Rev. 2014, 114, 3601–3658

hydroxylation of the aromatic ring of the substrate, which takes place in the following steps of the catalytic cycle.

It should also be noted here that, besides lending credence to the above-summarized mechanism involving the key iron−oxo intermediate, the DFT results showed that an alternative mechanism, whereby dioxygen is activated via binding to BH$_4$ without participation of iron, is very unlikely.

5.1.2. α-Ketoacid-Dependent Oxygenases. α-Ketoacid-dependent oxygenases (αKAOs) form a large group of enzymes catalyzing a broad range of oxidative transformations that include aliphatic and aromatic hydroxylation, halogenation, desaturation, epimerization, ring closing, and ring expansion.[133,134] These oxidation reactions are often parts of vital biological processes such as regulation of gene expression,[135−137] DNA or RNA repair,[138] synthesis of antibiotics,[139] or cellular oxygen sensing.[140] The biological significance of αKAOs and their widespread existence in nature has stimulated intensive research on αKAOs, including studies on their reaction mechanisms.

Already in 1982 it was suggested that the catalytic cycle of αKAOs consists of a dioxygen activation phase, when O$_2$ reacts with α-ketoacid cosubstrate to generate the reactive Fe(IV)=O species, and a subsequent two-electron oxidation of a primary organic substrate elicited by Fe(IV)=O, similar to that of PDHs discussed in the preceding subsection.[141] The generic catalytic cycle of αKAOs consistent with this proposal is presented in Figure 23. Structural and spectroscopic studies revealed that α-
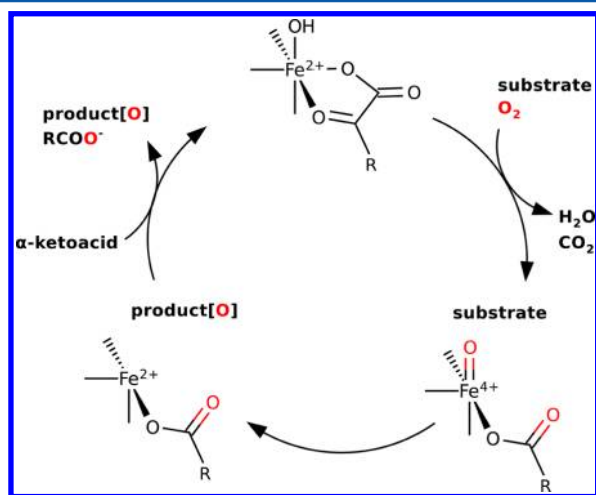

Figure 23. Generic catalytic cycle of α-ketoacid-dependent oxygenase.

ketoacid coordinates the ferrous ion via its keto and carboxylic groups, whereas the substrate binds in the immediate vicinity of the iron cofactor.[142−145] In analogy to PDHs, substrate binding triggers release of a water ligand and hence opens a coordination site suitable for binding of dioxygen.[146] Subsequent oxidative decarboxylation of the ketoacid yields the Fe(IV)=O reactive intermediate, which was trapped and characterized spectroscopically,[147−152] and which is involved in two-electron oxidation of the substrate.

The X-ray crystal structure of an active site of taurine dioxygenase (TauD), which is often regarded as a representative αKAO, is presented in Figure 24. Dioxygen is proposed to bind to the vacant coordination site (trans to His255), which is a site most exposed toward the substrate. Experimentally a ternary enzyme−α-ketoacid−O$_2$ complex has not been trapped yet, but NO-bound analogues were characterized with X-ray crystallography and spectroscopic methods.[153−155]
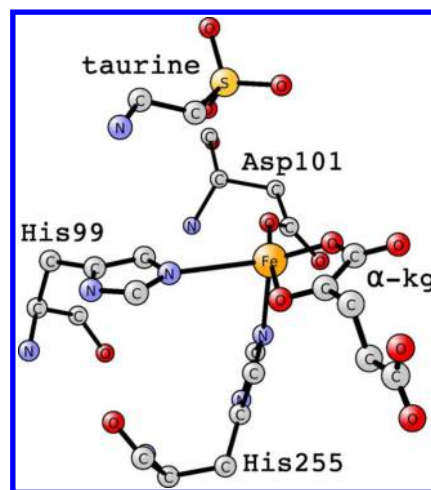

Figure 24. X-ray structure of the active site in a representative αKAO (TauD, PDB 1OS7).

Since none of the reaction intermediates formed after binding of O$_2$ and before generation of the ferryl species have been trapped so far, our insights into the mechanism of this part of the catalytic cycle rest on computational results, most of which were obtained with DFT methods. Several computational studies tackled the issue of O$_2$ activation by αKAOs; however, different results, leading sometimes to divergent conclusions, were obtained depending on the model and the density functional/basis set used.[156−159,155,160] The key intermediates found in these studies are shown in Figure 25. Species **A** is an end-on Fe−O$_2$
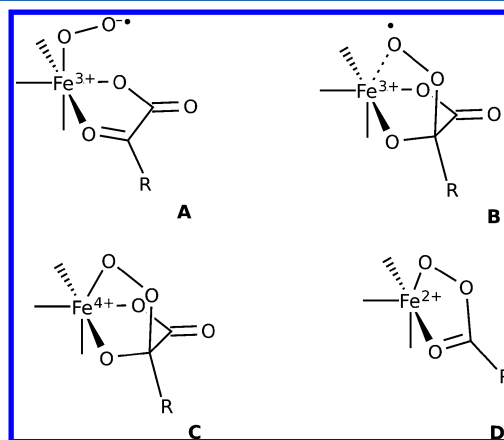

Figure 25. αKAO-oxygenated intermediates proposed to form prior to the ferryl species.

complex where an electron transfer between iron and dioxygen is fairly advanced, and hence, the structure is usually drawn with Fe(III) and a superoxide anion (cf. analogous species for PDHs, vide supra). Note that in species **A** the α-ketoacid is not directly involved in O$_2$ binding, which is opposite the situation in species **B**, **C**, and **D**. Species **B** differs from **A** in the mode in which the superoxide anion is bound; i.e., in **B**, it is attached to the keto carbon of the α-ketoacid and it only weakly interacts with the ferric ion. In species **C**, oxygen has been two-electron-reduced with both electrons provided by the iron and the peroxo group forms a bridge between Fe(IV) and the α-carbon of the cosubstrate. Species **D** results from decarboxylation of the α-ketoacid, and it features Fe(II) chelated by peroxoacid.

Table 2. Mechanisms for O$_2$ Activation by αKAOs Suggested on the Basis of DFT Computational Studies

mechanism no.	sequence of steps
1	Fe(II)−α-ketoacid + O$_2$ → ^{5}A → ^{5}D + CO$_2$ → ^{5}[Fe(IV)=O]
2	Fe(II)−α-ketoacid + O$_2$ → ^{7}A → ^{7}[Fe(III)−O$^{•−}$] + CO$_2$ → ^{5}[Fe(IV)=O]
3	Fe(II)−α-ketoacid + O$_2$ → ^{5}A → ^{5}B → ^{5}D + CO$_2$ → ^{5}[Fe(IV)=O]
4	Fe(II)−α-ketoacid + O$_2$ → ^{3}C → ^{5}D + CO$_2$ → ^{5}[Fe(IV)=O]

Table 3. Computed Barrier Heights (kcal/mol) and Models Used in DFT Studies on O$_2$ Activation by αKAOs

step	mechanism	barrier	model	functional	ref
^{5}A → ^{5}D	1	10.4	a	B3LYP	156
		3.2	b	B3LYP	157
		13.9	c	B3LYP	160
^{7}A → ^{7}[Fe(III)−O$^{•−}$]	2	13.9	b	B3LYP	156
		13.8	c	B3LYP	160
^{5}A → ^{5}B	3	12.9	c	B3LYP	158
		10.4	c	B3LYP	159
^{5}B → ^{5}D	3	3.1	c	B3LYP	158
		3.6	c	B3LYP	159
^{3}C → ^{5}D	4	11.2	d	BP86 + 10% HF	155
^{5}D → ^{5}[Fe(IV)=O]	1, 3, 4	5.7	a	B3LYP	156
		5.0	b	B3LYP	157
		ca. 5	c	B3LYP	160
		11.2	c	B3LYP	158
		17.6	c	B3LYP	159
		<1.0	d	BP86 + 10% HF	155
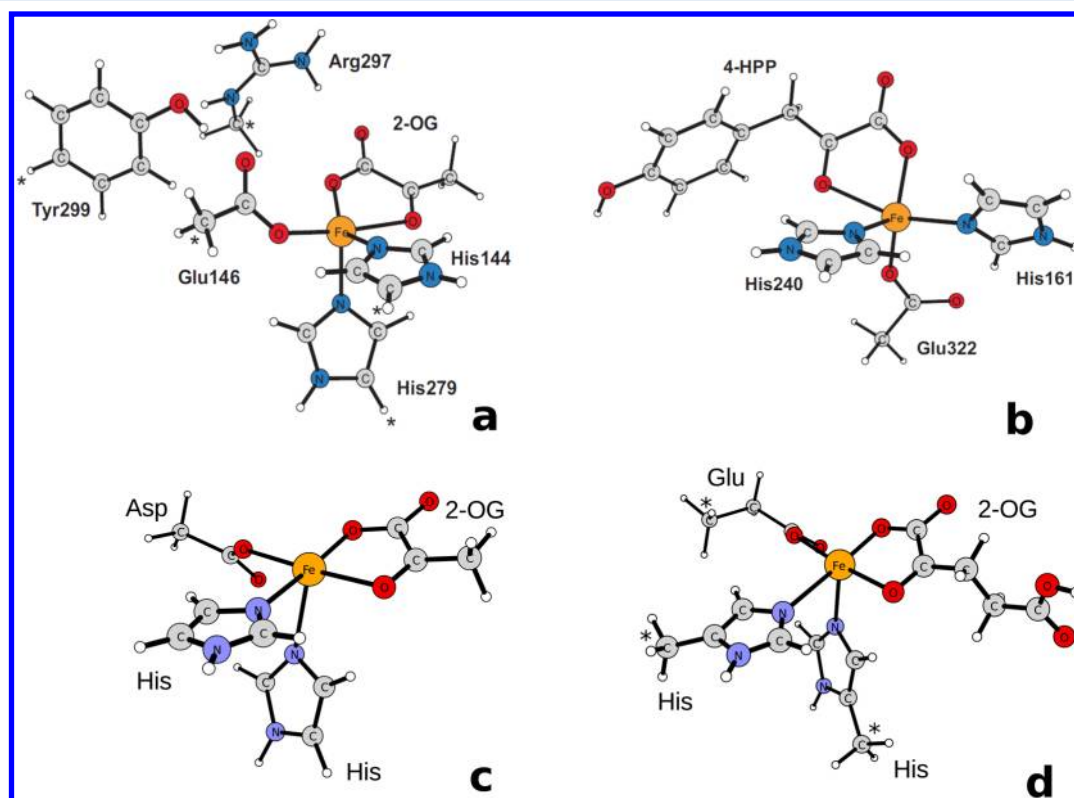
Figure 26. Active site models used in DFT studies on dioxygen activation by αKAOs. Atoms marked with an asterisk were kept fixed.

Four rather different mechanisms for oxidative decarboxylation of α-ketoacid were formulated on the basis of the DFT results, and they involve various combinations of species A−D, as summarized in Table 2. For mechanism 1 in a rate-limiting step, the quintet Fe(III)−superoxo species (^{5}A) transforms into the Fe(II)−peracid intermediate (^{5}D). Subsequent heterolysis of the

O−O bond yields the quintet ferryl species.[156,157,160] In mechanism 2 there is a single major reaction step leading from the septet Fe(III)−superoxo species (^{7}A) directly to the ^{7}[Fe-(III)−O$^{•−}$] intermediate; i.e., attack of the distal oxygen atom on the keto carbon of α-ketoacid and cleavage of the C−C and O−O bonds are coupled. Subsequent spin crossover from the ^{7}[Fe-

(III)−O$^{\bullet-}$] species to the ^{5}[Fe(IV)=O] species, which completes mechanisms 2, is supposed to be very fast.[157,160] Mechanism 3, like mechanism 1, proceeds on the quintet potential energy surface (PES), yet the attack on the keto carbon and the C−C cleavage are decoupled and take place in two consecutive steps; i.e., the attack of the distal oxygen yields the superoxo-bridged structure (^{5}**B**), which in the following step decarboxylates to the peracid species ^{5}**D**.[158,159] Finally, in mechanism 4 binding of O$_2$ to the Fe(II)−α-ketoacid takes place on the triplet PES and leads directly to the alkyl peroxo-bridged structure (^{3}**C**) featuring intermediate-spin Fe(IV). Spin crossover from the triplet to the quintet spin state elicits decarboxylation that yields ^{5}**D**.[155] The latter is cleaved as in mechanisms 1 and 3.

Barrier heights of the salient reaction steps are gathered in Table 3, where the applied functionals, models, and references to the original works are also listed. The composition of active site models used in these DFT studies is presented in Figure 26. Analysis of the data gathered in Table 3 leads to several observations of mechanistic relevance. First, for all mechanisms the rate-limiting barriers for decarboxylation (leading to ^{5}**D** or directly to the ferryl species) are below 14 kcal/mol and usually fall into a narrow range between 10 and 14 kcal/mol. Second, in mechanism 3 the transition state connected with the ^{5}**A** → ^{5}**B** step has an energy very similar to that of the TS for the ^{5}**A** → ^{5}**D** step in mechanism 1. Taking this together with the fact that the second step in mechanism 3, i.e., ^{5}**B** → ^{5}**D**, has a very small barrier (below 4 kcal/mol), it seems likely that minor differences in models and/or basis sets are the reason for the fact that in some studies species ^{5}**B** was identified while in other the nucleophilic attack of superoxide on the keto carbon was coupled to C−C bond cleavage. Thus, if this hypothesis holds, then mechanisms 1 and 3 are just two flavors of the same mechanism where dioxygen binds to Fe(II), is activated by an electron transfer from iron, and then, in the rate-limiting step proceeding on the quintet PES, attacks the keto carbon of the cosubstrate. Mechanism 2 is a septet variant of the same general reaction scheme where, due to instability of the septet analogue of species ^{5}**D**, the reaction proceeds directly to the ^{7}[Fe(III)−O$^{\bullet-}$] species. Furthermore, the cleavage of the O−O bond in the Fe(II)− peracid intermediate (^{5}**D**) is an easy step with a barrier usually around 5 kcal/mol. The barrier of 11.2 kcal/mol, obtained for this step in one study, can have its roots in the relatively small basis set used in calculations of the final energies; the reason for the largest barrier (17.6 kcal/mol), obtained in yet another study, is unclear.

In summary, the results of five studies conducted with the B3LYP functional provide a quite consistent picture of the mechanism and seem to converge to a "consensus" scenario for quintet and septet PESs. Of relevance here is the fact that the reliability of the B3LYP functional in describing the energetics of the ^{7}**A** → ^{7}[Fe(III)−O$^{\bullet-}$] step has been confirmed by CCSD(T) calculations.[160]

A considerably different mechanism (4) was proposed on the basis of a DFT study conducted with a functional calibrated to reproduce the geometry and electronic spectra of {FeNO}^{7} complexes, i.e., BP86 + 10% HF.[155] With this functional O$_2$ is predicted to bind to the Fe(II)−α-ketoacid complex on the triplet PES and directly form the bicyclic intermediate ^{3}**C** featuring a peroxo bridge and intermediate-spin Fe(IV). The subsequent step is proposed to be a spin crossover leading to ^{5}**D** and proceeding through a minimum energy crossing point located approximately 11.2 kcal/mol above. Thus, in mechanism

4 the oxidation state of iron changes from Fe(II) to Fe(IV) when O$_2$ binds, then back to Fe(II) during decarboxylation, and finally to Fe(IV) during the O−O bond cleavage; i.e., a stable Fe(III) species does not occur along this path. Mechanism 4 is certainly an interesting alternative to mechanisms 1−3, though it remains to be shown that the BP86 + 10% HF functional is reliable when it comes to the relative energies of species of interest. Moreover, the barrier for ordinary decarboxylation, i.e., not coupled to spin crossover, proceeding on the quintet or septet PES, was not reported for this functional, which precludes direct comparison of the two different mechanistic scenarios.

5.1.3. Isopenicillin N Synthase. Isopenicillin N synthase (IPNS) catalyzes a key step in the biosynthesis of penicillin and cephalosporin β-lactam antibiotics, i.e., the four-electron oxidative cyclization of the tripeptide δ-(L-α-aminoadipoyl)-L-cysteinyl-D-valine (ACV) to isopenicillin N (IPN) (see Figure 27). IPNS belongs to the two-His−one-carboxylate superfamily
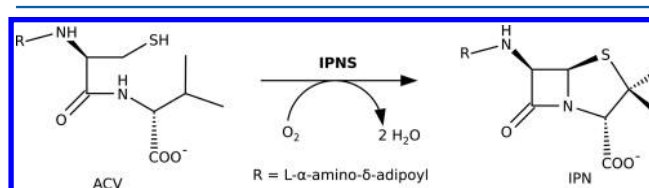

Figure 27. Enzymatic reaction catalyzed by IPNS.

of enzymes (Figure 29), and its mechanism of O$_2$ activation bears remarkable similarities to those of other members of this group. The consensus mechanism of the IPNS catalytic cycle is depicted in Figure 28. Computationally, the catalytic reaction of IPNS has been investigated at several levels of approximation: DFT-(B3LYP) applied to active site models,[161,162] a static QM/MM (ONIOM) hybrid method,[163,164] and a QM:[MM-FEP] approach, in which the effect of the MM part is described by free-energy perturbation (FEP).[165] In-depth and scrupulous comparison of the energy effects on the reaction energy profiles computed with these methods provided many valuable insights into "protein effects" as well as revealed strong and weak sides of the computational approaches used to study metalloenzyme catalysis. This detailed analysis has recently been published, and the interested reader is referred to that work.[132] Here, we will only briefly summarize the major findings pertaining to the O$_2$ activation part of the IPNS catalytic cycle.

In the substrate-bound form the ferrous cofactor of IPNS is five-coordinate with one face of the coordination octahedron occupied by the two-His−one-carboxylate motif and two other sites taken by the water ligand and the thiolate group of ACV (Figure 29). In analogy to NO, O$_2$ is suggested to bind trans to Asp216. For the IPNS−Fe−ACV−O$_2$ complex several close in energy species were found, the side-on septet (Fe(III)−O$_2$$^{\bullet-}$) being the ground state. With the active site model the O$_2$-binding step was computed to be endergonic by 10.3 kcal/mol, which taken at face value would boost a barrier for subsequent reaction steps to a prohibitively high level.[162] A solution of this problematic issue was found thanks to comparison of the results of the active site model and QM/MM(ONIOM) studies. In particular, it was revealed that the active site model allows for unrealistically large geometrical changes of the first-shell ligands, which artificially stabilizes the unbound state by ca. 6 kcal/mol. Endergonicity of O$_2$ binding is reduced further by another 4−5 kcal/mol attributed to nonbonding interactions (mostly van der Waals) between the QM and MM parts of the system.[163] Thus, at
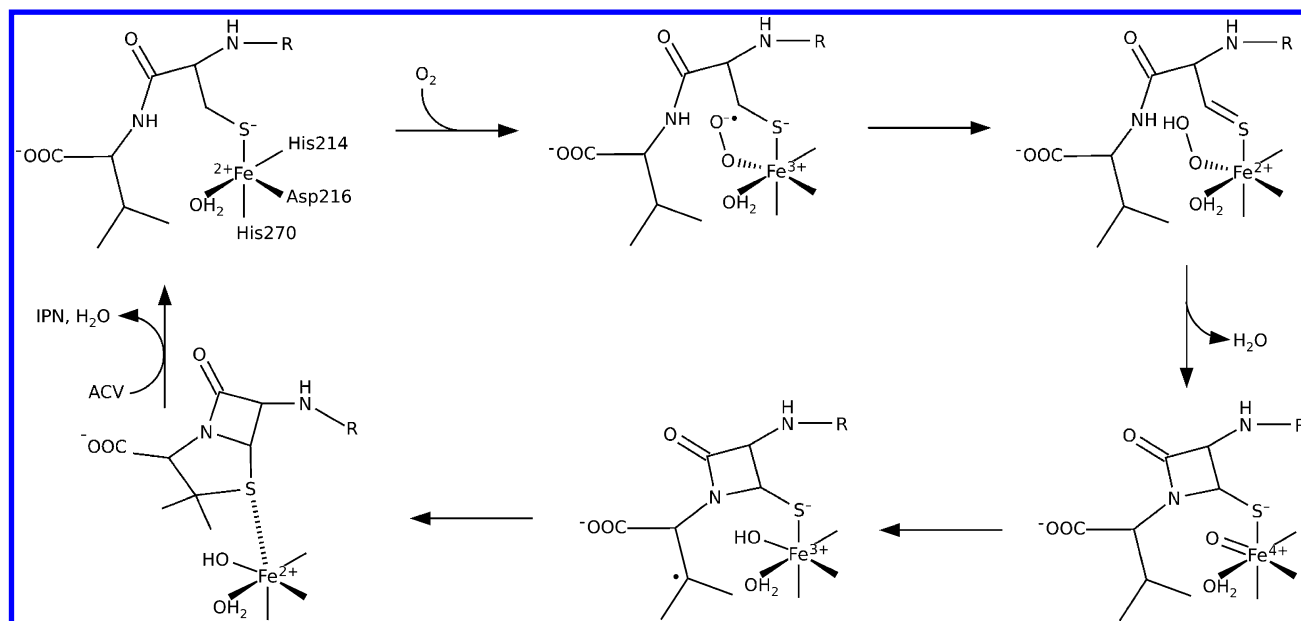
Figure 28. Proposed reaction scheme for the catalytic cycle of IPNS.
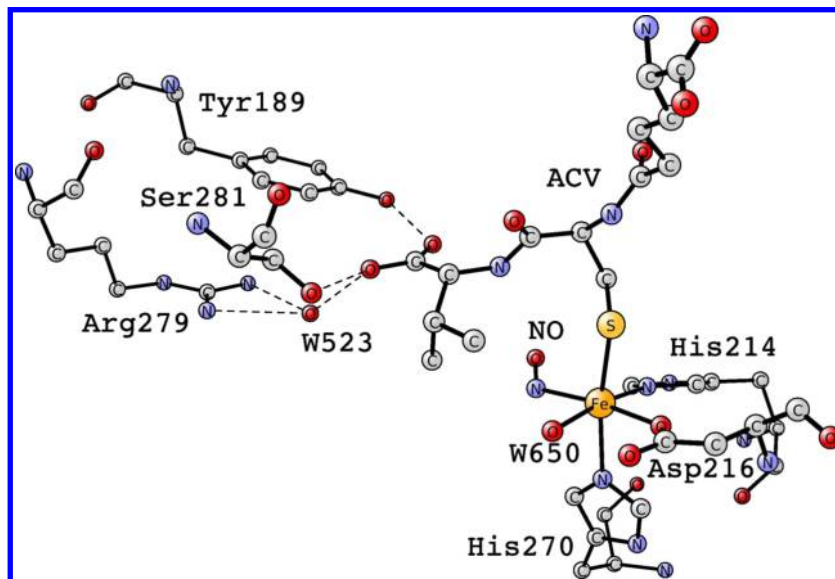

Figure 29. X-ray structure of the active site of IPNS with ACV and NO bound (PDB 1BLZ).

the QM/MM(ONIOM) level O_2 binding to IPNS is computed to be only slightly endergonic (2−3 kcal/mol).

The end-on Fe(III)−$O_2^{\bullet-}$ species is an oxidant strong enough to cleave the C−H bond at the β-carbon adjacent to the deprotonated thiolate group of ACV. Septet, quintet, and triplet spin states were tested, and the lowest barrier for Cβ−H cleavage was located on the quintet PES.[162]

A noticeable difference between the results obtained with the active site and QM/MM models concerns the stability of the Fe(II)−OOH species (**5 INT** in Figure 30). With an active site model it is located more than 10 kcal/mol below the reactant level, whereas in QM/MM(ONIOM) and QM:[MM-FEP] it is clearly above zero. The difference has been attributed to unfavorable electrostatic interaction between the Fe(II)−OOH species and the protein matrix.

Yet another difference concerns the mechanism itself (Figure 31). The so-called ligand donor mechanism has been put forth in

the study using an active site model.[162] In this mechanistic proposal, the *aqua* ligand (green in Figure 31) delivers a proton, neutralizing the leaving OH group, and the hence formed water molecule acts as a mediator for subsequent proton transfer from the substrate's NH group to the OH ligand. In the ligand donor mechanism the energy barrier for the O−O cleavage computed with an active site model is around 10 kcal/mol; in the static QM/MM(ONIOM) calculations it is of the same value, but drops below 10 kcal/mol after inclusion of dynamic effects via QM:[MM-FEP]. The subsequent reaction step, i.e., water-mediated proton transfer, turned out to be difficult (Figure 32). Its barrier computed with the active site model is 19.8 kcal/mol,[162] whereas a lower bound limit obtained with QM/MM supported by some molecular dynamics (MD) sampling is 20.7 kcal/mol.[164] Irrespective of these high values of the barrier, the ligand donor mechanism was not excluded since, as the authors argued, "the modeled reaction is restricted to residues in the QM
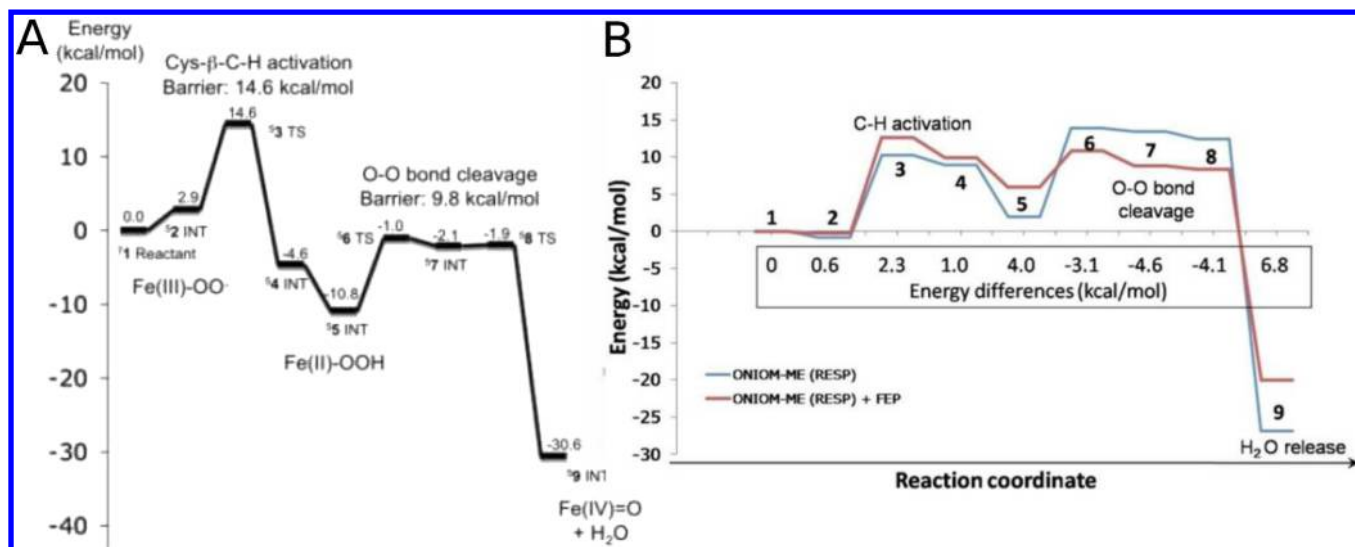
Figure 30. Reaction energy profiles for generation of ferryl species (ligand donor mechanism) in the IPNS catalytic cycle obtained with (A) the active site model and (B) the QM/MM(ONIOM) and QM:[MM-FEP] models. Reprinted from refs 162 (panel A) and 165 (panel B). Copyright 2008 and 2011, respectively, American Chemical Society.
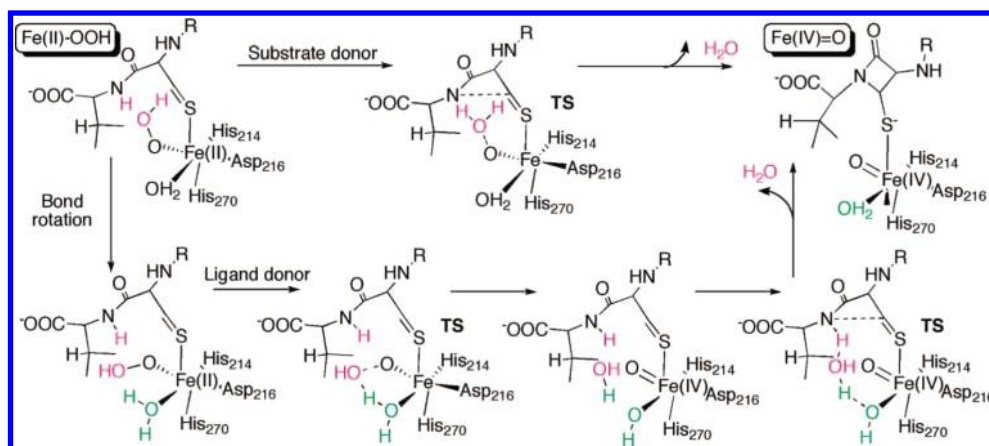

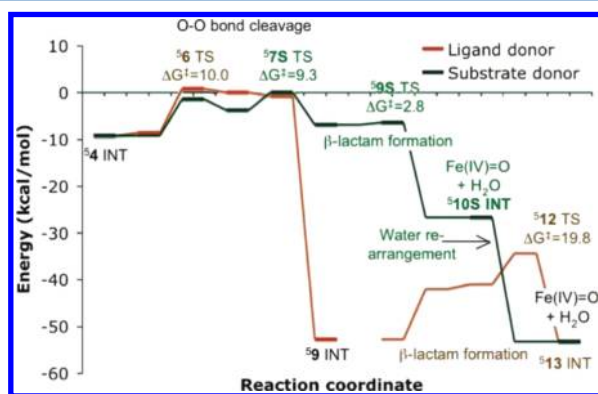**Figure 31.** Two mechanisms for O−OH bond cleavage and β-lactam ring formation. Reprinted from ref 164. Copyright 2009 American Chemical Society.

Figure 32. Energy profiles for the two mechanisms for O−OH bond cleavage and β-lactam ring formation. Reprinted from ref 164. Copyright 2009 American Chemical Society.

system, and alternative pathways may be available in the real protein".[164]

In the second proposal, called the substrate donor mechanism (Figure 31), which is also consistent with the consensus mechanisms of IPNS (Figure 28), the proton is taken from the NH group of ACV.[164] A low-barrier pathway for this mechanism was found in the QM/MM(ONIOM) study when the QM part of the model was extended to include residues stabilizing, via hydrogen-bonding interactions, the carboxyl group of the substrate (Tyr189, Arg279, Ser281, W523; see Figure 29). The barrier for O−O bond cleavage in the substrate donor mechanism is 9.3 kcal/mol, which is close to the barrier in the ligand donor mechanisms. However, in the substrate donor mechanism closing the β-lactam ring involves only a tiny barrier, whereas in the ligand donor there is a barrier of around 20 kcal/mol.

Clearly, the mechanism of O_2 activation by IPNS reveals similarities to that described above for PDHs, with the features in common including the reaction proceeding on the quintet PES, formation of a peroxo intermediate, and cleavage of the O−O bond with protonation of the leaving OH group. The final steps of the IPNS catalytic cycle (Figure 28) involve C−H bond cleavage elicited by iron−oxo species and a subsequent closing of the penam ring.

5.1.4. Apocarotenoid Oxygenase. Carotenoids play multiple protective and regulatory roles in plant and animal

physiology.[166,167] The biologically active forms are often apocarotenoids that are synthesized from the parent compounds by an oxidative cleavage reaction catalyzed by a family of non-heme iron enzymes.[166,168] For example, apocarotenoid oxygenase (ACO) from cyanobacterium *Synechocystis* sp. PCC 6803, which is the only enzyme from this family with a known structure, cleaves its substrate at the C15−C15′ bond (Figure 33).
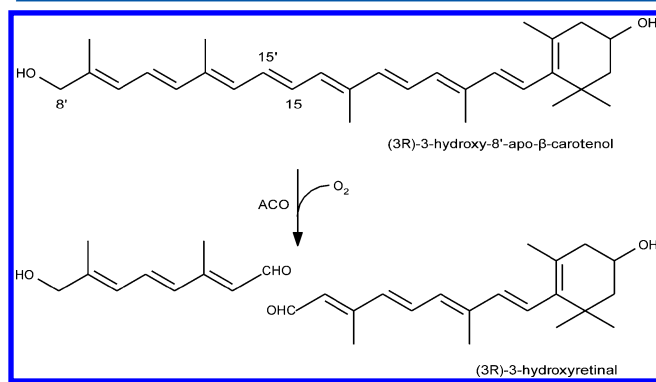

Figure 33. Oxidative cleavage reaction catalyzed by ACO.

The X-ray crystal structure was solved for an ACO−substrate complex, and it revealed an unusual architecture of the active site (Figure 34).[169] In ACO the ferrous ion is bound by four histidine side chains, and in the first coordination shell there are no negatively charged protein ligands. Instead, three glutamates are placed in the second shell, and they form hydrogen bonds with the first-shell histidines. The coordination site exposed toward the substrate is occupied by a water ligand; the site trans to His304 remains empty. A hydrophobic channel passing by the metal cofactor is the place where the substrate binds with its C15−C15′ bond, which is to be cleaved, positioned close to the water ligand.

The mechanism of the oxidative cleavage catalyzed by ACO was studied with the B3LYP functional applied to an active site model, which included the whole methyl-substituted π-conjugated system of the substrate, first-shell histidines, Glu150, and Glu370.[170] The third second-shell glutamate, i.e.,

Glu426, forms a salt bridge with Arg52, and hence, it was not included.

Reaction energy profiles constructed for two different mechanisms involve comparable barriers for their rate-limiting steps, and hence, any definite discrimination between these two alternatives is precluded. In the first scenario, called the "dioxetane mechanism" (Figure 35), the key intermediate is the dioxetane species **4**. The second mechanism, hereafter called the "expoxide mechanism", features the key epoxide intermediate **11**. Both mechanisms begin with dioxygen binding at the coordination site close to the substrate occurring with a shift of the water ligand to the site trans to His304. Notably, O$_2$ accepts an electron from the substrate, which is oxidized to a radical cation. The ground state of species **2** is a spin quintet with high-spin Fe(II) and antiferromagnetic coupling between the organic radical and the superoxide. The computed energy of O$_2$ trapping is +1.4 kcal/mol.

The lowest barrier path to the dioxetane intermediate proceeds through, first, protonation of the distal oxygen by the water ligand coupled to reduction (by Fe(II)) of the superoxide to a hydroperoxo group (**2 → 7**), second, attack of the proximal oxygen on C15′ (**7 → 8**), and, third, transfer of the proton back to the OH ligand coupled to formation of the four-membered ring (**8 → 4**). The subsequent steps of O−O and C−C cleavage are fast and proceed with barriers not exceeding 11 kcal/mol. First, the O−O bond is cleaved with the help of the ferrous ion, which reduces one oxyl radical to O$^-$ stabilized by a bond to Fe(III) (**4 → 9**). Second, the C−C bond is cleaved, yielding the aldehyde products and the active site iron in the ferrous state **6**.

In the epoxide mechanism, it is the distal oxygen atom of species **2** that attacks C15′ (Figure 35; **2 → 10**). In the rate-limiting step (**TS9**; 16.6 kcal/mol), the peroxo bridge intermediate undergoes a heterolytic O−O cleavage, leading to Fe(IV)=O and the substrate epoxide (**11**). The water ligand plays a catalytic role in the subsequent step, when the oxirane ring is opened, as it provides a proton to neutralize the negative charge on O$^-$ (**11 → 12**). Finally, the iron−oxo species attacks C15′, introducing the second oxygen into the substrate, and thereby prepares it for the subsequent C−C cleavage proceeding as in the dioxetane mechanism.
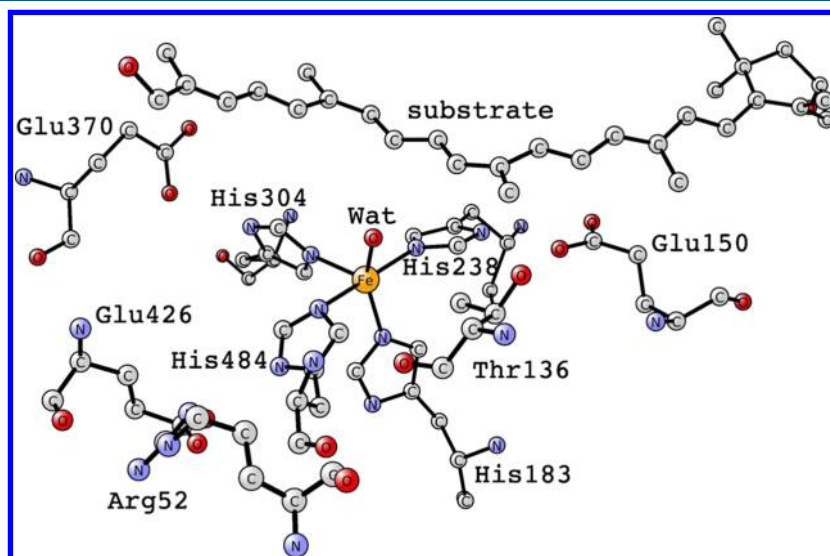

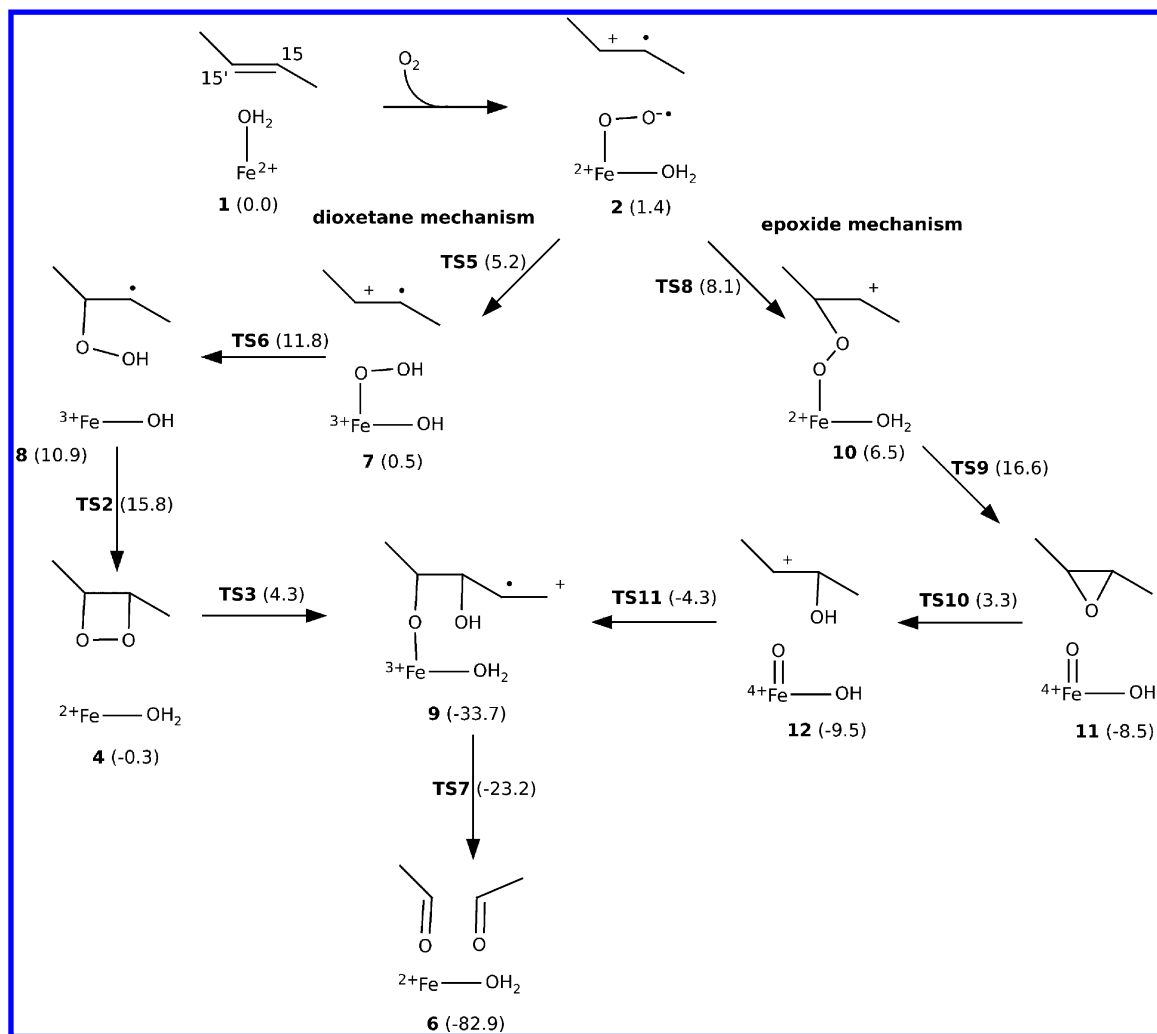**Figure 34.** X-ray structure of the active site of ACO (PDB 2BIW).

Figure 35. Dioxethane and epoxide reaction mechanisms proposed for ACO on the basis of the results of a DFT study.[170] Energy values are given in kilocalories per mole.

5.1.5. 1-Aminocyclopropane-1-carboxylic Acid Oxidase. In plants, ethylene plays the role of a signaling molecule involved in such biological processes as fruit ripening, seed germination, flower senescence, and leaf abscission. The ultimate step in ethylene biosynthesis is catalyzed by a non-heme iron(II) enzyme, 1-aminocyclopropane-1-carboxylic acid oxidase (ACCO). The catalytic reaction of ACCO couples four-electron reduction of O_2 to two water molecules with oxidation of 1-aminocyclopropane-1-carboxylic acid (ACC) and ascorbate. Moreover, CO_2, presumably in the form of HCO_3^- or CO_3^{2-}, plays the role of enzyme activator. From experimental results it follows that a substrate radical is produced during the catalytic cycle and that the ACC chelates the active site ferrous ion with its amino and carboxyl groups.[171−174] These data allowed for formulation of a mechanistic hypothesis presented in Figure 36. According to this proposal, both substrates, i.e., ACC and O_2, coordinate to iron when bound in the active site, whereas bicarbonate locates in the second coordination shell and provides a hydrogen bond to the O_2 ligand. The resulting Fe(III)−$O_2^{•−}$ species is then one-electron-reduced to form an Fe(III)−OOH intermediate that is a precursor for the ferryl species featuring an N-centered substrate radical. Finally, the radical decomposes to ethylene, CO_2, and CN^- concomitantly with reduction of the ferryl species to an Fe(III)−OH intermediate. Reduction of the
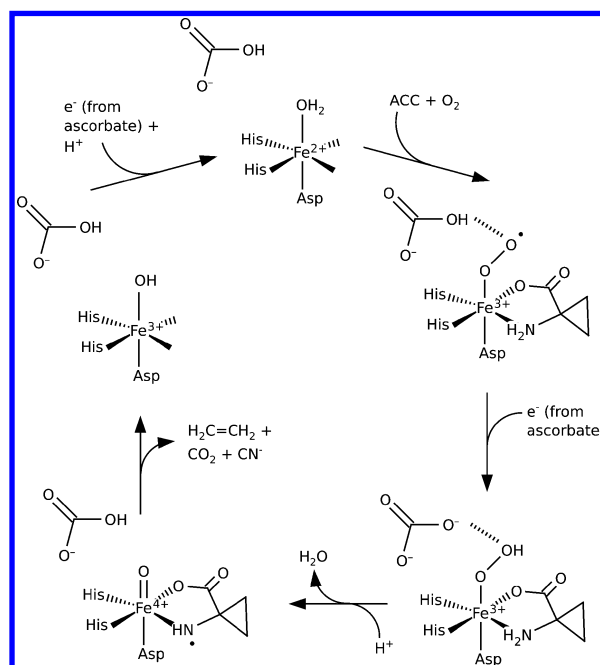

Figure 36. Proposed general mechanism for the ACCO catalytic cycle.

3628

dx.doi.org/10.1021/cr400388t | Chem. Rev. 2014, 114, 3601−3658

latter by the second electron provided by ascorbate completes the catalytic cycle.

The feasibility of the above-sketched mechanism of ACCO was probed with the B3LYP functional applied to an active site model (see Figure 37) constructed on the basis of an X-ray
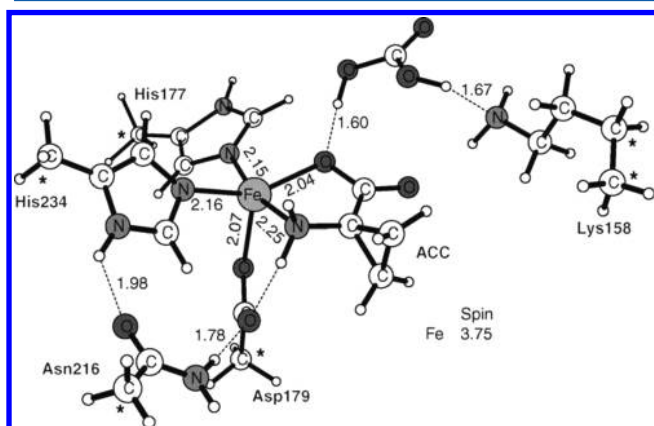

Figure 37. Active site model used in the DFT study on the mechanism of ethylene synthesis by ACCO. Reprinted with permission from ref 176. Copyright 2006 Wiley.

crystal structure of ACCO from *Petunia hybrida*.[175] Protein ligands were modeled with methylimidazole and acetate groups; from the second shell, the side chains of Asn216 and Lys158 were included. Bicarbonate was placed to bridge between Lys158 and the first-shell ligands. ACC chelates iron with its amino group bound trans to His117 and the carboxyl group trans to His234. The inverse arrangement was also tested, but it led to very similar results. Atoms marked with an asterisk were constrained in the geometry optimization.

The results of the computational study confirmed the overall reaction scheme from Figure 36 and provided some genuinely new insights into the ACCO reaction mechanism (Figure 38).[176] First, the results showed that the Fe(II)−O$_2$ adduct, i.e., the species present after O$_2$ binding yet before the first reduction by

ascorbate, is not capable of generating a N-based substrate radical. This means the one-electron reduction by ascorbate is a prerequisite for progress of the reaction. Second, instead of the originally proposed Fe(III)−OOH intermediate, it is the Fe(II)−O$_2^{\bullet -}$ species that is responsible for the N−H bond cleavage. Moreover, the ferryl intermediate is generated after opening of the cyclopropyl ring, not before. The reaction sequence suggested in Figure 36, i.e., O−O bond cleavage preceding opening of the cyclopropane ring, was also probed, yet it led to a somewhat higher (by 3 kcal/mol) activation barrier. As follows from the DFT results, decomposition of ferryl species to ethylene and cyanoformate proceeds as depicted in Figure 38 with barriers not exceeding 3 kcal/mol. As cyanoformate is known to be kinetically unstable in aqueous media with respect to its constituents, CN$^-$ and CO$_2$, the actual pathway of its decomposition was not probed with DFT.

5.1.6. (Hydroxyethyl)phosphonate Dioxygenase and (S)-(2-Hydroxypropyl)phosphonic Acid Epoxidase. The reaction mechanisms of two non-heme iron enzymes catalyzing oxidation reactions for related phosphonate compounds (Figure 39) were investigated with DFT methods. (Hydroxyethyl)-
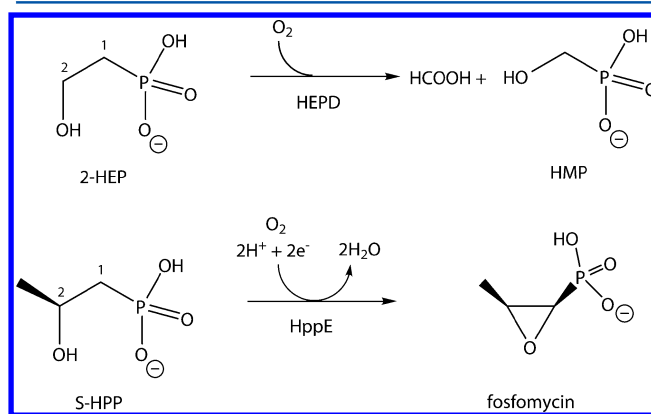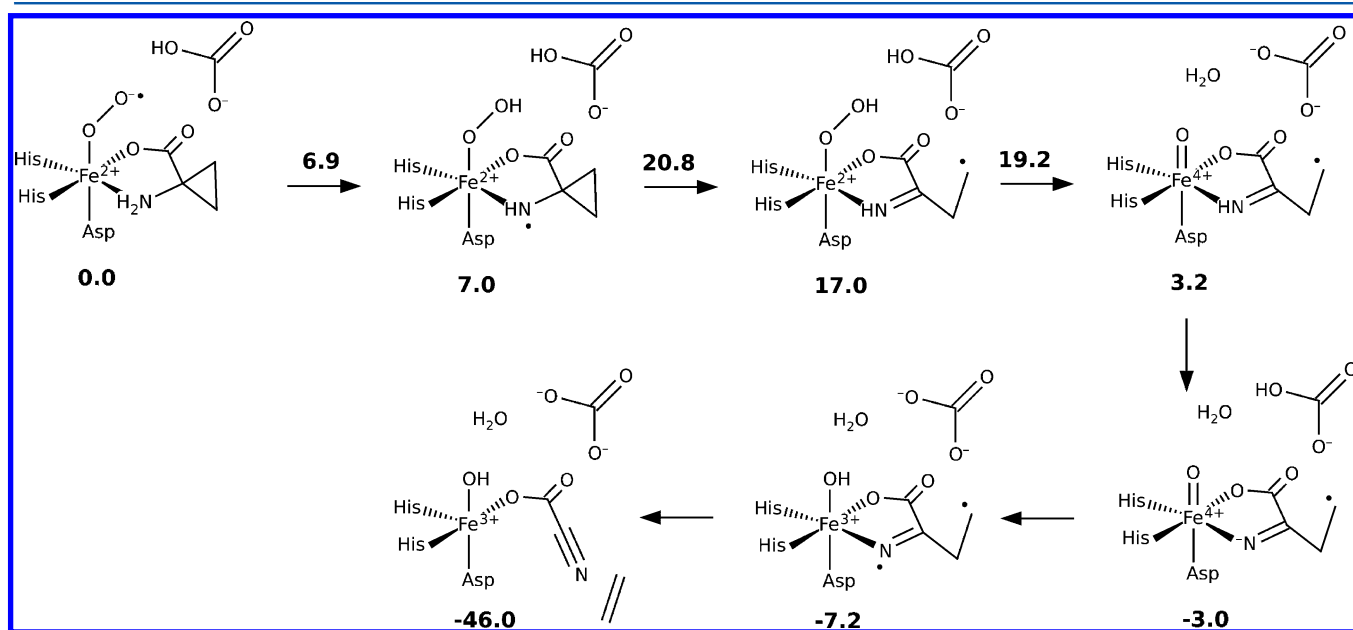

Figure 39. Reactions catalyzed by HEPD and HppE.

Figure 38. Reaction mechanism suggested for ACCO on the basis of the results of a DFT study.[176] Energy values are given in kilocalories per mole.
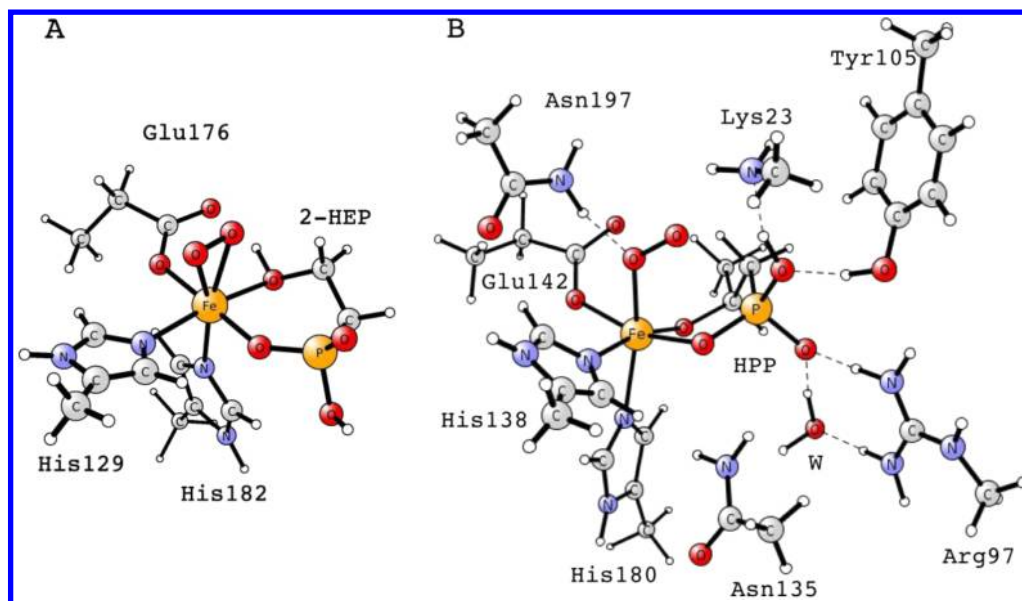
Figure 40. Active site models used in DFT studies on reaction mechanisms of (A) HEPD[177] and (B) HppE.[179]
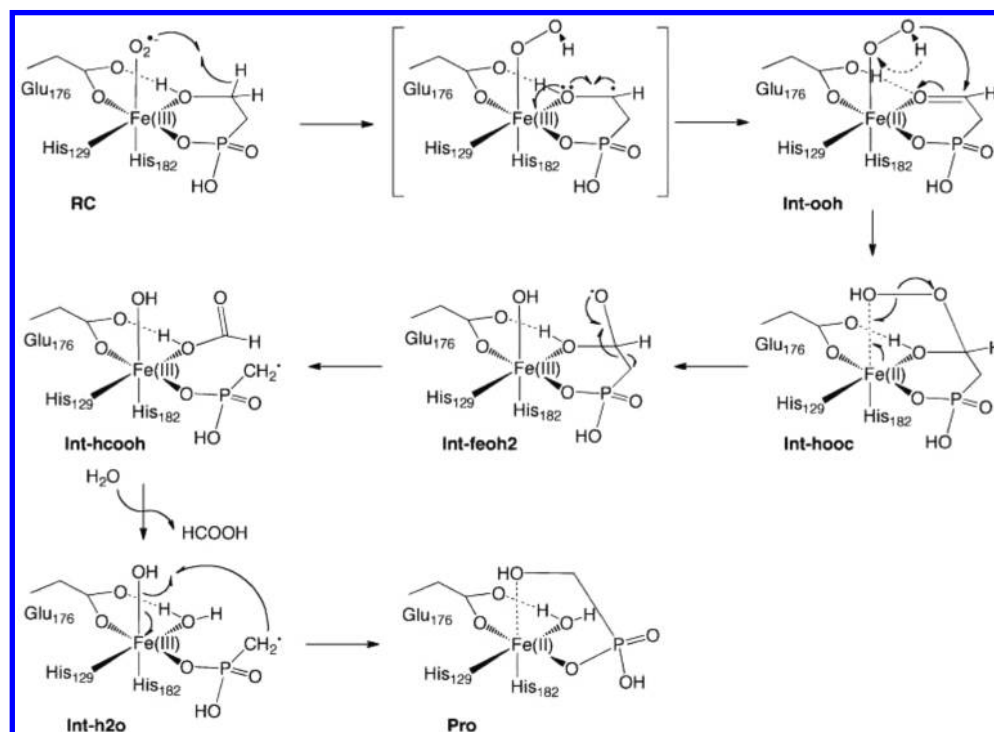

Figure 41. Mechanism proposed for the HEPD reaction. Reprinted from ref 177. Copyright 2010 American Chemical Society.

phosphonate dioxygenase (HEPD) is an Fe(II)-dependent dioxygenase catalyzing oxidative cleavage of (2-hydroxyethyl)-phosphonate (2-HEP) to formic acid and (hydroxymethyl)-phosphonate (HMP). The second enzyme is (S)-(2-hydroxypropyl)phosphonic acid epoxidase (HppE), which catalyzes the ultimate step in biosynthesis of fosfomycin. Similarly to HEPD, HppE is also an Fe(II)-dependent enzyme. Its catalytic reaction involves oxidative cyclization of (S)-(2-hydroxypropyl)phosphonic acid ((S)-HPP) coupled to reduction of O_2 to water with two electrons provided by (S)-HPP and two by the external reductant, e.g., NADH (reduced nicotinamide adenine dinucleotide).

The reaction mechanisms of HEPD and HppE were investigated with the B3LYP functional applied to active site models (Figure 40) constructed on the basis of available X-ray crystal structures. For HEPD the model included the first-shell ligands and for some critical reaction steps also the second-shell Tyr98, which forms a hydrogen bond with the phosphonic group of 2-HEP.[177] The rest of the protein was taken into account in the follow-up ONIOM(DFT:MM) study, yet inclusion of the protein in the computational model left the mechanism basically unchanged.[178] The active site model of HppE contained the first-shell ligands and all polar groups from the second shell that form hydrogen bonds with the first-shell ligands.[179] An important difference between the active site models used for HEPD and
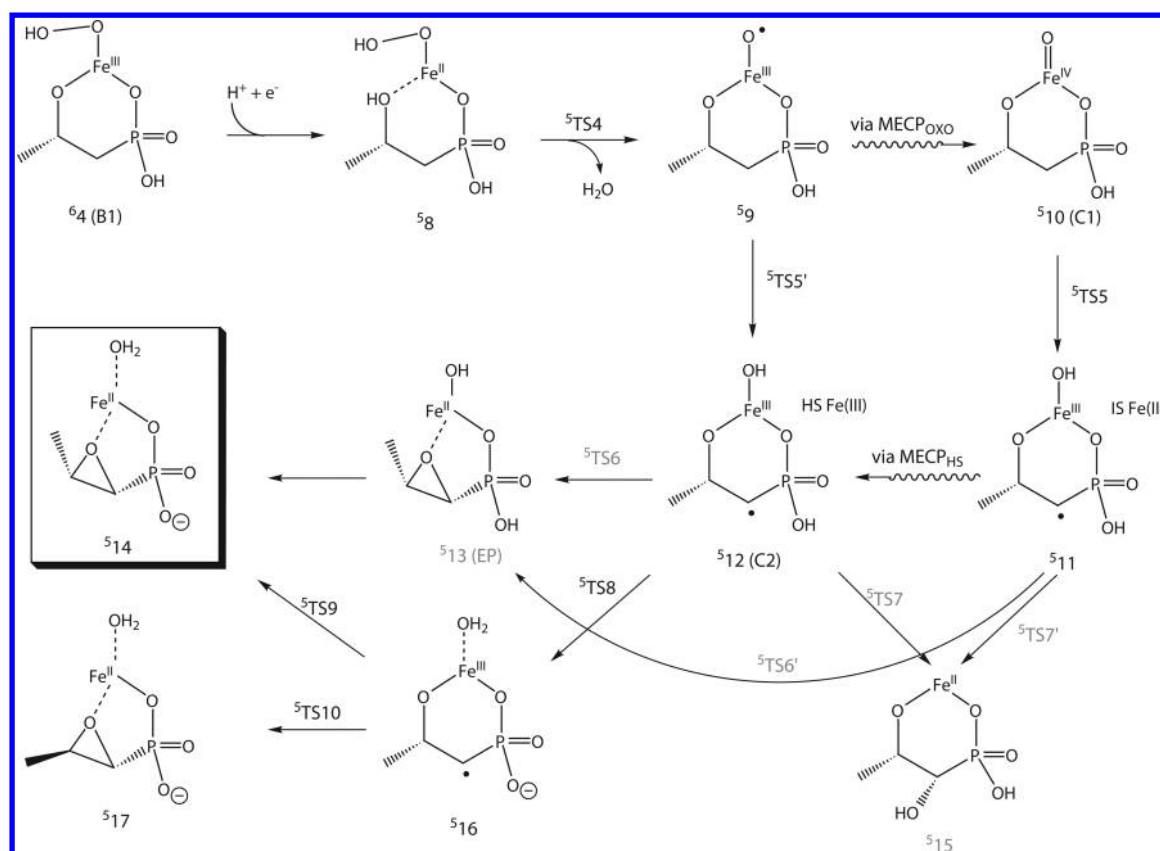
Figure 42. Mechanism proposed for the HppE reaction. Reprinted with permission from ref 179. Copyright 2013 Wiley.

HppE concerns the protonation state of the substrate's hydroxyl group: for HEPD the group keeps its proton, whereas for HppE it is deprotonated. Both choices are motivated by the structures of the active sites in the enzyme—substrate complexes revealed by X-ray crystallography, though for HEPD the structure was solved with Cd(II) instead of Fe(II).

Reaction energy profiles computed for several mechanisms previously proposed in the literature for HEPD and HppE allowed the researchers to propose the most likely mechanistic scenarios for the two enzymes. More specifically, for HEPD heterolytic mechanisms invoking a Criegee-type rearrangement or a heterolytic C—C bond cleavage were ruled out,[177] whereas for HppE it was shown that only the Fe(IV)=O/Fe(III)—O•− species is an oxidant powerful enough to efficiently cleave the C1—H bond of (S)-HPP.[177]

The mechanism of HEPD suggested on the basis of the DFT study is presented in Figure 41.[177] In the reactant state (**RC**) the dioxygen molecule has been reduced to a superoxide anion by Fe(II), and as already mentioned, the alcohol group of 2-HEP is assumed to be protonated at this stage. The DFT-predicted ground state of **RC** is a septet with side-on-bound O_2, whereas the quintet end-on variant lies 5.3 kcal/mol above it. The latter end-on quintet form is reactive; i.e., its distal oxygen atom accepts a hydrogen from C2 of 2-HEP. With a protonated alcohol group, the barrier to this step is quite high (30.3 kcal/mol without zero-point energy (ZPE)), yet for a model with a deprotonated hydroxyl group, it was lowered to 18.1 kcal/mol. This step is similar to the first reaction step of IPNS (see Figure 28) since the resulting intermediate **Int-ooh** features Fe(II)—OOH and two-electron-oxidized substrate, i.e., aldehyde. In the next step the peroxo group is transferred from Fe(II) to the aldehyde group with the help of the phosphonate group; i.e., the latter shuttles a

proton from the distal to the proximal oxygen atom. Subsequent homolytic cleavage of the O—O bond yields a *gem*-diol radical intermediate, **Int-feoh2**, that undergoes homolytic C—C cleavage, yielding the first product, i.e., formic acid. It is proposed that in the last two steps formic acid is replaced by a water molecule and the CH_2-centered radical couples with the OH ligand, forming the second product, i.e., HMP.

The mechanism of HppE suggested on the basis of the DFT study is presented in Figure 42.[179] The catalytic cycle is proposed to begin with two-electron reduction of the Fe(II)—(S)-HPP—O_2 reactant complex by the external reductant. Reduction coupled with uptake of two protons yields species ^{5}**8**, i.e., the Fe(II)—OOH intermediate similar to **Int-ooh** from HEPD, yet with the substrate molecule not oxidized yet. In the next step the O—O bond is cleaved (the leaving OH group accepts a proton from the alcohol group of the substrate), affording a very reactive Fe(III)—O• species (^{5}**9**) that can either directly abstract the C1-bound hydrogen of (S)-HPP or decay to the more stable Fe(IV)=O form (^{5}**10**), which subsequently cleaves the C1—H bond. Both reaction branches converge at species ^{5}**12** featuring high-spin Fe(III)—OH and a C1-based substrate radical, a situation somewhat similar to that of **Int-hcooh/Int-h2o** from HEPD. However, instead of OH rebound, which would lead to C1-hydroxylated product ^{5}**15**, the OH ligand is protonated with a proton provided by the phosphonate/Lys23 pair (see Figure 40B) to yield intermediate ^{5}**16**, which easily transforms to the final product fosfomycin (^{5}**14**) or its less sterically hindered trans epimer (^{5}**17**).

5.1.7. Cysteine Dioxygenase. Cysteine dioxygenase (CDO) is a non-heme iron enzyme requiring Fe(II) for activity and catalyzing oxidation of cysteine to cysteinesulfinic acid (Figure 43). CDO participates in controlling the level of cysteine

in the human body, and its decreased activity has been associated with some neurological disorders.
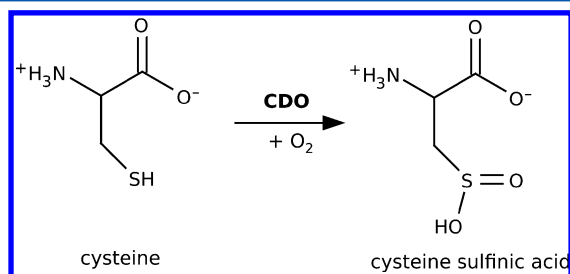

Figure 43. Reaction catalyzed by CDO.

In the enzyme–substrate (cysteine) complex of CDO the ferrous ion is coordinated by three imidazole groups of histidine protein ligands and chelated by the substrate cysteine with its thiolate and amino groups. The remaining sixth coordination site is used for binding of dioxygen. The reaction mechanism of CDO was studied with DFT applied to an active site model[180,181] and then with a QM/MM method.[182] In both cases, the reaction energy profiles were computed with the B3LYP functional and a similar fragment of the enzyme–substrate complex was treated with DFT (Figure 44).

The mechanism of the CDO catalytic reaction that is supported by the results of the computational studies can be followed in Figure 44 depicting the reaction energy profile and the key features of the reaction coordinate as derived from QM/MM studies. Quite atypically, the ground state of the reactant

CDO–Fe(II)–cysteine–O_2 complex is a spin singlet with quintet and triplet species less stable by 5.8 and 13.8 kcal/mol, respectively. Irrespective of this stability of the singlet species, which most probably has its origin in the identity of the first-shell ligands (four nitrogen ligands and one thiolate), the reaction proceeds on the quintet and partly on the triplet potential energy surfaces. In the first step, which is the slowest in the whole reaction, the distal oxygen atom attacks the thiolate group of the substrate cysteine, forming a peroxo-bridged intermediate (^5B), similar to that encountered for other non-heme enzymes. The O–O bond is subsequently severed to afford the iron(IV)–oxo species **C** with a triplet ground state. Thus, up to this point the reaction proceeds on the quintet PES. The following rotation of the S–O group (**C → C′**), which replaces sulfur with oxygen as the donating ligand, proceeds most easily with spin crossover back from the triplet to the quintet PES. The rotation exposes sulfur for attack by the Fe(IV)=O group, which proceeds with a small barrier again on the quintet PES and yields the final product—cysteinesulfinic acid.

In the QM/MM study on CDO, an alternative mechanism that postulates an attack of the proximal oxygen of the peroxo group on thiolate was also tested, yet on the grounds of the very high activation energy, it was ruled out.[182]

5.1.8. Extradiol Dioxygenases. Extradiol dioxygenases form a subgroup of mononuclear non-heme enzymes that catalyze oxidative cleavage of the aromatic ring in catechol substrates. Their name reflects the fact that they cleave the aromatic ring at the bond adjacent to the diol group of the catechol substrate (Figure 45). Extradiol dioxygenases are mainly involved in microbial aerobic degradation of catechol substrates,
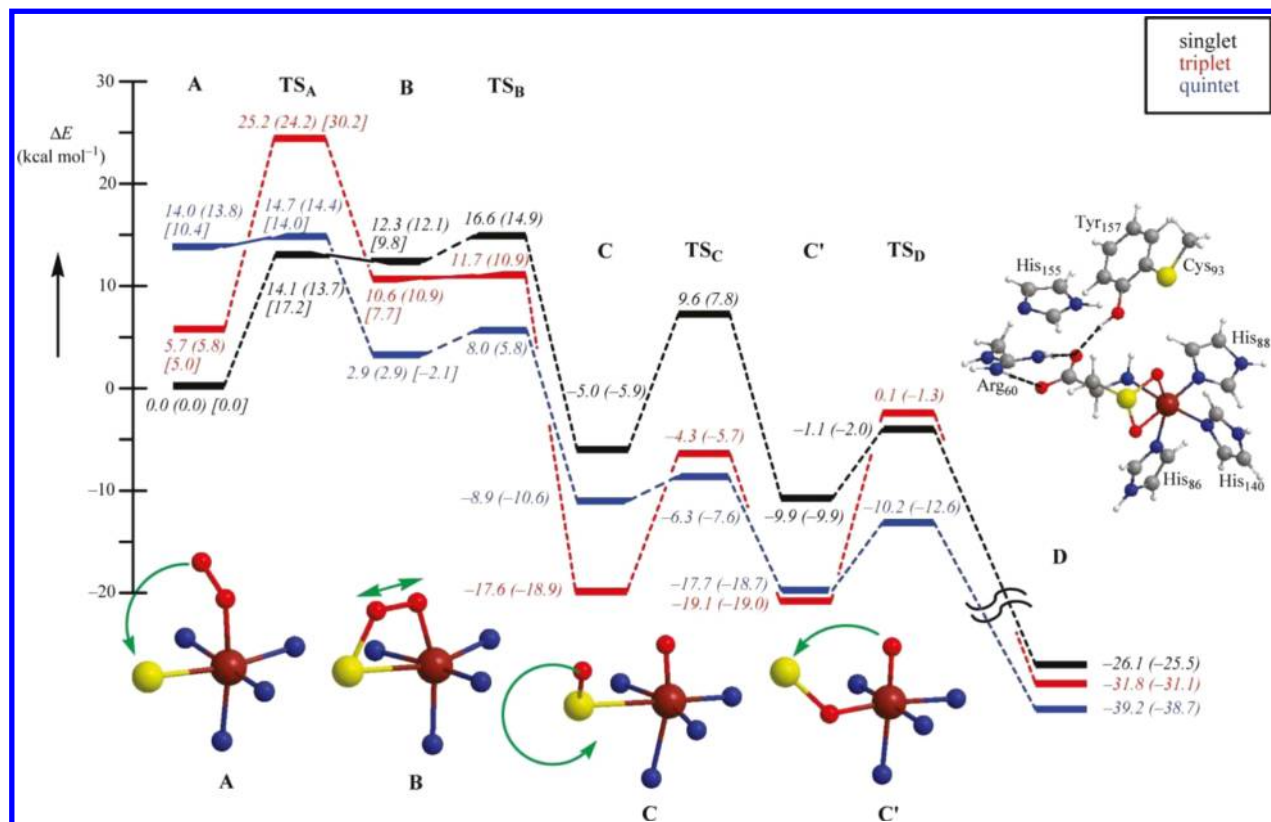

Figure 44. Reaction potential energy profiles derived from QM/MM studies on CDO. The reported values are relative energies. Values in parentheses include ZPE corrections, and values in brackets are relative energies obtained for geometries optimized with a larger basis set. Reprinted from ref 182. Copyright 2011 American Chemical Society.
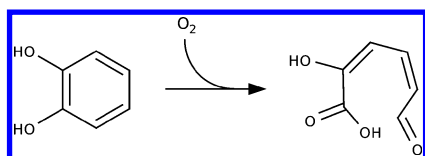
Figure 45. Reaction catalyzed by extradiol dioxygenases.

yet a closely related enzyme, homogentisate 1,2-dioxygenase (HGD), is found in higher organisms, including *Homo sapiens*.

Extradiol dioxygenases belong to Fe(II)- or Mn(II)-dependent enzymes with a two-His—one-carboxylate metal-binding motif in the active site. Spectroscopic and crystallographic results indicate the catechol substrate chelates the metal with its two oxygens, yet one of them remains protonated in a native substrate—enzyme complex.[183,184] As usual for enzymes activating O_2, the remaining sixth coordination site is used for binding of dioxygen.

Several DFT(B3LYP) studies were dedicated to the reaction mechanism of ring cleavage by extradiol dioxygenases, and their results are by and large consistent with each other. Historically the first of such studies used an active site model of 2,3-dihydroxybiphenyl 1,2-dioxygenase (BphC; Figure 46A),[185] whereas more recent studies used homoprotocatechuate 2,3-dioxygenase (HPCD) as a representative extradiol dioxygenase (Figure 46B,C).[186−190] Active site models were comprised of two imidazoles and acetate or formate, which modeled the metal-binding triad, and catechol or homoprotocatechuate anions. From the second coordination sphere the models included two histidines (imidazoles): one (His241 or His248) positioned close to the substrate's ring and glutamate metal ligand and the second (His195 or His200) located in the vicinity of the O_2-binding site. Additionally, a tyrosine forming a H-bond with catecholate was also included. The model of the BphC active site also takes into account Asp244 and a nearby water molecule, whereas models for HPCD incorporate Asn157. In the most recent study, Arg243, which forms a salt bridge with a carboxylic group of the substrate, was also taken into account.

The reaction mechanism that is supported by the results of B3LYP studies is presented in Figure 47, and this mechanism applies to both iron- and manganese-dependent extradiol

dioxygenases. O_2 binds to the metal at the coordination site located trans to the glutamate ligand, and it is one-electron-reduced to a superoxide radical. The electron is provided either by the metal ion (**b1**) or by the substrate (**b2**). In the first B3LYP study a species with a mixed **b1/b2** character was described for the septet spin state, yet for the reactive quintet state the electronic structure is best represented by **b2**.[185] For HPCD the active site model shown in Figure 46B gave the electronic structure consistent with **b2**, yet when the model was extended to include Arg243 (Figure 46C), the ground-state structure changed to **b1**. These results indicate that a delicate balance between the two forms exists, and although structure **b1** is most consistent with the interpretation of the recent spectroscopic data obtained in freeze−quench experiments performed with an electron-deficient 4-nitrocatechol substrate,[191] it is likely that the **b2** form lies on the reaction path, at least for faster, electron-rich substrates.

Irrespective of the actual electronic structure of species **b** at this stage of the reaction, the substrate is fully deprotonated, and in the quintet spin state it reacts readily with the superoxide moiety, forming a peroxo-bridged intermediate (**c**). Protonation of the proximal oxygen (**c → d**) is a prerequisite for efficient O−O bond cleavage that yields a metastable *gem*-diol radical (**e**). The latter collapses, forming an epoxide ring (**f**) which easily opens via C−C cleavage, affording a seven-membered lacton radical intermediate (**g**). OH rebound (**g → h**) and opening of the seven-membered ring (**h → i**) complete the reaction.

B3LYP mechanistic studies significantly contributed to our understanding of the catalytic mechanism of extradiol dioxygenases. Most notably, they consistently showed that (a) the metal ion is redox-active during catalysis, (b) an intermediate with a peroxo bridge between the metal and the substrate participates in the reaction, and (c) the homolytic O−O bond cleavage precedes ring expansion/cleavage. Moreover, an alternative mechanistic hypothesis invoking a heterolytic O−O cleavage concerted with ring expansion was ruled out.[192,190] X-ray crystal structures obtained for peroxo and *gem*-diol intermediates add credence to the B3LYP-based mechanistic hypothesis (Figure 47).[193,194] The reaction mechanism of homogentisate dioxygenase involves an analogous peroxo-bridged intermediate undergoing homolytic O−O bond
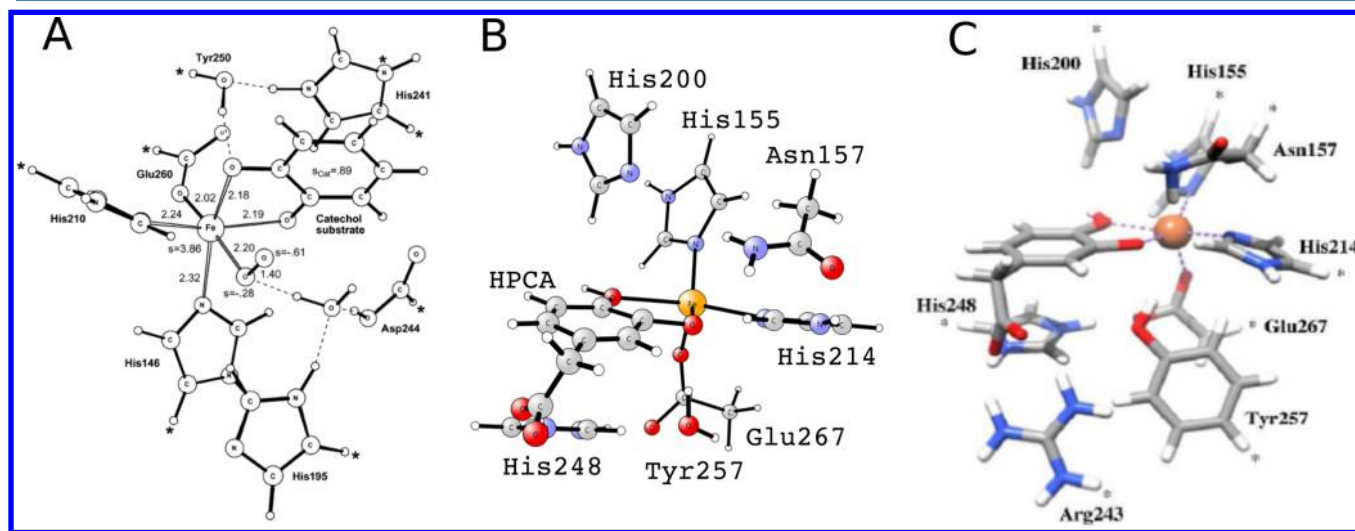

Figure 46. Active site models used in selected DFT investigations on the reaction mechanism of extradiol dioxygenases. (A) Reprinted from ref 185. Copyright 2004 American Chemical Society. (B, C) Reprinted with permission from ref 186. Copyright 2012 Royal Society of Chemistry.
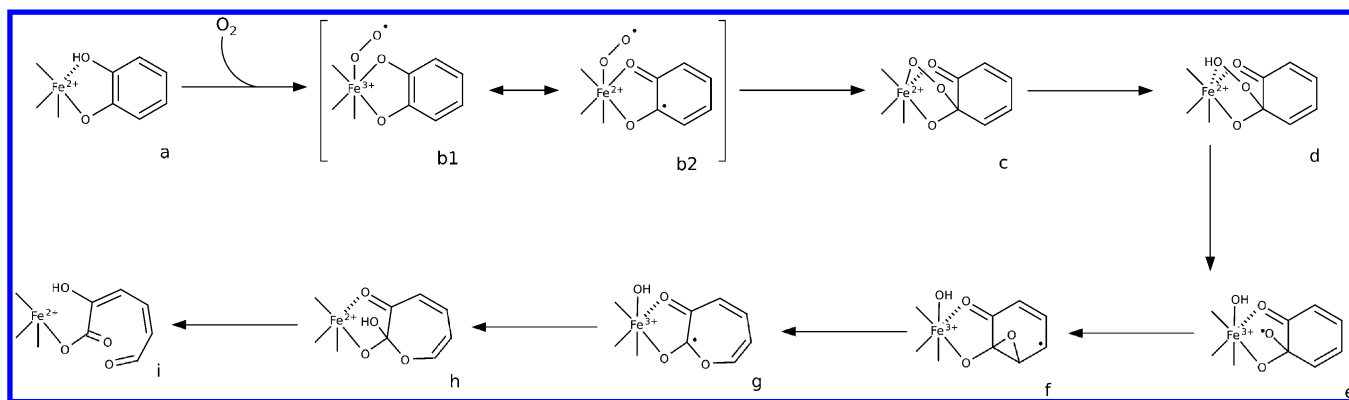
Figure 47. Reaction mechanism for extradiol dioxygenases supported by B3LYP studies.

cleavage, yet the ring-opening steps are somewhat different owing to the different structure of the substrate.[195]

5.1.9. β-Diketone-Cleaving Dioxygenase. β-Diketone-cleaving dioxygenase (Dke1) is a non-heme iron enzyme with a metal-binding motif composed of three histidine residues. Dke1 catalyzes oxidative cleavage of acetylacetone (acac) with incorporation of both atoms of dioxygen into the products: methyl glyoxal and acetate (Figure 48).[196]
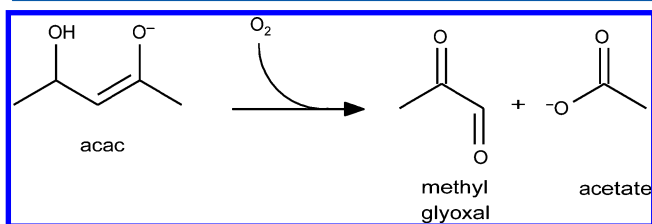

Figure 48. Reaction catalyzed by Dke1.

The reaction mechanism of Dke1 was investigated with the BP86 + 10% HF functional applied to an active site model including the ferrous ion, its three histidine ligands, and the acac substrate chelating the metal.[197] As the Dke1 reaction coordinate supported by the results of the computational study (Figure 49) shows remarkable similarities to pathways already encountered for other mononuclear non-heme enzymes, it is only very briefly presented here. Thus, O$_2$ binding leads to a reactive quintet Fe(III)−superoxo species that by attacking an electron-rich central carbon of acac transforms into a peroxo-bridged intermediate. Subsequent heterolysis of the O−O bond, which yields a ferryl species, proceeds with attack of the leaving distal oxygen on the keto group; i.e., as usual, the leaving oxygen atom develops a second covalent bond. Opening of the epoxide ring followed by attack of the ferryl species on the ester carbon completes the reaction.

5.1.10. Intradiol Dioxygenases. Diol dioxygenases fall into two broad categories: the Fe(II)-dependent extradiol dioxygenases covered in one of the preceding subsections and intradiol dioxygenases which require Fe(III) for their activity and catalyze
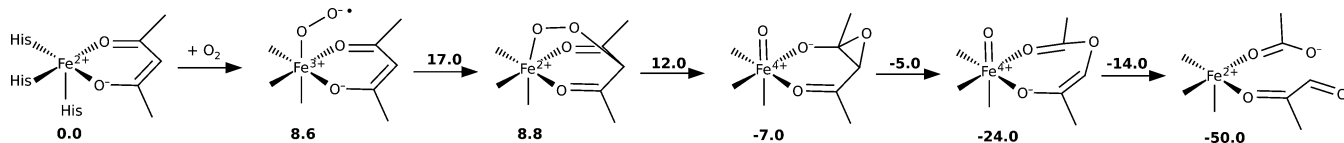
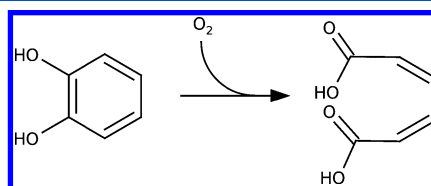oxidative cleavage of catechol rings at the C−C bond within the diol fragment (Figure 50).

Figure 50. Reaction catalyzed by intradiol dioxygenases.

The change of iron oxidation state when going from extra- to intradiol enzymes is paralleled by differences in the ligands coordinating the metal ion. Thus, in the native state the active site Fe(III) is bound by two histidines, two tyrosinates, and one OH ligand. When the catechol substrate binds to the metal with its two hydroxyl groups ionized, the OH and one tyrosine are displaced from the first coordination sphere (Figure 51). From the second coordination sphere, Arg457 and Gln477 form direct hydrogen bonds with the substrate's oxygens. The active site model depicted in Figure 51 was used in a B3LYP study on the reaction mechanism of intradiol dioxygenases, and its results revealed several new details not anticipated previously.[198]

The reaction mechanism (with plausible side reactions) supported by the B3LYP study involves four major chemical steps (Figure 52): (a) binding of O$_2$, yielding a peroxo-bridged intermediate, **3**, that undergoes a conformational change, opening a coordination site on iron (**3** → **3′**), (b) binding to the vacant coordination site a charge-neutral ligand that delivers a proton to the proximal oxygen atom of the peroxo group (**3′** → **4** → **5**) (the ligand might be a water molecule or Tyr447), (c) cleavage of the O−O bond, which could proceed either according to a heterolytic mechanism where O−O cleavage is coupled to C−C breaking and ring expansion (**5** → **6**) or according to a homolytic mechanism where Tyr408 provides an electron, reducing the OH radical to OH⁻ (**5** → **9** → **6**), and (d) attack of OH on the anhydride and opening of the ring (**6** → **7** → **8**). A novel finding of this B3LYP computational study was the
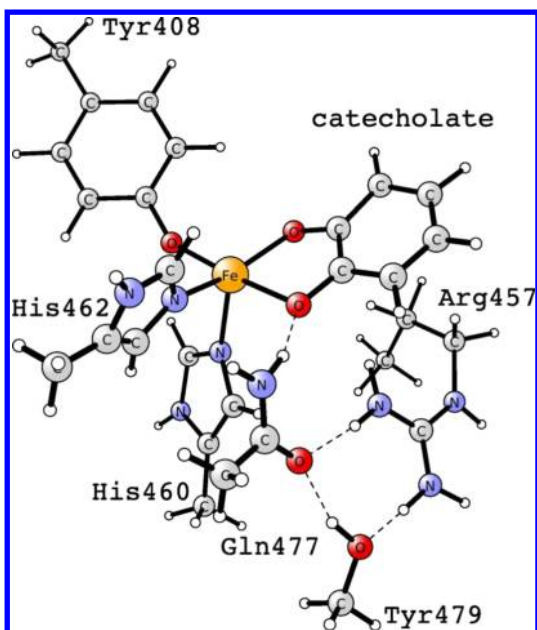

Figure 49. Reaction mechanism for DKe1 supported by the results of a DFT study.[197] Energy values are given in kilocalories per mole.

Figure 51. Active site model used in a DFT investigation on the reaction mechanism of intradiol dioxygenases.[198]

observation that the conformational change of the peroxo intermediate (**3** to **3′**) is critical for the cleavage specificity. It

places the O−O bond in approximately the same plane as the C−C bond of the ring which needs to be cleaved. Such an arrangement guarantees an intradiol type of cleavage irrespective of the detailed mechanisms for this step. Concerning the O_2-binding step, a relatively straightforward mechanism was supported by the B3LYP results, and it includes binding of O_2 to the metal coupled to one-electron oxidation of the catecholate anion (**1 → 2**). Subsequent coupling of the superoxide radical with the semiquinonate (**2 → 3**) leads to the peroxo-bridged intermediate in a sextet ground state.

An alternative mechanism for O_2 binding was proposed on the basis of the results of spectroscopic studies supported by DFT and INDO/S-CI calculations.[199] On the basis of a spectroscopy-derived electronic structure description of the enzyme−catecholate complex, it was suggested that O_2 binding could proceed on the quartet PES and the process would be a single-step O_2 trapping, leading directly to a peroxide intermediate featuring an intermediate-spin Fe(III). However, the process itself has not been probed with electronic structure methods, and it is currently not known if it is energetically viable.

5.1.11. Naphthalene 1,2-dioxygenase. The catalytic reaction of naphthalene 1,2-dioxygenase (NDO), a representative Rieske dioxygenase, involves cis-dihydroxylation of naphthalene coupled to two-electron oxidation of NADH (Figure 53). In its active site, NDO hosts a mononuclear non-heme iron cofactor with a two-His−one-carboxylate binding motif (Figure 54) and a Rieske Fe_2S_2 cluster located in the immediate vicinity
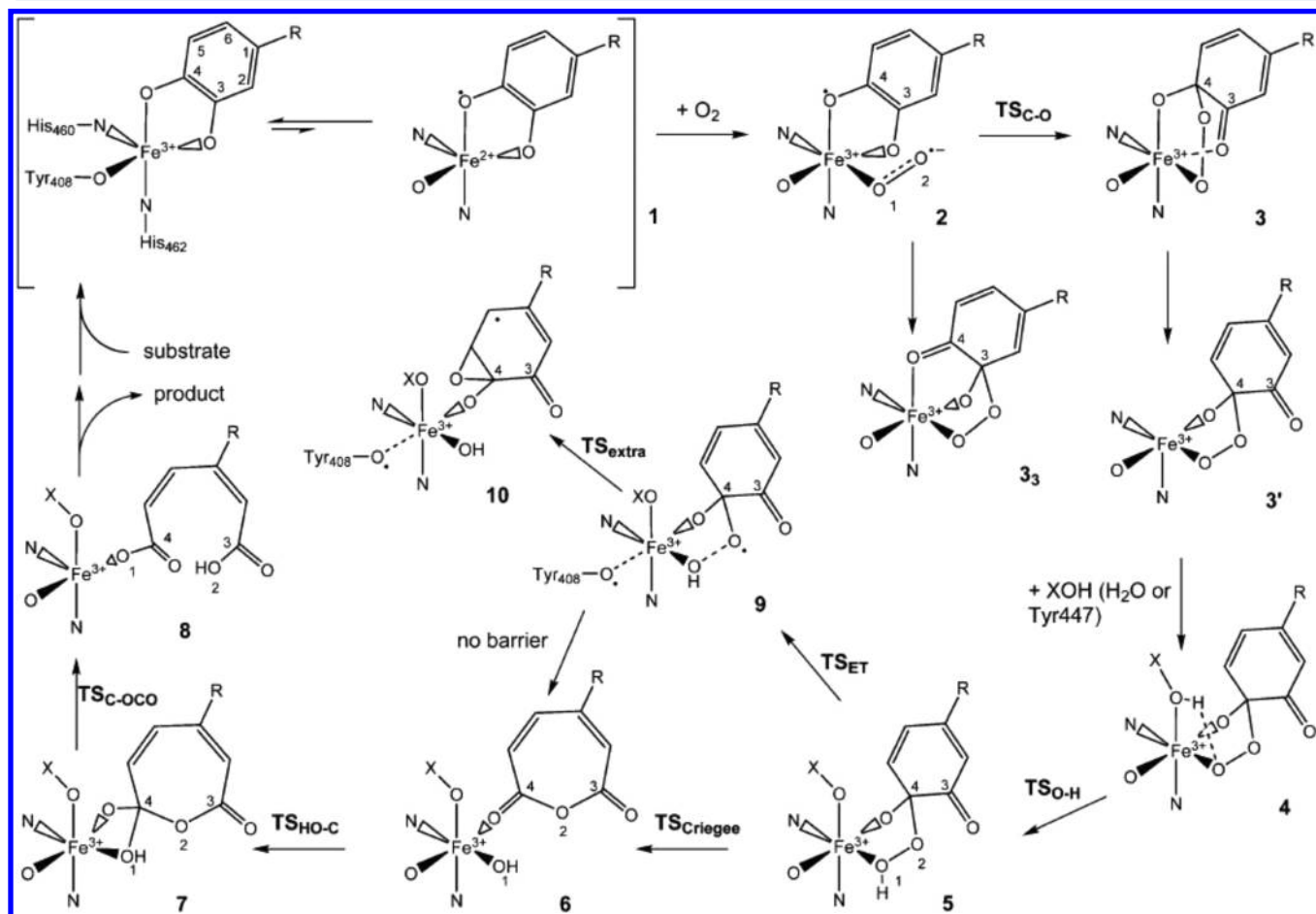

Figure 52. Reaction mechanism for intradiol dioxygenases supported by the results of a DFT study. Reprinted from ref 198. Copyright 2006 American Chemical Society.
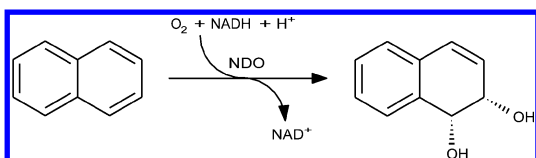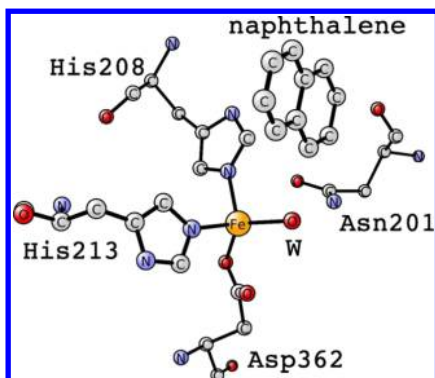
Figure 53. Reaction catalyzed by NDO.

Figure 54. X-ray structure of the non-heme iron cofactor in the NDO active site (PDB 1O7G).

of the non-heme center. Crystal structures revealed that O_2 binds to the non-heme iron in a side-on fashion, whereas the aromatic substrate locates nearby.[200] Results of single-turnover experiments unequivocally showed that the dihydroxylation reaction is feasible even if the NADH reductase component of NDO is missing provided the non-heme cofactor is in a ferrous state and the Rieske cluster is reduced, i.e., two electrons are accessible when O_2 binds.[201] These results limit somewhat the number of plausible mechanisms for dihydroxylation (under the single-turnover conditions), yet there are still at least several plausible detailed mechanistic scenarios that could be invoked. A B3LYP study by Bassan et al. tackled these issues and provided valuable insights into the course of the transformation of naphthalene to the *cis*-diol by NDO.[202]

The active site model used in the DFT study included two methylimidazoles and an acetate modeling histidines and aspartate protein side chains and the naphthalene and O_2 substrates. A slightly larger model, involving Asn201 and Val203 from the second coordination shell, was employed to test the stability of the results for the most critical reaction steps. Binding of O_2 was investigated with a model deprived of naphthalene.

The results of the DFT study provided several interesting insights into the NDO reaction. First, they showed that dioxygen needs to be two-electron-reduced and protonated to be prepared for further reaction steps. An iron-bound superoxo species was

found not to be capable of efficient attack on the aromatic hydrocarbon. Second, heterolysis of the O−OH bond in the Fe(III) species without involvement of the organic substrate was found to require a prohibitively high activation barrier, and hence, a mechanism invoking participation of an Fe(V)=O species was not supported. In contrast, when one more electron is available, the O−O heterolysis begins with an Fe(II) species, and the process is both facile and exothermic and yields an Fe(IV)=O intermediate that might be responsible for oxidation of the organic substrate. However, in the single-turnover experiment this second electron is definitely not available, and hence, a different mechanism was sought. Such a mechanism, which was not previously anticipated for NDO, was indeed found, and it is presented in Figure 55. More specifically, the O−O bond is cleaved in the Fe(III)−OOH species concerted with formation of two C−O bonds in the arene oxide, which means the hydrocarbon is two-electron-oxidized without the need to form a high-valent iron−oxo species. Epoxidation involves a barrier of around 18 kcal/mol, and it is the slowest step. Subsequent opening of the epoxide to form a carbocation and recombination of the latter with the OH ligand are predicted to be very fast (barriers lower than 8 kcal/mol).

5.1.12. Chemistry of Oxygenated Species in Mononuclear Non-Heme Iron Enzymes. In the preceding subsections, we have reviewed selected DFT studies aimed at the reaction mechanisms of mononuclear non-heme enzymes activating O_2. Here we summarize these results with a focus on the chemistry that is available for various oxygenated species encountered in the catalytic cycles of these enzymes. Trends and similarities revealed in such compilations should both be useful in systematizing our understanding of the full breadth of chemistry at work in the so-far-studied non-heme enzymes and also serve as a reference in future studies on novel enzymes from this vast superfamily.

The superoxide radical bound to Fe(III) or Fe(II) is capable of abstracting a hydrogen atom from substrates with relatively weak X−H bonds (Figure 56). Such a situation was found in the catalytic cycle of ACCO, where cleavage of the N−H bond is facilitated by the ferrous ion capable of (partly) reducing the resulting N-based radical to an anion. In the catalytic cycle of HEPD and in the reaction of HppE with an enantiomer of the native substrate, a C−H bond at the carbon hosting a deprotonated alcohol group is severed by the superoxide. In these cases transfer of a hydrogen atom to the superoxide is coupled to one-electron reduction of Fe(III) to Fe(II), which yields aldehyde or ketone products. In a similar way a thioaldehyde is produced during the initial steps of the IPNS catalytic cycle.
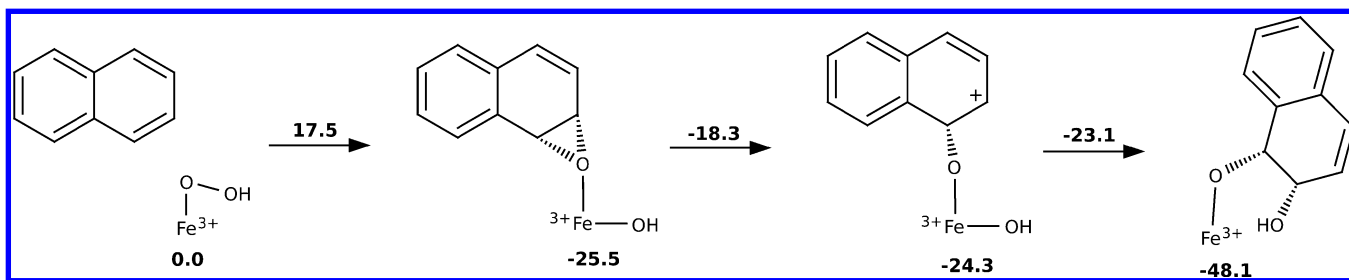

Figure 55. Reaction mechanism for the dihydroxylation reaction catalyzed by NDO suggested on the basis of the results of a DFT study.[202] Relative energy values in kilocalories per mole are given beneath the structures shown and above the arrows for the transition states connecting them.
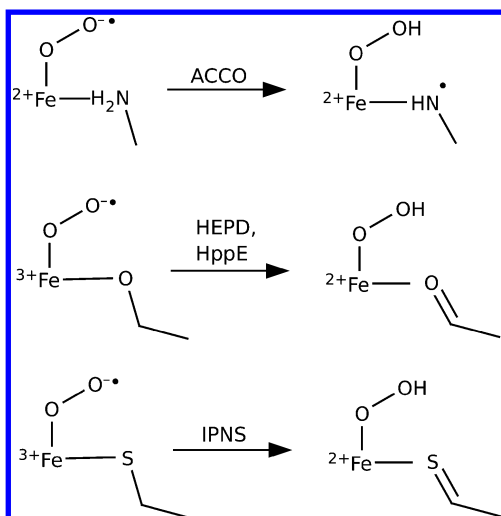
Figure 56. Examples of Fe(II)/Fe(III)−O$_2$$^{•−}$ reactions involving hydrogen atom abstraction. Only the most relevant fragment of the substrate is shown.

The most often encountered reaction of the Fe(III)−O$_2$$^{•−}$ species is an electrophilic attack on an electron-rich (co)substrate that yields an Fe(II) intermediate with a peroxide bridge between the ferrous ion and an organic molecule (Figure 57). In all examples shown in the figure the reactive spin state is a quintet with high-spin Fe(III) antiferromagnetically coupled to the superoxide radical. This particular electronic structure allows for a smooth two-electron reaction, leading to a ferrous intermediate featuring a high-spin Fe(II) ion, i.e., also lying on a quintet PES.

When the substrates are easily one-electron-oxidized, as, for example, carotenoids or catecholates, already the ternary enzyme−dioxygen−organic substrate complex may contain an organic radical along with the superoxide anion stabilized by coordination to the metal (Figure 58). With proper (anti-ferromagnetic) alignment of the spins of the unpaired electrons on the two radicals, direct coupling between them proceeds with a straightforward formation of a new C−O bond.

With the O$_2$ ligand already protonated, several different reaction scenarios are usually plausible, and one of them, arguably the simplest, involves a transfer of the HOO group from the metal ion to the organic substrate (Figure 59). In the reaction of HEPD, it is the distal, i.e., originally protonated, oxygen atom that attacks the aldehyde group and the proton is transferred to the second (proximal) oxygen atom with the help of a phosphonic group of the substrate. In this reaction HOO acts as a nucleophile. In the case of HGD, the HOO ligand has a partial radical character, and hence, in its attack on the aromatic ring, it behaves as an electrophilic reagent. Moreover, in the HGD and ACO cases, it is the proximal oxygen atom that is directly transferred from the metal ion to the organic radical, i.e., the proton remains on the same oxygen atom throughout the reaction.

When a catalytic reaction involves a homolytic O−O bond cleavage, one end of the peroxo group is in contact with the metal ion, and it is reduced to HO$^-$ or RO$^-$ when the O−O bond breaks (Figure 60). The electron required for the reduction is provided usually by the ferrous ion; in intradiol dioxygenases, which host Fe(III) in the active site, a tyrosinate ligand can serve as a reductant.

Heterolytic cleavage of the O−O bond typically yields high-valent iron(IV)−oxo species, and such a reaction requires Fe(II),
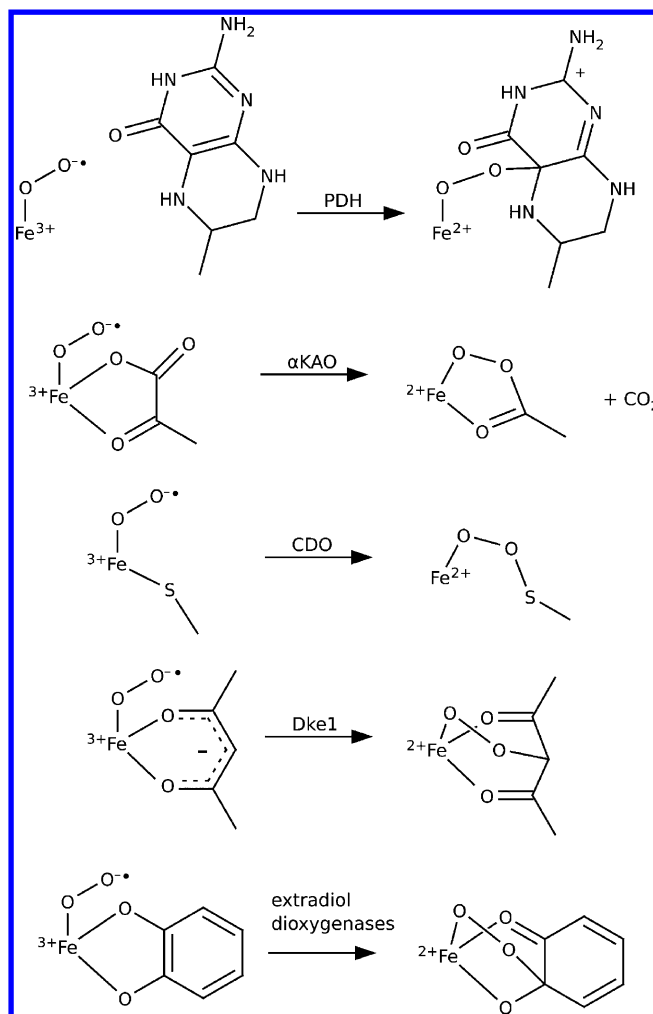
Figure 57. Examples of Fe(III)−O$_2$$^{•−}$ reactions involving electrophilic attack and two-electron oxidation of an organic (co)substrate.

Figure 58. Examples of Fe(II)/Fe(III)−O$_2$$^{•−}$ reactions involving radical coupling between the superoxide and an organic radical. Only the most relevant fragment of the substrate is shown.
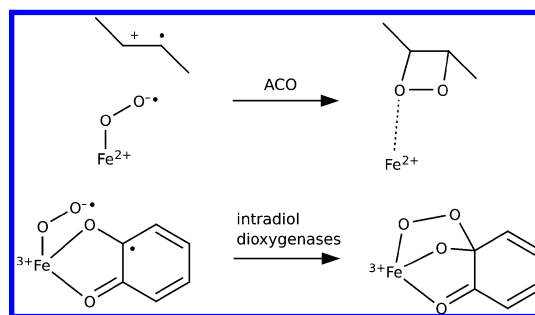
a deprotonated proximal oxygen atom, and usually also that the distal oxygen atom has a chance to develop a second covalent bond when the O−O gets broken (Figure 61). The bonding partner for the distal oxygen can be a hydrogen (PDHs, IPNS, ACCO) or a (co)substrate's carbon (αKAOs, ACO, Dke1) atom. Heterolysis to Fe(IV)=O usually proceeds on the quintet PES.

Finally, heterolytic O−O bond cleavage may proceed without changing the oxidation state of the metal but instead with coupled two-electron oxidation of an organic substrate (Figure

Figure 59. Examples of HOO transfer reactions. Only the most relevant fragment of the substrate is shown.

Figure 60. Examples of O−O bond homolysis facilitated by one-electron reduction of the proximal oxygen atom. Only the most relevant fragment of the substrate is shown.

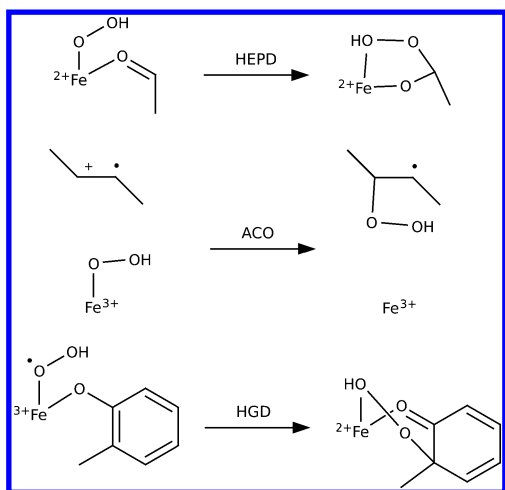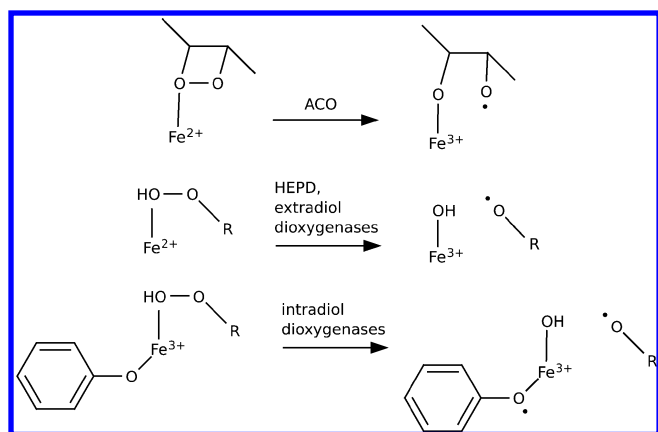62). In both cases depicted in the figure, a hydroperoxo group is bound to high-spin Fe(III), and when the O−O bond cleaves, the OH group remains on iron and the other oxygen atom forms two covalent bonds with the organic substrate. This kind of heterolytic O−O cleavage requires that the donor orbital of the organic substrate, i.e., the one that provides two electrons for reduction of the peroxo group, has a good overlap with the O−O σ^* orbital.

5.2. Dinuclear Non-Heme Iron Enzymes

5.2.1. Methane Monooxygenase. MMO is an enzyme which inserts one oxygen from O_2 into methane to form methanol. The active site of the soluble form of MMO[203] is shown in Figure 63. It contains an iron dimer complex linked by oxygen-derived ligands and has four glutamates and two histidines. Due to the presence of a well-resolved X-ray structure, and the technical importance of the reaction catalyzed, this was actually the first redox-active enzyme mechanism that was treated with the cluster model using modern DFT functionals in 1997.[4] Several groups were active at an early stage, and the most essential parts of the reaction mechanism were determined more than a decade ago. A comprehensive review of this development was written by Friesner et al.[204] In short, the active species (compound **Q**) has a diamond core structure with two bridging oxo groups and is in an $Fe_2(IV,IV)$ state, one of the most oxidized
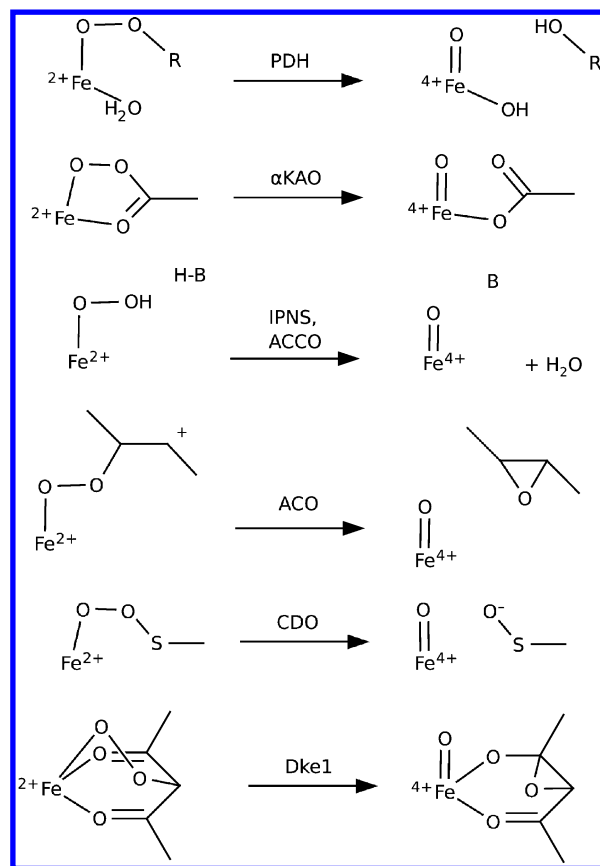
Figure 61. Examples of heterolytic O−O bond cleavage yielding iron(IV)−oxo species.
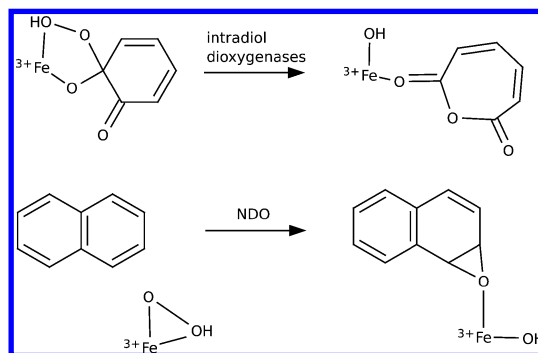
Figure 62. Examples of heterolytic O−O bond cleavage proceeding with direct two-electron oxidation of the organic molecule.

species in nature. One of the oxo groups of compound **Q** activates methane by an abstraction of one hydrogen atom. The TS is linear in C···H···O to form an $Fe_2(III,IV)$ state and a methyl radical.[4,204,205] The loss of entropy at the TS is a large part of the barrier. In the second step, the methyl radical recombines with the bridging hydroxide formed in the first step. The TS for this step was first located by Basch et al.[206] This rebound mechanism was criticized by interpretations of radical clock experiments,[207] which appeared to show that there could not be a sufficiently long-lived alkyl radical to be consistent with a two-step mechanism. A concerted mechanism with simultaneous cleavage of the C−H bond and formation of the C−O bond was therefore suggested. Several explanations were suggested to resolve this apparent discrepancy between experiment and theory. In one of them, it was concluded that the radical clock probe molecules

Figure 63. Active site of methane monooxygenase.

were chemically so different from methane that different mechanisms were likely.[208] The probes are much easier to ionize and could form cations instead of radicals. Another suggestion was a so-called two-channel mechanism of the dynamics involving a bound radical intermediate.[209] A third possibility could be something analogous to the two-state reactivity mechanism suggested for P450 to explain similar discrepancies in that case,[76] bu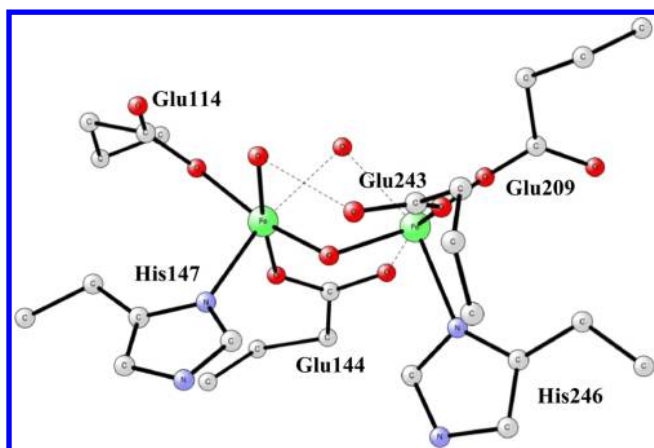t this has not been tested. In summary, a concerted mechanism, as suggested by the experiments, has never been found in DFT modeling calculations for methane hydroxylation by MMO, at least when reasonable models have been tried, and the suggestion has therefore not survived.

In the initial phase of the MMO studies, there were problems converging to proper electronic states. These problems were solved by Friesner et al.,[204] who were able to obtain the correct antiferromagnetic coupling of compound **Q** with two high-spin irons. A state of key importance is also the first intermediate after **Q**, with an electronic structure characterized as $Fe_2(III,IV)-O^\bullet$,[208] discussed further below in connection with mixed Mn−Fe dimers. It was found that already at the TS for hydrogen abstraction the iron dimer is in an $Fe_2(III,IV)$ state as it is in the product of this step. The bridging oxygen radical would then act as a hydrogen atom abstractor. At the TS, the spins are divided between a bridging oxo ligand and the methyl, while the iron spins stay essentially constant from the $Fe_2(III,IV)-O^\bullet$ state to the product.

The O−O bond cleavage to reach compound **Q** is also a significant step in the catalytic cycle. Again, several groups were involved in studying this step at an early stage.[208,210−212] There was essential agreement among these studies on the mechanism. First, a peroxide (compound **P**) is formed between the two irons in an $Fe_2(III,III)$ state. Several different structures of **P** are nearly degenerate. In the TS for the O−O cleavage, the oxygens are symmetric, but only one of the irons is redox-active. In the final
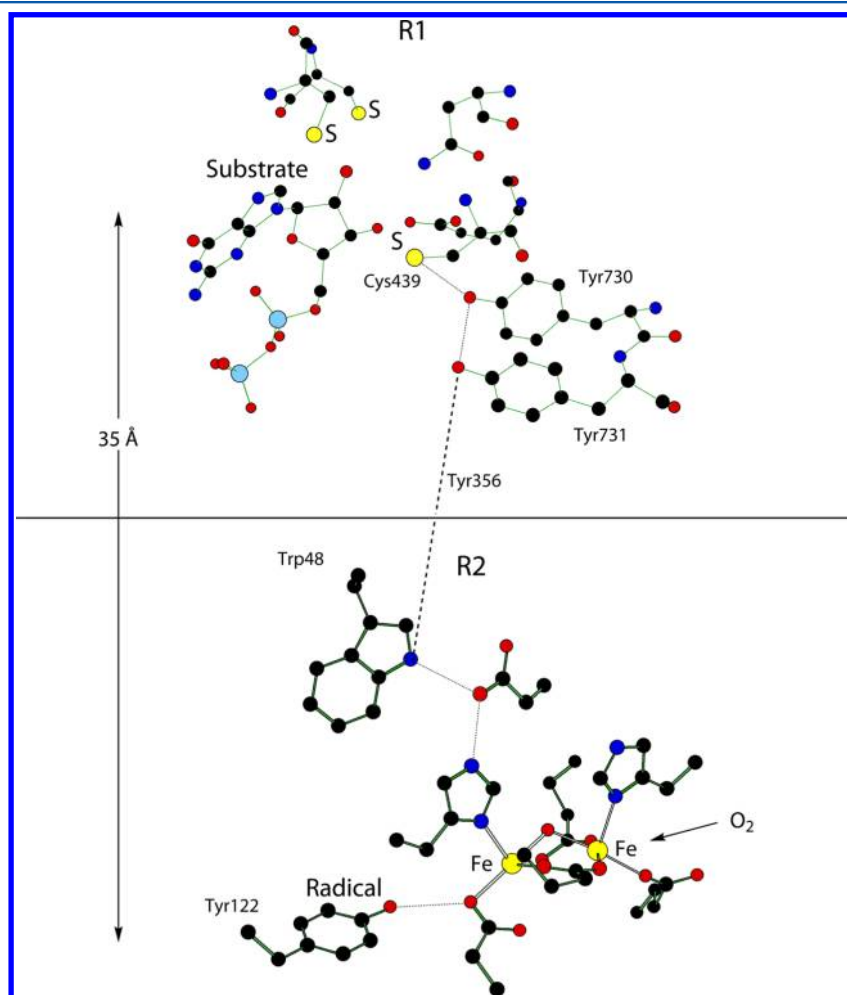

Figure 64. R1 and R2 proteins in RNR.

stage, the other iron also changes its oxidation state to IV, and compound **Q** is formed. In the study by Friesner et al., it was claimed that a large model of 100 atoms is needed to reproduce the experimental reaction energy. This conclusion was drawn to explain the difference obtained compared to results from other groups, who used much smaller models of 40−50 atoms. However, it was later shown that the size of the model was not the reason for the difference in the results,[28] which was instead due to a convergence to the wrong local minimum in the calculations with the large model. More recent work has discussed the role of protons in dioxygen activation.[213]

Methane activation by particulate methane monooxygenase (pMMO) has also been considered using quantum chemical calculations.[214,215] In contrast to the soluble MMO, pMMO uses copper to affect its reaction.[216] Calculations by Shiota and Yoshizawa have suggested that the binuclear copper center is the likely site for the reaction[214a] and that the active species is a bis(μ-oxo)Cu(II)Cu(III) cluster.[214b]

5.2.2. Ribonucleotide Reductase. Ribonucleotide reductase (RNR) is another enzyme which was studied early with DFT, using cluster models.[210,212,217] Class I RNR has two subunits, R1 and R2;[218,219] see Figure 64. In R2 a very stable Tyr122 radical[220] is created by a reaction between dioxygen and an iron dimer complex, very similar to that in MMO. The only difference between the complexes is that one of the glutamate ligands is replaced by an aspartate. When the ribonuclotide substrate becomes bound in R1, there is a docking between R1 and R2, and the radical in R2 is transferred 35 Å to Cys439, close to the substrate. The cysteine radical then acts as a catalyst for replacing a hydrogen with a hydroxide on the ribonucleotide to form a deoxoribonucleotide, the building block for DNA. After this transformation, the radical returns to the tyrosine in R2. A few hundred cycles can be performed before the tyrosyl radical needs to be regenerated.

The dioxygen cleavage in RNR differs on a few important points from that described above for MMO. Unlike the case in MMO, there are a few ionizable residues in the neighborhood of the iron dimer in RNR. One of them, Trp48, donates an electron to the iron complex in the process of the dioxygen cleavage, ending up in an Fe$_2$(III,IV) complex termed compound **X**. A DFT comparison has been made of the dioxygen cleavage in MMO and RNR,[221] suggesting that the incoming electron from the tryptophan could be the reason the O−O cleavage is 2 orders of magnitude faster in RNR than in MMO in spite of the large similarity between the iron complexes.

An interesting question at a very early stage for RNR was how the radical is transferred such a long distance without any apparent redox-active cofactors along the way. An electron transfer over a distance of 35 Å would be prohibitive using normal rules of electron transfer. Theoretical modeling suggested that a large part of the transfer occurs by moving a hydrogen atom between a neutral and a radical amino acid, for example, between Tyr730 and Tyr731 in the figure, rather than just an electron.[217,222] Other steps still occur by the more conventional type of proton-coupled electron transfer (PCET), where the electron goes between two amino acids, but the proton has quite different donors and acceptors, the latter often bulk water. This picture of the radical transfer agrees almost perfectly with results from more recent advanced experiments involving site-specific replacement of tyrosine with 3-aminotyrosine.[223]

The RNR substrate reaction was studied very early with DFT using cluster models.[224a] In fact, the first study was so early that the models were not entirely developed, and the clusters were

quite small. Two important features missing at that stage were the fixation of coordinates from the X-ray structure and the procedure for choosing proper protonation states. Still, the mechanism derived contains parts that are still considered correct. A refinement with improved models was made a few years later,[224b] and good agreement with the experimentally suggested mechanism was obtained. In the later study, a transition state for a long-range (8 Å) electron transfer step was obtained for the first time. In another similar study at the same time, the substrate mechanism for the anaerobic RNR was also characterized including the transition state for another long-range electron transfer of 6 Å.[224c] In these transition states, there are strong couplings between many degrees of freedom, some of them involving proton motion. Unlike what is generally assumed for long-range electron transfer, the number of degrees of freedom directly involved in the motion is very large, actually larger than in most TSs not involving electron transfer. All of these different motions are grouped together in one single coordinate with one harmonic frequency in the Marcus model.[225] It is quite impressive that this model usually works so well. A review has been written on mechanisms of other enzyme substrate reactions catalyzed by radicals,[205] and the reader is referred to that review for further details.

5.2.3. Enzymes with Mixed MnFe Dimers. During recent years a new class of RNRs have been discovered containing a mixed MnFe dimer, rather than the normal Fe$_2$ dimer.[226] An equally important feature of these enzymes is that they lack the tyrosyl radical. Still, the same long-range radical transfer exists, and the substrate reaction can be catalyzed in a way similar to that of the iron dimer RNR. These surprising features have been studied recently by DFT and cluster models.[227a] It was shown that Mn(IV)Fe(III) has the same redox potential as the tyrosyl radical. The metal complex is thus able to serve as the radical-harboring site, performing exactly the same substrate catalysis as the Fe$_2$(III,III) complex with a tyrosyl radical.

Still another class of RNRs have recently been confirmed containing a Mn$_2$ dimer in the same position as the Fe$_2$ dimer.[228,229] In contrast to the Fe$_2$ dimer and the MnFe dimer, the Mn$_2$ dimer is not able to cleave dioxygen. Comparative calculations performed show that the cleavage of dioxygen is actually more exergonic for the Mn$_2$ dimer than for the Fe$_2$ dimer complex.[227b] However, the barrier for the cleavage is indeed higher for the Mn$_2$ dimer, in agreement with the suggestions by experiments. The reason for this is that, for the Mn$_2$ dimer, a very stable end-on asymmetric peroxide is formed. The high stability is due to the presence of two Jahn−Teller (JT) active metals. To cleave dioxygen, a symmetric form first needs to be formed, breaking the optimal JT distortions, which is quite costly. For the Fe$_2$ dimer and MnFe dimer, the symmetric form of the peroxide is quite stable, and the barrier is therefore lower. Tentative, but complete, energy diagrams for the radical transfer in the Fe$_2$ dimer and MnFe dimer enzymes were also presented in the same study. An important feature of these diagrams is that they appear to explain how the radical could be so stable and still allow a fast transfer through the H-bonded chain to the substrate, without invoking an effect of the docking of R1 and R2 or the presence of an additional proton from the solvent. The driving force for the radical transfer is supplied by the exergonicity of the substrate reaction. The formation of the cysteinyl radical from the tyrosyl radical is slightly endergonic, and the driving force for the radical transfer is supplied by the exergonicity of the substrate reaction. The theoretical energy profile is in almost exact agreement with the thermodynamic profile for the radical transfer on the basis of

electrochemical measurements presented in a recent experimental study.[230]

The two-electron chemistry, as performed by the iron complex of MMO, has also been compared among the three different dimers discussed above.[227c] It was shown that $MnFe(IV,IV))$ has a substantially higher barrier for hydrogen abstraction than $Fe_2(IV,IV)$. As mentioned above, a significant part of the barrier is due to the loss of entropy for the incoming substrate. However, if the substrate is bound in the enzyme, there is no loss of entropy, and the MnFe dimer can therefore have a role as, for example, an oxidase in that case. The Mn_2 dimer will have a high barrier even if there is no entropy loss.

6. COPPER ENZYMES

6.1. Enzymes with an Active Complex with a Single Copper

Copper-containing amine oxidases (CAOs) form a family of redox-active enzymes which catalyze the oxidative deamination of primary amines by dioxygen to form aldehydes, ammonia, and hydrogen peroxide.[231] Catalysis requires a protein-based o-quinone cofactor, 2,4,5-trihydroxyphenylalaninequinone, referred to as topa-quinone (TPQ). The crystal structure for yeast *Hansenula polymorpha* (HPAO) (among other CAOs) has been solved to 1.6 Å resolution.[232] At the active site a Cu atom is coordinated to the imidazole side chains of three histidines and weakly coordinated to two water molecules. The deeply buried TPQ cofactor and copper are in close proximity, but they are not coordinated to each other; see Figure 65.
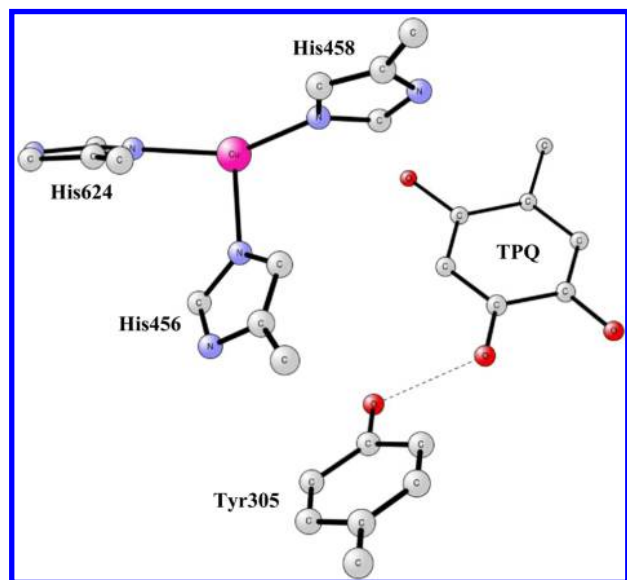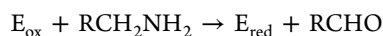

Figure 65. X-ray structure of the active site of copper-containing amine oxidase.[232]

Experiments have shown that the CAOs utilize a two-step, ping-pong-type mechanism in their catalytic cycle.[233] The process can be formally divided into reductive and oxidative half-reactions, with the reductive half-reaction being

$$E_{ox} + RCH_2NH_2 \rightarrow E_{red} + RCHO$$

and with the oxidative half-reaction being

$$E_{red} + O_2 + H_2O \rightarrow E_{ox} + H_2O_2 + NH_3$$
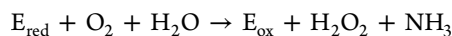
The early theoretical studies of these reactions were reviewed in 2003.[205] At the time it was thought that copper was not redox-

active in this process, but simply acted as a "spin catalyst" to help in the spin transition when O_2 was activated. Recently, new DFT investigations have been done to reinvestigate the role of copper.[234] It was then found that a redox-active Cu(I) is needed to catalyze reduction of O_2 to H_2O_2. According to the DFT calculations for the oxidative half-reaction, the binding of dioxygen to the Cu(I) metal in an end-on fashion leads to the formation of a $Cu(II)-O_2-I-TPQsq$ intermediate. This intermediate is reduced by an electron transfer concomitant with a proton transfer from a tyrosine (see figure) through a network of hydrogen bonds involving a water molecule. After the TS, the tyrosine abstracts an electron and a proton from TPQ to generate a $Cu(II)-O_2-II-TPQox$ complex. The tyrosine plays a key role in this process by shuttling an electron and proton from the TPQ cofactor to the $Cu(II)-O_2-I$ moiety. By substituting copper with cobalt, it was also found that Co(II) is functional. From early experimental[235] and DFT[236] work, it was already known that copper is redox-active in the biogenesis of the TPQ cofactor. A tyrosine will be transformed to the TPQ by binding axially to copper. Dioxygen will bind equatorially. This structure leads to a Cu(II) complex with a superoxo and a tyrosyl radical. The superoxo ligand will then attack the tyrosyl and form a bridging peroxide. At that point the O–O bond is cleaved accompanied by proton transfers. This is followed by a water attack, leading to a hydroxide attack on the ring, followed by proton transfers. Biogenesis is completed by yet another O_2 molecule, which takes two protons and two electrons from the quinone, forming H_2O_2 and TPQ.[205]

Another mononuclear copper enzyme that has been studied with quantum chemistry is galactose oxidase (GO), which catalyzes the two-electron oxidation of primary alcohols to their corresponding aldehydes, coupled with reduction of dioxygen to hydrogen peroxide.[237] One of the copper ligands is a cysteine-linked tyrosyl radical that interacts in an antiferromagnetic fashion with the Cu(II) center. Calculations using both the cluster approach[238] and QM/MM[6] have helped establish the reaction mechanism of GO. The substrate binds equatorially to the Cu(II) ion and loses a proton to an axial tyrosine residue. Hydrogen atom transfer from the substrate to the tyrosyl radical then takes place, resulting in a substrate ketyl radical, which subsequently reduces the copper to yield Cu(I) and the aldehyde product. Finally, molecular oxygen oxidizes the Cu(I) and the tyrosine to regenerate the Cu(II) ion and the tyrosyl radical, also giving the hydrogen peroxide product. In addition to the mechanistic studies, the calculations have also provided insight into the electronic and magnetic properties of the cysteine-linked tyrosyl radical in GO.[239]

The one-electron reduction of NO_2^- to NO, one of the steps in the denitrification process, occurs in two classes of enzymes. One class uses a d_1-heme cofactor, and it is briefly discussed in section 4.3 above. The other class uses two copper atoms, and it is briefly discussed here. The catalytic reaction in copper nitrite reductase takes place at the T2 copper site, with three histidine ligands and a second-shell aspartate, shown in Figure 66.[240] A DFT study of the reaction mechanism in the copper nitrite reductase has been performed using a model complex including the residues shown in Figure 66 plus two water molecules.[241] A mechanism was suggested where two protons enter via the aspartate (Asp92) near the active site and reach the NO_2^- substrate via a water molecule. The first proton enters after, or in concert with, the binding of the negatively charged substrate to Cu(II), and the second proton enters after the one-electron reduction to Cu(I) by an external electron, entering via the other
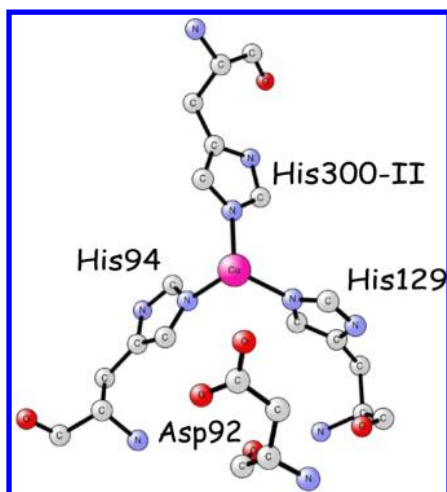
Figure 66. X-ray structure of the catalytically active T2 copper site in copper nitrite reductase.[240]

Figure 67. X-ray structure of the active site of tyrosinase.[246]

copper site. The calculations suggest that there is no hydroxyl intermediate formed, but rather a state with a protonated nitrite bound to the reduced copper. The N−O bond is cleaved when the second proton, located on the aspartate (Asp92), attacks the protonated nitrite oxygen, forming NO and a water molecule.[241]

Quercetin 2,3-dioxygenase (2,3QD) is the only known dioxygenase which contains copper. The substrate quercetin is a 3,5,7,3′,4′-pentahydroxyflavone. The full mechanism has been studied by cluster models using hybrid DFT.[242] The active site has a single copper ligated to three histidines, one glutamate, and one water. First, the substrate replaces the water and binds to copper. Like in several other metal enzymes, O_2 binds in a bridging mode between the metal and the substrate. However, unlike the other ones, the O−O bond is not cleaved at that stage. Instead, the metal−oxygen bond is first broken to form a second C−O bond to the substrate. Only at that stage is the O−O bond broken in an unusually complicated TS, where besides the O−O bond also two C−O bonds are broken and CO is released. In the entire area of chemistry, this is a very uncommon form of TS.

6.2. Enzymes Containing a Copper Dimer

The type 3 copper proteins have a dinuclear copper complex at the active site, with each copper coordinated by three histidine ligands. Tyrosinase, catechol oxidase, and hemocyanin belong to this class. Tyrosinase catalyzes two different reactions, the oxidation of phenol (tyrosine) to *o*-quinone and the conversion of *o*-diphenols to *o*-quinones (Figure 68), both with the help of dioxygen. Catechol oxidase has only diphenolase activity, while hemocyanin is an oxygen transport protein without phenolase or diphenolase activity. Crystal structures of hemocyanin[243,244] and catechol oxidase[245] have existed for some time, while the X-ray structure of tyrosinase is rather recent;[246] see Figure 67.

The mechanisms of both tyrosinase and catechol oxidase have been studied using hybrid DFT methods.[247,248] An interesting aspect of the experimentally advocated mechanisms for both enzymes[249,250] is that protons are suggested to enter and leave the complex, while the overall reaction does not need any protons from the outside. This would imply that there should be many amino acids that could function as catalytic bases around the active site. However, the crystal structures show no such base. From calculations for catechol oxidase, it has been possible to suggest a mechanism in which no protons are entering or leaving the dicopper complex, thereby keeping the charge of the complex
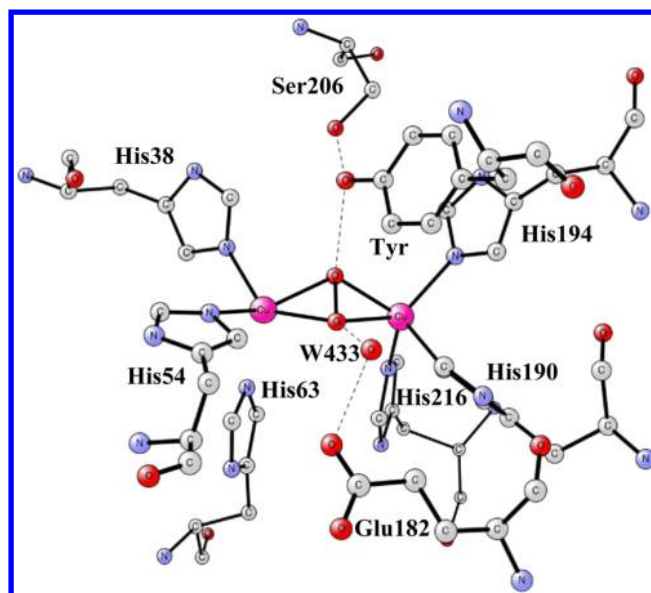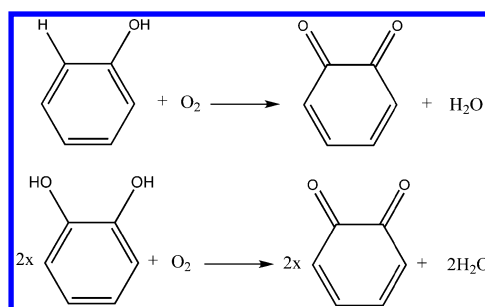
Figure 68. Reactions catalyzed by tyrosinase.

constant at +2. For tyrosinase, on the other hand, this has so far not been found possible.

The theoretical mechanism for catechol oxidase[248] is shown in Figure 69. It starts out with the binding of an oxygen molecule to
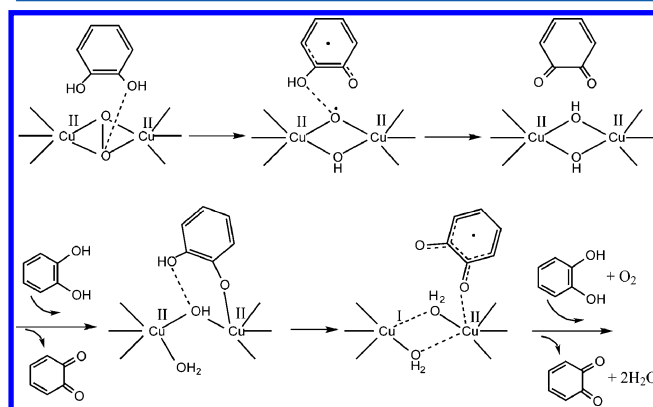
Figure 69. DFT-suggested catalytic cycle for catechol oxidase.[248]

a $Cu_2(I,I)$ complex, forming a $Cu_2(II,II)$ complex with a bridging $\mu\text{-}\eta^2\text{:}\eta^2$ peroxide. In the first half-cycle, the peroxide abstracts a hydrogen atom (both proton and electron) from the first chatechol substrate in a PCET step. The product is a $Cu_2(I,II)$ with a radical quinol complex. After this, the O−O bond of the peroxide is cleaved in the rate-limiting step of the catalytic cycle. The product is a $Cu_2(II,II)$ complex with metal-bridging

hydroxide and oxyl radical ligands. The substrate remains a radical quinol. By having two radicals, the enzyme avoids the costly formation of the Cu(III) state. In the next and final step of the first half-cycle, the second hydrogen atom of the substrate is abstracted by the oxyl radical in another PCET step. The quinone is released, and the second substrate enters. In the first step of the second half-cycle, a proton of the substrate is abstracted by one of the hydroxide groups to form a water ligand bound to a Cu$_2$(II,II) state and with a copper–catecholate bond to the substrate. In the final step, the second proton is abstracted from the substrate by the remaining bridging hydroxide, and the Cu–O bond to the substrate is broken, leading to a second quinone, which is released, leaving an electron to the complex. After release of the two water molecules, the product Cu$_2$(I,I) complex can start a new catalytic cycle.

In contrast to catechol oxidase, no mechanism consistent with the experimental X-ray structure and a neutral incoming substrate has yet been found. However, if the phenol is deprotonated prior to arrival at the active site, a mechanism with a reasonable rate-limiting barrier can be obtained.[247b] Alternatively, and almost equivalently, a low-barrier mechanism can be obtained if the starting structure is a Cu$_2$(I,I) complex with a bridging hydroxide;[247a] see Figure 70. In that case, the
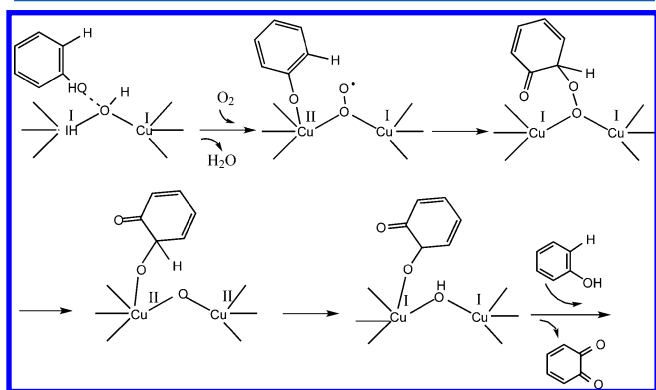

Figure 70. DFT-suggested catalytic cycle for tyrosinase.[247a]

mechanism starts with an abstraction of a proton from the phenol substrate by the bridging hydroxide, which will then leave as a water molecule. In this process the phenolate substrate will bind to one of the coppers, followed by binding of O$_2$ as a superoxide. In the next step, the superoxide will attack the phenol substrate to form a bridging peroxide with one of its oxygens binding to the substrate and the other one between the coppers. This is followed by the rate-limiting step in which the peroxide is cleaved. The remaining bridging oxide will finally abstract a hydrogen atom from the substrate, which will be transformed to a catechol and leave, and the cycle can start all over again. A major problem with this mechanism is that there will never be an asymmetrically bridging peroxide, as strongly implicated by experiments. Alternatives with a proton abstraction of the incoming phenol by a histidine ligand, or by an amino acid quite far away from the active site, have been tried but so far without success.[247b] In a QM/MM study, a mechanism appeared to be demonstrated where the requirement for an outside base was not necessary.[251] The mechanism suggested was quite similar to one which was attempted earlier and rejected. A new interesting feature of the QM/MM mechanism was that, in the transition state, one of the histidines left copper to form a hydrogen bond to the peroxide. However, it was later shown that there are technical

errors in the QM/MM study, and the new mechanism had to be abandoned.[247b] The problem of how the incoming phenol substrate is deprotonated therefore remains for future studies.

6.3. Multinuclear Copper Enzymes

Enzymes containing multinuclear copper sites catalyze a variety of redox reactions.[252] Quantum chemical calculations have been used to study the properties of the active sites and elucidate the reaction mechanisms of a number of these enzymes.[253−255] A very recent review by Rulisek and Ryde summarizes the results on multicopper oxidases.[256]

Here, we discuss the results concerning a multicopper reductase, namely, nitrous oxide reductase (N2OR). This bacterial enzyme catalyzes the reduction of N$_2$O to N$_2$, which constitutes the final step of the denitrification process in the global nitrogen cycle.[257] N2OR is a homodimer, and each monomer contains two multinuclear copper centers, Cu$_A$ and Cu$_Z$.[258] Cu$_A$ is a binuclear copper center involved in transferring electrons to the catalytic center, while Cu$_Z$ is a μ_4-sulfide-bridged tetranuclear copper cluster (see Figure 71) where the substrate reaction is believed to take place. The catalytically active form of Cu$_Z$ has been demonstrated to be the fully reduced state (4Cu(I) oxidation state).[259]
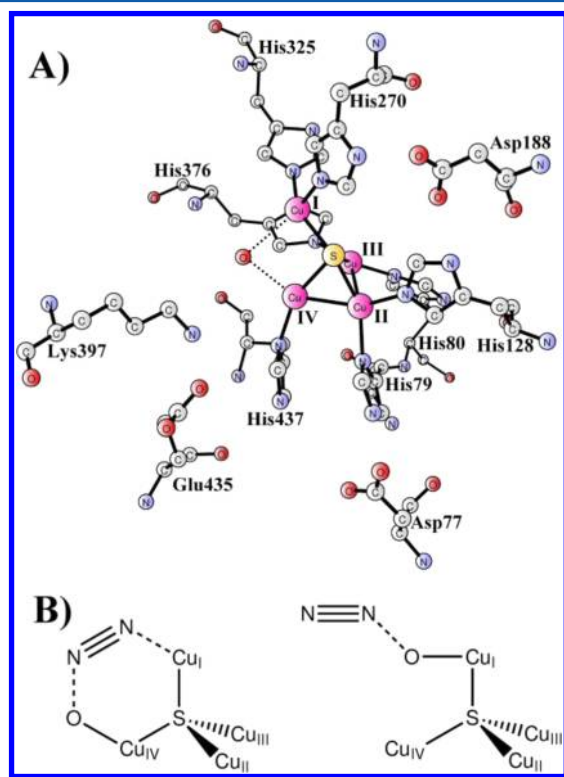
Figure 71. (A) Active site structure of N2OR.[258c]. (B) Two alternative mechanisms for N2OR.

DFT calculations have been performed on models of Cu$_Z$, both to study the electronic structure of the cluster and to investigate the mechanism of the N−O bond cleavage step. Solomon and co-workers performed calculations on a [Cu$_4$S-(Im)$_7$]$^{2+}$ model and concluded that the N$_2$O substrate binds to the fully reduced Cu$_Z$ in a bent μ-(1,3)-O,N fashion, bridging the Cu$_I$ and Cu$_{IV}$ centers, upon which the N−O bond dissociates (see Figure 71).[254]

Later calculations by Ertem et al.[255] using both the [Cu$_4$S(Im)$_7$]$^{2+}$ model and also a somewhat larger model that

includes some second-shell residues have suggested an alternative mechanism in which the N$_2$O substrate coordinates terminally to the Cu$_Z$ cluster before N−O bond cleavage takes place (Figure 71). This pathway resembles the mechanism suggested for the reduction of N$_2$O by a dinuclear $[(LCu)_2S_2]^+$ biomimetic model complex.[260] It turns out that the bridging and terminal mechanisms have quite similar barriers and the DFT calculations can therefore not conclusively determine which one is operative for N2OR.

Very interestingly, recent crystallographic studies have shown that the Cu$_Z$ cluster under some conditions contains an additional sulfur atom that bridges the Cu$_I$ and Cu$_{IV}$ centers.[261] More experimental and theoretical work is thus required to establish the significance of this new finding in the reaction mechanism of N2OR.

7. HYDROGENASE

Combining water oxidation, releasing protons and electrons as discussed above, with the use of these protons and electrons to produce dihydrogen is an attractive way to diminish the need for fossil fuels. In nature, hydrogenases are the enzymes designed to form dihydrogen from protons and electrons in a reversible process:
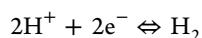
$$2H^+ + 2e^- \Leftrightarrow H_2$$

Hydrogenases are divided into three main classes by specifying the transition-metal content of their active sites. These classes are the NiFe,[262] the FeFe,[263] and the iron−sulfur cluster-free[264] hydrogenases. Of the two main classes, the NiFe enzymes are primarily used for hydrogen oxidation and the FeFe enzymes for proton reduction.[265−267] There are two rather recent reviews on theoretical work on hydrogenases.[268,269] Most of the work has considered H−H bond cleavage, but the reaction is commonly considered as easily reversible by external means, and the mechanism is therefore assumed to also be the same for the H−H bond formation. The pathway for H−H bond cleavage will be discussed here.

The X-ray structure of the active site for the reduced form of NiFe hydrogenase is shown in Figure 72 for a Ser499Ala mutant.[270] There are four cysteinate ligands, two of them bridging between nickel and iron and two of them terminally bound to nickel. Iron has in addition three diatomic ligands, two of which are cyanides and one of which is a carbonyl, which is very unusual for a biological metal complex.

The catalytic cycle of NiFe hydrogenases is usually illustrated by a scheme such as that in Figure 73A.[271] It contains the three intermediate states observed experimentally, Ni$_a$-C*, Ni$_a$-S, and Ni$_a$-SR. Ni$_a$-C* is the EPR-active resting state, which has a bridging hydride between the metals. The EPR-silent Ni$_a$-SR state is reached by reduction of Ni$_a$-C*, while Ni$_a$-S, which is also EPR-silent, is obtained by oxidation. To complete the cycle, Ni$_a$-SR can be reached by adding dihydrogen to Ni$_a$-S. Several other states have been observed under varying conditions but will not be discussed here. An interesting alternative scenario to the one in Figure 73A, shown in panel B in the same figure, has also been suggested.[272] The main difference between these mechanisms is that Ni$_a$-S does not participate in the active cycle. Instead, catalysis starts only after an initial reaction between Ni$_a$-S and dihydrogen where Ni$_a$-C* is created. Ni$_a$-C* is then only in equilibrium with Ni$_a$-SR during turnover.[273] The structural implications of this suggestion have not been completely clear, but it has been suggested that a bridging hydride may be present all the time during catalysis.[272]
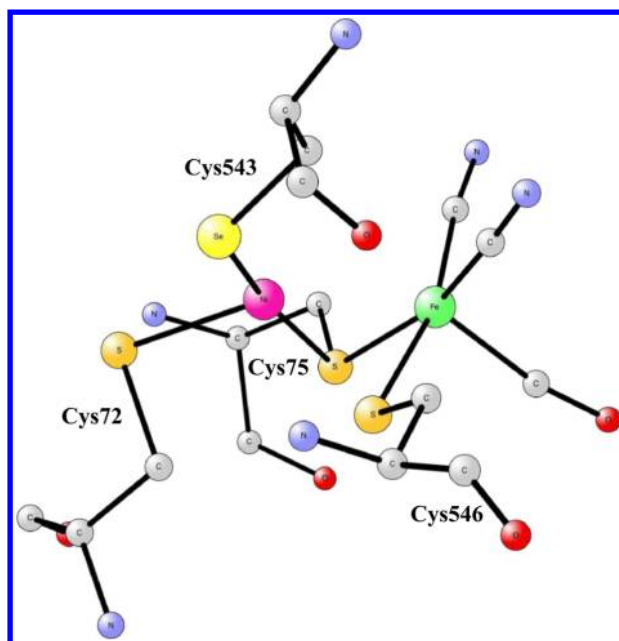
Figure 72. X-ray structure of the active site for the reduced form of NiFe hydrogenase.[270]
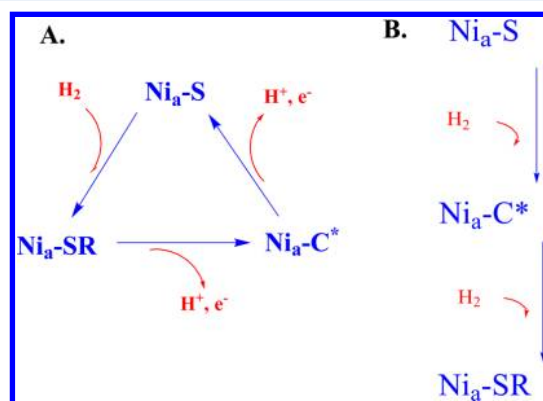
Figure 73. Two different types of catalytic cycles for NiFe hydrogenases suggested by experiments.

In the early period, all theoretical studies on NiFe hydrogenases led to a mechanism following the scheme in Figure 73A. A TS with a heterolytic cleavage of the H−H bond was found. There is essential agreement among all studies on most details of this type of mechanism.[268,269] The cleavage of the H−H bond is heterolytic, with one hydrogen ending up as a bridging hydride and the other one as a proton on Cys543. Due to the character of the TS, it can be referred to as the heterolytic mechanism. A disagreement exists concerning the oxidation state of nickel, which is assigned as Ni(II) by most, but with one suggestion being Ni(III).[274] However, in the case of Ni(III) the reaction is unlikely to be reversible. This would imply a quite different mechanism for H−H bond formation, which can not be ruled out at the present stage. The iron is in all studies a low-spin Fe(II).

Even though near consensus on the mechanism was reached, the search for the mechanism in Figure 73B was continued. An interesting state in the context of a new mechanism was a Ni(I) state, appearing at the end of the heterolytic mechanism. These attempts were eventually successful.[275] A TS for oxidative addition was found leading to two hydrides, one bridging and one bound to nickel. The new mechanism would then start out with

only one turn of the heterolytic mechanism and after that proceed with cycles based on the oxidative addition mechanism, leading to a scheme such as that in Figure 73B.

There is a large current interest in the oxidized states of NiFe hydrogenase. The reason for this is the problem of connecting the hydrogenase process with water oxidation, producing O_2. Two main oxidized states of the NiFe cofactor have been identified. In Ni-B, there is a bridging hydroxide between Ni(III) and Fe(II). It is inactive for H_2 cleavage, but is relatively easily activated. The Ni-A state is more problematic and is difficult to reactivate. At the highest resolution (1.1 Å) it was concluded that Ni-A is a peroxide with one oxygen bridging between the metals and the other oxygen on nickel.[270,276] Only a few theoretical studies of the formation and reactivation of Ni-A have been made,[277,278] and the peroxide structure was used only in one of them.[268,278] The calculations suggested that the peroxide was easily cleaved upon acceptance of one electron and one proton into one terminal (on nickel) and a bridging hydroxide ligand. Its activation requires two additional electrons and protons and is therefore slow. Several oxygen-insensitive NiFe hydrogenases have been found. In these enzymes, the Ni-A state is activated by two electrons supplied from the proximal FeS cluster.[279] Two DFT studies have been performed for the details of the mechanism of how the electrons are released from the cluster.[280,281]

The second major class of hydrogenases are the FeFe hydrogenases, which are generally found to catalyze H−H bond formation in contrast to most of the NiFe hydrogenases. The X-ray structure of the active site, known as the H cluster, is shown in Figure 74.[282,283] It consists of an iron dimer, the
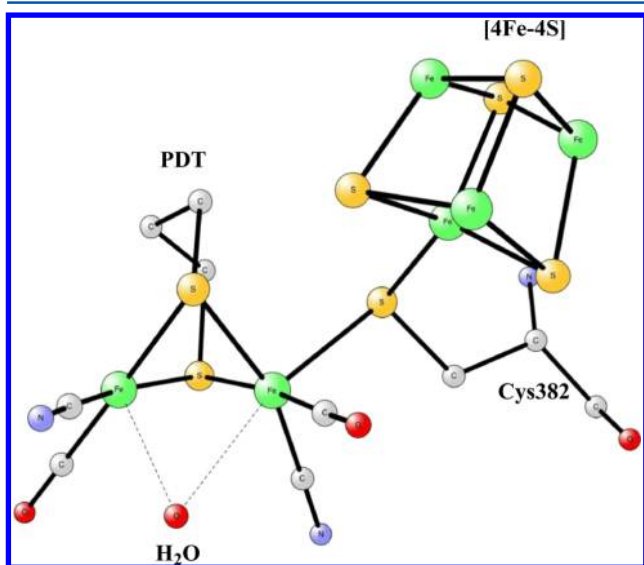

Figure 74. X-ray structure of the active site for FeFe hydrogenase.[282]

putative site of H_2 cleavage, bridged by a cysteine to an FeS cluster. Each iron atom of the dimer is coordinated by one terminally bound cyanide and one terminally bound carbonyl ligand. The two irons are bridged by a five-atom dithiolate.

The most accepted mechanism for H_2 cleavage has been suggested by Hall et al.[284] Dihydrogen is cleaved heterolytically by an Fe(II)Fe(II) form of the iron dimer, where a proton ends up at the nitrogen of the μ-SCH_2NHCH_2S (PDT) and the second hydrogen becomes a bridging hydride. De Gioia et al.[285] suggested an alternative to the Hall mechanism, in which the μ-

CO-Fe(I)Fe(II) form rearranges to a form where the bridging carbonyl moves to a terminal position. Dihydrogen is then cleaved between the irons, where the bridging CO was originally bound. One proton ends up on a sulfur atom of the bridging dithiolate, rather than on a nitrogen of PDT as in the Hall mechanism; the other one becomes a bridging hydride.

There are some clear similarities between the mechanisms for NiFe hydrogenase and FeFe hydrogenase. In both mechanisms, there is an activation step that leads to a catalytically active metal dimer at the (I,II) redox level. In the oxidative addition part of the NiFe mechanism and in the Hall version of the FeFe mechanism, the activation of H_2 furthermore occurs at a terminal position of one of the metals. A major difference is that heterolytic cleavage is used throughout in the FeFe case, while this type of cleavage is only used in the initial activation in the NiFe case.

8. NITROGENASE

The molybdenum-containing nitrogenase catalyzes the reduction of dinitrogen to two ammonia molecules and one hydrogen molecule consuming eight electrons, eight protons, and sixteen ATP molecules. The active site catalyst of the most common nitrogenases is a cluster with seven iron atoms and one molybdenum atom connected by sulfide bridges; see Figure 75. The mechanism of this enzyme is one of the most challenging ones in the area of biochemistry.
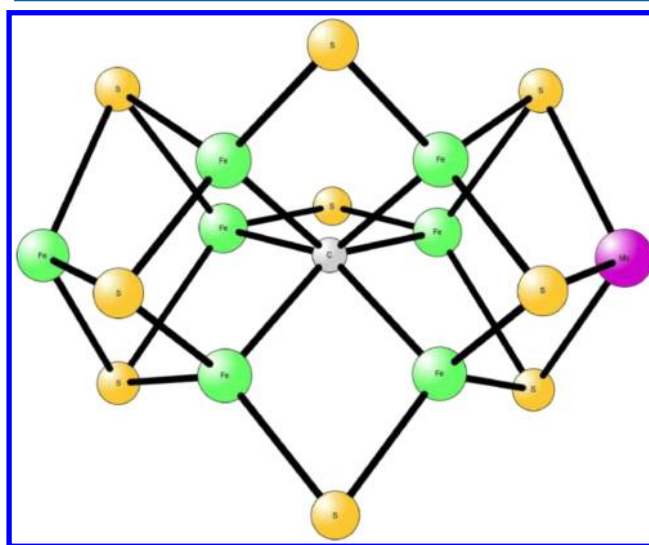
Figure 75. FeMo cofactor of nitrogenase.

A very surprising feature of the FeMo cofactor is that there is an atom X in the center of the cluster, whose origin was unknown until quite recently. In fact, even the presence of X was unknown as long as a decade after the first 2.7 Å resolution structure of the enzyme appeared in 1992.[286] The central atom was seen only when a very high resolution structure with 1.16 Å resolution was determined in 2002.[287] X was suggested to be carbon, nitrogen, or oxygen. Two years ago, a combined X-ray emission and theoretical study finally revealed that X is a carbon atom.[288] In parallel, an X-ray structure with an even higher resolution came to the same conclusion.[289]

The current status on the mechanism of nitrogenase has recently been reviewed by Seefeldt et al.[290] and computational studies by Tuzcek.[291] A severe difficulty has been to trap any intermediates in the reaction, but there has recently been some progress. Spectroscopic analysis of species derived from four

substrates, dinitrogen, hydrazine, methyldiazene, and diazene, reveals that each is bound with a single type of nitrogen. All substrates appear to bind to a single FeS face. The state activated for N_2 binding is obtained by reduction and accumulation of four protons and electrons. The limited current information tends to favor a pathway where the N−H bonds are formed on the two nitrogens in an alternating fashion, with cleavage of the N−N bond at a late stage. This is in contrast to the industrial Haber−Bosch process for ammonia synthesis, where this cleavage occurs before the protonations of the nitrogens.[292,293]

During the first decade after the first X-ray structure, mainly two theoretical groups, the groups of Noodleman[294] and Dance,[295] were involved in mechanistic work. This work was, of course, quite hampered by the fact that the presence of X was not known. Nevertheless, very detailed investigations of optimal redox states were made using advanced broken symmetry techniques. Without the interstitial atom, Noodleman et al.,[294] using a variety of density functionals, concluded that the resting state should be $Mo^{4+}6Fe^{2+}Fe^{3+}$, which produced metal hyperfine and Mössbauer isomer shifts that agreed well with experimental results. Interestingly, the geometries were also in excellent agreement with experiments even without the atom X. A later study including the atom X gave the assignment $Mo^{4+}4Fe^{2+}3Fe^{3+}$. It was found difficult to conlude the identity of X on the basis of comparisons to spectroscopic results.

Using DFT with the BLYP functional, Dance derived a chemical mechanism for ammonia formation.[295] An important part of the mechanism is that the protons are supplied via a chain of residues including water molecules that end at two specific sulfurs. A full diagram including transition states for 21 steps was calculated. N_2 was found to be η^2-coordinated to an endo position of one Fe atom of a prehydrogenated FeMo cofactor, and the reaction passes through N_2H_2 and N_2H_4 intermediates. Hydrogenation of N_2 and the intermediates is intramolecular and does not involve direct protonations from surrounding residues. The interstitial X atom was chosen as nitrogen.

Blöchl et al. studied N_2 binding to the FeMo cofactor using Car−Parrinello molecular dynamics with the PBE functional and found axial and bridging binding modes of N_2 to the prismane Fe sites followed by cleavage of a protonated sulfur bridge.[296] The binding to molybdenum was found to be endergonic. Two different pathways for ammonia formation were found, one starting with a bridging N_2 and the other one an axially bound N_2. These pathways were found to connect at an early stage in the mechanism. Nørskov et al. studied the entire mechanism, including N_2H_2 and N_2H_4 intermediates.[297] Protonations were found to occur in an alternating fashion, with the initial reduction of N_2 being rate-limiting. Ahlrichs et al. studied several steps in the catalytic cycle using the BP86 and B3LYP functionals.[298] They found N_2 binding in a cavity of the cluster with a $Mo^{4+}6Fe^{2+}Fe^{3+}$ configuration. A nitrogen was used as X. Full protonations of one nitrogen of N_2 was found to occur before protonation of the other nitrogen started. Recently, Szilagyi et al., using the BP86 and B3LYP functionals, suggested a more oxidized resting state, $Mo^{4+}2Fe^{2+}5Fe^{3+}$, than those from earlier proposals.[299] A central carbon atom was used, and the homocitrate ligand was found hydroxyl-protonated. Even more recently, Yan et al.[300] performed a combined experimental (FTIR) and theoretical (DFT with PBE) study of CO bound to the FeMo cofactor. The structures with the best match between measured and calculated frequencies were used to identify the binding positions.

9. METHYL-COENZYME M REDUCTASE

Methyl-coenzyme M reductase (MCR) is a nickel-containing enzyme responsible for the formation of the major part of the naturally produced methane. X-ray structures have been obtained for several forms of the enzyme.[301a,b,c] The active site of MCR (see Figure 76) contains a nickel porphyrinoid cofactor
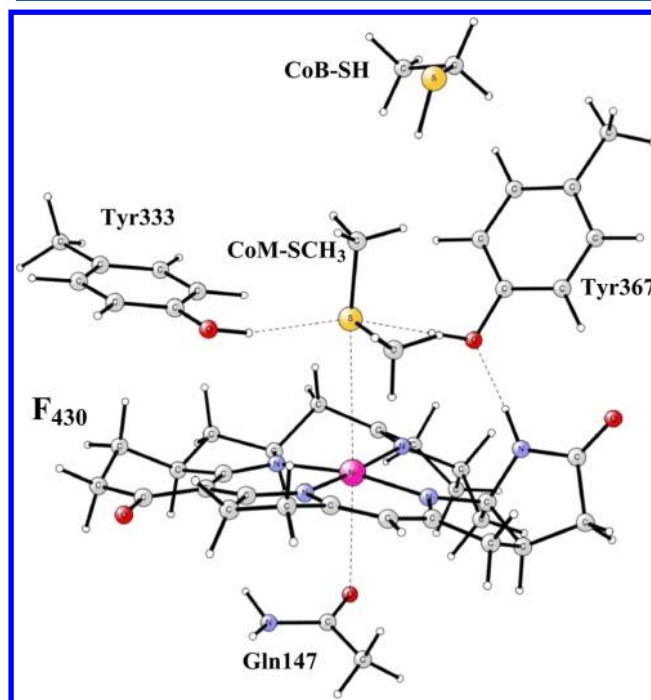
Figure 76. Optimized structure of the active site of MCR.

denoted F_{430}. It is deeply buried and accessible from the outside through a long channel, through which the two substrate cofactors CoB and CoM can reach F_{430}. The sulfurs of the cofactors end up about 6 Å from each other. For the optimal structure, the sulfur of CoM is hydrogen-bonded by two tyrosines and a weakly bound glutamine is the proximal ligand of nickel. In view of the presence of Ni−C bonds in other Ni enzymes and of Co−C bonds in many derivatives of the well-known and somewhat related coenzyme B_{12}, the mechanisms suggested experimentally for methanogenesis have all involved formation of a Ni−CH₃ bond at some point, usually followed by protonolysis to release methane[301a,b,c,302a] following the equation

$$CoB-S-H + CoM-S-CH_3 \rightarrow CoB-S-S-CoM + CH_4$$
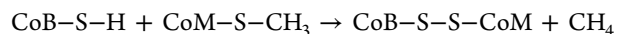
The energetics obtained by DFT calculations suggests a quite different mechanism.[303a] In this mechanism, an intermediate is formed with a Ni−S bond rather than a Ni−C bond. The Ni−S bond is formed to CoM concertedly with the cleavage of the S−CH₃ bond. Also, in near concert with that reaction step, the methyl radical released abstracts a hydrogen from CoB and forms methane. Subsequently, in a separate second step, the S−S bond is formed between CoM−S and CoB−S. The mechanism is not in conflict with any known experimental results. Instead, a few key experimental results support this mechanism. First, the methyl group is found to be inverted at carbon. Second, optimized transition states for smaller models without any constraints have a distance between the sulfurs of 6.2 Å, which is very close to the distance found in the X-ray structure of

MCR.[301b] This means that the enzyme is perfectly set up for this type of TS. The mechanism is also in line with results obtained for the substrates $CHF_2-S-CoM$ and $CF_3-S-CoM$, where the latter is inactive. This is explained by a too high barrier for inversion of the CF_3 radical.

The theoretical mechanism has been questioned several times on the basis of new experiments. First, a $Ni-CH_3$ intermediate was found for the substrates CH_3I.[302b] However, model calculations showed that there is a large energetic difference between the formation of the $Ni-CH_3$ intermediate for the natural substrate and for CH_3I. In the latter case, it is indeed a stable intermediate, while in the former it is far from stable.[303b] In another experiment, the reverse reaction with anaerobic oxidation was observed.[301d,e] The different steps of the mechanism found were consistent with the theoretical mechanism, including two separate transition states and a rather stable intermediate, but the relative rates for the forward and backward reaction were not in agreement with the calculations in the first MCR study.[303a] Calculations were therefore repeated with a more accurate treatment of entropy and dispersion, leading to excellent agreement with the new experiments.[303c]

10. COENZYME B$_{12}$-DEPENDENT ENZYMES

Cobalamin, commonly known as vitamin B_{12}, is a cofactor involved in many enzymatic reactions. It contains a low-spin hexacoordinated Co(III) that is equatorially ligated by four nitrogen atoms of a corrin ring. An optimized structure of this cofactor is shown in Figure 77. The different chemical forms of
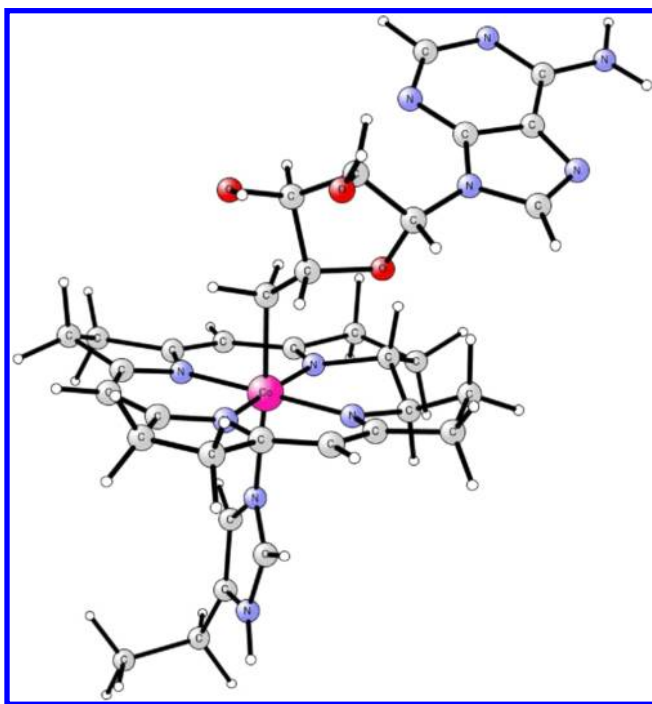

Figure 77. Optimized structure of the AdoCbl cofactor.

cobalamin differ by the upper axial ligand, which can be a methyl group or an adenosyl group. The electronic structure and spectroscopic properties of cobalamin have been extensively studied using quantum chemical methods, and the results were recently summarized by Brunold and co-workers.[304] In (5′-deoxyadenosyl)cobalamin (AdoCbl)-dependent enzymes, the reaction starts by a homolytic cleavage of the Co−C bond,

leading to the formation of a deoxyadenosyl radical (Ado radical) and Co(II). This Ado radical then abstracts a hydrogen atom from the substrate to generate a substrate radical, which subsequently rearranges to form a product radical. In the final step, the hydrogen atom is transferred back from Ado to the product radical, and the resulting Ado radical recombines with Co(II) to close the catalytic cycle.

A large number of theoretical studies have been concerned with the energetics of the Co−C dissociation process. It has been studied in both model complexes and different enzyme environments, using various levels of theory.[305] A recent review by Jensen and Ryde summarizes many of the results and puts them in a historic context.[308]

Different DFT functionals gave considerably different results. B3LYP, for example, yielded bond dissociation energies (BDEs) that were underestimated by about 20 kcal/mol,[305a] while BP86 gave much better results. However, very importantly, it was later found that inclusion of empirical dispersion corrections to B3LYP (B3LYP-D) gave much better agreement with experiments.[306,307] The trans axial N-base was found to have only a minor effect on the homolytic Co−C bond dissociation,[305b,c,d,f] while the effect is more significant for the heterolytic cleavage.[305d]

In enzymes, the Co−C bond dissociation energy has to be considerably reduced for catalysis to take place. Experimentally, this is now known to be accompanied by a large structural change of the enzyme caused by binding of the substrate. Crystal structures with substrates show broken Co−C bonds.[309,310] Several theoretical studies have analyzed the reason for the reduction of the Co−C bond strength.[311−315] Other quantum chemical studies have also considered the reaction mechanisms and other aspects of the chemistry of B_{12}-dependent enzymes.[306,316−321] For example, using QM/MM calculations, Jensen and Ryde studied glutamate mutase and obtained a BDE of the Co−C bond of about 2 kcal/mol, which can be compared to 32 kcal/mol in vacuum.[311] Several factors were suggested to contribute to this large catalytic effect, such as the cage effect, the electrostatic stabilization of the dissociated product, the stabilization of the protein itself, and the distortion of the coenzyme. Empirical valence bond calculations on the methylmalonyl-CoA mutase enzyme by Warshel and co-workers instead suggested that strain effects had no major impact and that the catalytic power is associated with electrostatic interaction between the substrate and the enzyme surroundings.[312]

Very recently, calculations were done on the D-ornithine 4,5-aminomutase using both molecular dynamics and QM/MM calculations. The reconstruction pathway was followed from the open, catalytically inactive, to the closed, catalytically active, forms of the enzyme.[315] It was concluded that the Co−C bond is activated through the synergy of steric and electrostatic effects arising from tighter interactions with the surrounding enzyme.

11. TUNGSTEN-DEPENDENT ENZYMES

Three families of tungsten-dependent enzymes are known to date: aldehyde oxidoreductases (AORs), formate dehydrogenases (FDHs), and acetylene hydratases (AHs).[322] In all of them, the tungsten ion is ligated by two pterin cofactors through the four dithiolene sulfur atoms. The reaction mechanisms and various aspects of catalysis and selectivity of members of both AORs and AHs have been studied recently using quantum chemical methods, and the main findings are summarized here.

Acetylene hydratase catalyzes the transformation of acetylene to acetaldehyde.[323] The crystal structure shows that, besides the

two pterin molecules, a cysteine residue and a water molecule are bound to the tungsten ion (see Figure 78).[324] A second-shell Asp residue is also known to play an important role in the reaction.[325]
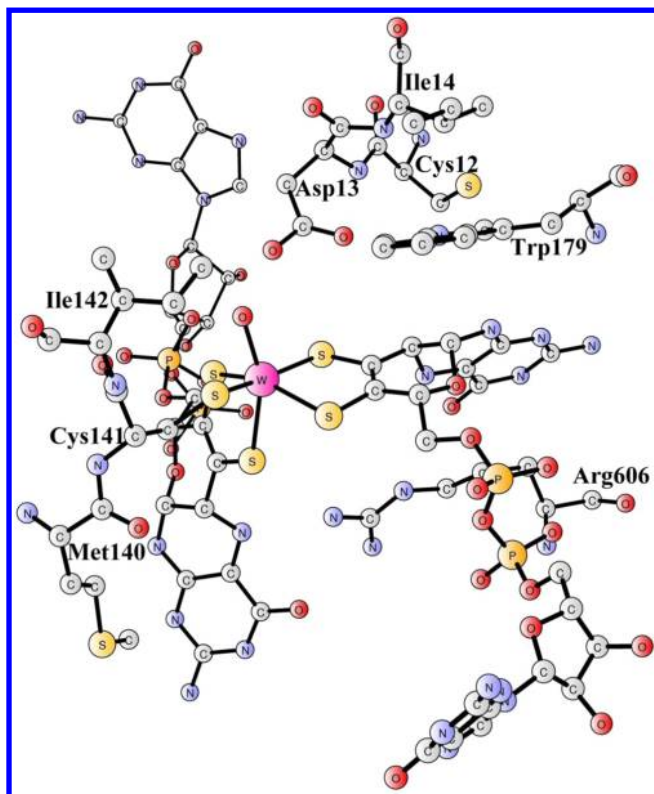

Figure 78. Crystal structure of the acetylene hydratase active site.[324]

DFT-cluster model calculations have suggested a first-shell mechanism as shown in Figure 79.[326] The reaction starts with a ligand exchange in which the acetylene substrate displaces the tungsten-bound water molecule. The water then performs a nucleophilic attack on the acetylene concomitantly with a proton transfer to the anionic second-shell aspartate to yield a vinyl alcohol anion intermediate. The proton is subsequently transferred back from Asp to the vinyl alcohol anion to afford vinyl alcohol. Finally, a fast tautomerization of vinyl alcohol to acetaldehyde can take place either at the tungsten center, with the assistance of the aspartate, or outside the enzyme. This mechanism thus requires the second-shell Asp residue to be in the ionized form to activate the nucleophilic water. This was in conflict with pH titration calculations using continuum electrostatics and statistical thermodynamics, which indicated that the

residue should be protonated.[324] It should also be mentioned that this mechanism was subsequently reinvestigated using QM/MM methodology, and the conclusions were essentially the same as with the cluster approach.[327] Interestingly, a similar first-shell mechanism has also been suggested for acetylene hydration catalyzed by a biomimetic tungsten complex.[328]

Other possible reaction mechanisms have also been examined, such as a second-shell electrophilic addition mechanism,[326] a first-shell water attack mechanism with the assistance of a neutral Asp13 residue,[329] and a first-shell mechanism via a $W=C=CH_2$ vinylidene intermediate,[330] but all these possibilities turned out to be associated with high-energy barriers.

With the suggested mechanism of Figure 79, it was also possible to rationalize some aspects of the observed chemoselectivity of AHs.[331] For example, the facts that propyne binds better to the tungsten than acetylene and that the barrier for its hydration is higher explain why propyne functions as a competitive inhibitor of AHs.

A member of the AOR family has also been studied quantum chemically, namely, formaldehyde ferredoxin oxidoreductase (FOR), which catalyzes the oxidation of formaldehyde to formic acid using water as the oxygen source and ferredoxin as the electron acceptor.[332] Liberation of two electrons and two protons from the $W(IV)-H_2O$ complex results in the formation of a $W(VI)=O$ species, which is believed to be the starting oxidant for the following reaction.[333] The reaction mechanism of FOR has been investigated using the cluster approach, and among several reaction pathways considered, a possible first-shell mechanism was suggested.[334] After coordination of the aldehyde substrate to the tungsten, the $W=O$ performs a nucleophilic attack on the formaldehyde carbon, resulting in the formation of a tetrahedral intermediate. An important second-shell glutamate residue then acts as a general base to abstract a proton from the intermediate, coupled with a two-electron reduction of the tungsten ion.

In a number of molybdenum and tungsten enzymes, these two metals can replace each other.[335−338] This is, however, not the case for FOR, since incorporation of Mo instead of W results in the inactivation of the enzyme.[339] Calculations have been used to rationalize this result, and on the basis of experimental and calculated redox potentials, it is suggested the reason is that the formation of the $Mo(VI)=O$ species is highly unfavorable.[340]

12. ZINC-DEPENDENT ENZYMES

Zinc is silent to most spectroscopic methods, and calculations can therefore provide an excellent complement to the experimental work. Over the years, a large number of different zinc-dependent enzymes have been studied with quantum
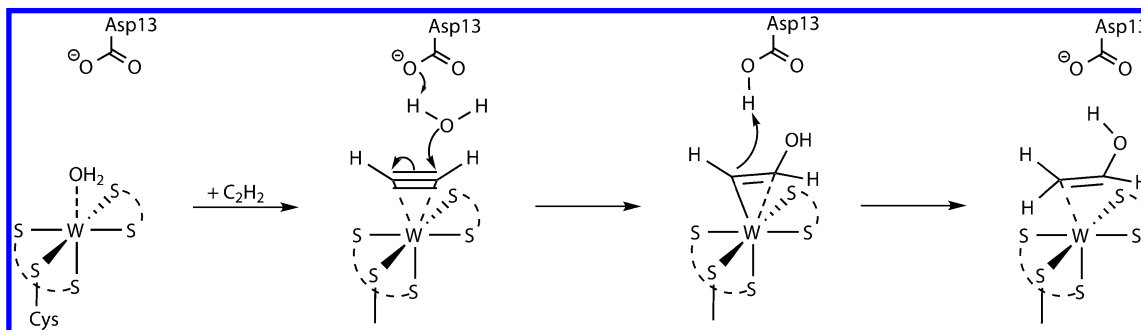

Figure 79. Reaction mechanism of acetylene hydratase suggested on the basis of DFT calculations.[326]
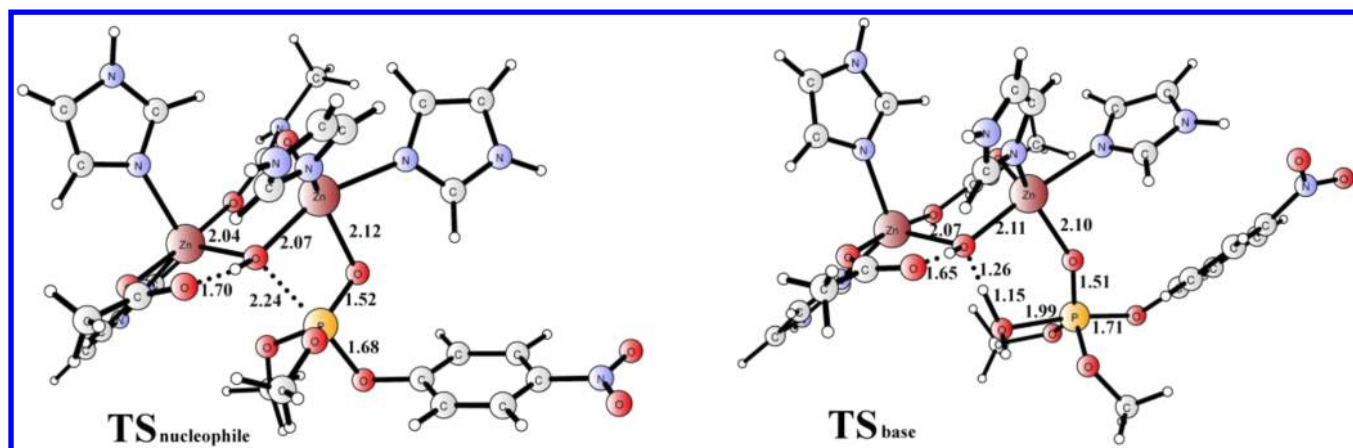
Figure 80. Optimized transition states for nucleophilic vs base mechanisms in phosphotriesterase.[343a,c]

chemical methods, using both the cluster approach and various QM/MM techniques.[341,342] It is beyond the scope of this review to discuss all these studies. Instead, we will only give a couple of examples with focus on multinuclear zinc enzymes to illustrate the capabilities of the methods and some of the main mechanistic results.

In recent years, quantum chemistry has been employed to investigate the reaction mechanisms of quite a number of dinuclear zinc enzymes. These include phosphotriesterase (PTE),[343] RNase Z,[344] aminopeptidase from *Aeromonas proteolytica* (AAP),[345] dihydroorotase (DHO),[346] human renal dipeptidase (hrDP),[347] glyoxalase II,[348] *N*-acylhomoserine lactone hydrolase (AHL lactonase),[349] alkaline phosphatase (AP),[350] β-lactamase,[351] glutamate carboxypeptidase II,[352] prolidase,[353] nucleotide pyrophosphatase/phosphodiesterase,[354] and methionine aminopeptidase.[355]

The enzymes catalyze a wide variety of hydrolytic reactions, such as phosphate, peptide, and ester bond hydrolyses. A common feature of these enzymes is that the two zinc centers are bridged by a hydroxide ion, and one of the important questions in this regard is whether the bridging hydroxide acts as a nucleophile, attacking the substrate directly, or as a general base, activating a water molecule that in turn performs the nucleophilic attack.[356] Other questions concern the specific roles of the two zinc ions and how they cooperate to affect the reactions.[357] The calculations have in many cases been able to resolve these issues.

Here, as an illustrative example, we briefly discuss the case of phosphotriesterase, for which both cluster and QM/MM calculations have been performed in recent years. PTE catalyzes the hydrolysis of a range of organophosphate triesters, which are extremely toxic compounds.[358] Besides the hydroxide, the two zinc ions are bridged by a carboxylated lysine residue.[359]

Cluster calculations using an active site model consisting of the zinc ions and truncated models of the first-shell residues (less than 100 atoms; see Figure 80) were performed to investigate the PTE reaction mechanism.[343a] The substrate was found to bind monodentately to one of the zinc ions, and the reaction was calculated to follow a stepwise associative mechanism in which the bridging hydroxide performs the nucleophilic attack to yield a pentacoordinate phosphorus intermediate which then decays to release the leaving group. The resulting diethyl phosphate was found to bind bidentately to the binuclear metal center.

Similar calculations were performed to study the alternative mechanism in which a Zn-bound water molecule performs the nucleophilic attack, activated by a proton transfer to the bridging hydroxide (Figure 80).[356b] The calculations showed that this scenario is associated with a higher barrier than the direct nucleophilic attack by the bridging hydroxide (ca. 6 kcal/mol higher).[343c] The conclusions of the cluster calculations are consistent with crystal structures showing the product phosphodiester binding to the dizinc center through two of its oxygens.[343c]

Several QM/MM studies employing different setups have also been performed to investigate the PTE reaction.[343d,e,f] Overall, these studies predict reasonable barriers for the hydrolysis reaction, although in some cases the barriers are a bit overestimated compared to experimental rate constants.[343d,f] Mechanistically, they differ in some important aspects from the cluster calculations and differ also among each other. For example, one study yielded a stepwise mechanism,[343d] while in two others the mechanism was found to be concerted; i.e., no pentacoordinate intermediate was located.[343e,f] Also, all studies found the diethyl phosphate product to bind monodentately to the metal center, which seems to be at odds with the crystallographic results.[358]

Similar mechanistic studies have been performed for trinuclear zinc enzymes. Three such enzymes are known to date, namely, phospholipase C (PLC),[360] nuclease P1 (NP1),[361] and endonuclease IV (Endo IV),[362] all of which are involved in phosphate hydrolysis. The reaction mechanisms of all three enzymes have been studied theoretically, PLC[363] and NP1[364] with the cluster approach and Endo IV with QM/MM.[365]

Here, we briefly mention the main results obtained from the calculations for the case of PLC. This enzyme catalyzes the hydrolysis of phospholipids to yield diacylglycerol and a phosphorylated headgroup.[366] One of the mechanistic questions is whether the substrate phosphate oxygen displaces the hydroxide bridging Zn1 and Zn3 (Figure 81).[367,368] If this is the case, a Zn1-bound water molecule acts as the nucleophile for the reaction.[367] Alternatively, the hydroxide bridging Zn1 and Zn3 can perform the nucleophilic attack.[368] Both mechanistic scenarios have been considered using a cluster model of the enzyme.[363] In line with the experimental estimates,[369] and similarly to the PTE case, the calculated barrier for the hydroxide attack was found to be ca. 6 kcal/mol lower than for the attack by a terminal water.
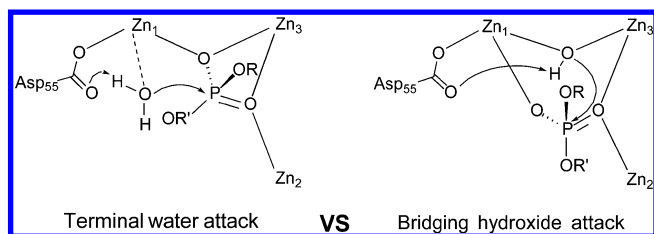
Figure 81. Two possible mechanisms considered for phosphate hydrolysis by PLC.[363]

13. MOLYBDENUM-DEPENDENT ENZYMES

Molybdenum enzymes catalyze a wide range of redox reactions.[370,371] The active sites usually contain one or two pterin cofactors bound to the metal (Figure 82). In recent years,
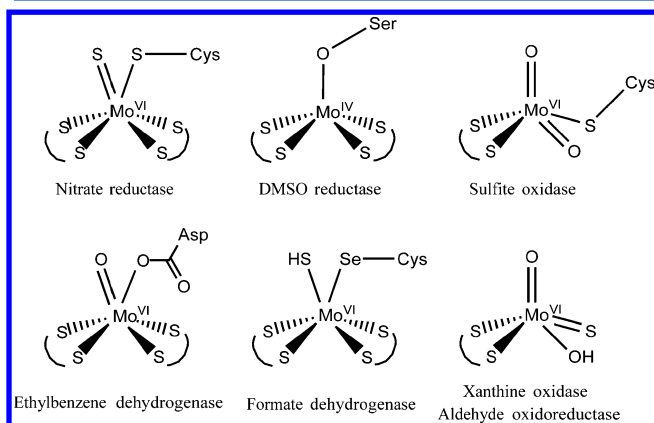

Figure 82. Schematic drawing of the metal sites of some Mo-dependent enzymes.

quite a number of Mo-dependent enzymes have been studied using quantum chemical methodology, such as nitrate reductase,[372] DMSO reductase,[373] sulfite oxidase,[374] ethylbenzene dehydrogenase,[375] aldehyde oxidoreductase,[376] xanthine oxidase,[377] and formate dehydronegase.[378] The results have been summarized in a recent review by Metz and Thiel.[379] Here, to illustrate some of the concepts, we mention briefly some of the important findings for a couple of these enzymes that turn out to have quite different reaction mechanisms, namely, nitrate reductase[372] and xanthine oxidase.[377]

Nitrate reductase catalyzes the reduction of nitrate to nitrite, which is one of the important reactions in biological nitrogen metabolism. Russo and co-workers first reported DFT calculations[372a] to elucidate the N—O bond cleavage mechanism using the crystal structure available at that time, in which the Mo(VI) ion is ligated to two pterin cofactors and a cysteine.[380] The calculations showed that the oxygen transfer proceeds via a first-shell mechanism and that the singlet state is slightly preferred compared to the triplet state. However, subsequent revision of the crystal structure revealed an extra sulfido ligand to the metal.[381] On the basis of this new information, new calculations have shown that Mo(VI) can be reduced to Mo(IV) by forming a S—S bond between the sulfido and cysteine ligand, which creates an empty site for the coordination of the nitrate substrate.[372d,e,f] Subsequently, an oxygen atom is transferred from nitrate to Mo(IV) to generate the Mo(VI)=O product complex. For this first-shell mechanism, two different scenarios have been considered, one with and one without the interaction of cysteine with the metal. This interaction facilitates the oxygen

transfer and lowers the barrier somewhat.[372f] The second-shell mechanism, in which the oxygen atom is transferred to the sulfur atom, turns out to have a very high barrier.[372e,f] From the calculations it could thus be concluded that the first-shell mechanism involving direct coordination of substrate to metal is more favorable.

The second example is xanthine oxidase, which catalyzes the transformation of xanthine to uric acid in the last step of the purine nucleotide metabolism. Its molybdenum coordination environment is composed of a pterin molecule, an oxo group, a hydroxide, and a sulfido group (Figure 82).[382] QM/MM calculations by Metz and Thiel have demonstrated that a second-shell glutamate residue plays an important role in the deprotonation of the Mo—hydroxide to generate an oxyanion, which then performs a nucleophilic attack on the substrate to form a tetrahedral intermediate.[377b] In the subsequent step, a hydride is transferred from the substrate to the sulfido group, coupled with two-electron transfer to the metal. This hydride transfer was calculated to be the rate-limiting step.[377b] One of the important findings from the calculations is that the substrate has several different tautomers and also different protonation states, and two possible orientations are accessible in the enzyme–substrate complex.[377b] The substrate-binding mode suggested on the basis of calculations has been used to rationalize the fact that the enzyme has activity toward 1-methyl-2,6-dioxopurine but no activity toward 1-methyl-6-oxopurine.[383,384] QM/MM calculations have also been used to investigate the effects of replacing the hydride acceptor sulfido ligand by an oxo or a selenido ligand.[377c] The oxo form was found to have a very high barrier, in agreement with experimental findings,[385] while the selenido form gave a barrier similar to that of the sulfido form.

14. SUMMARY

In the present review we have described the status of high-accuracy, mainly DFT, studies of mechanisms for metalloenzymes. From being of marginal importance, this area has during the past 15 years gradually grown to become of at least equal importance compared to traditional spectroscopic studies. By far most of the studies of redox mechanisms until now have used the cluster approach, but there are also a significant number where the QM/MM approach has been used, in particular for P450.

The most challenging mechanisms studied have been the ones where electrons and protons are entering or are being released. The methods available are at present not sufficiently accurate for determining absolute pK_a values and redox potentials. However, relative values are often of high accuracy, which can be used to make the calculations predictive. This normally requires empirical information as described in the sections on photosynthesis (PSII) and respiration (CcO). The knowledge of the total driving force, obtained from experimental redox potentials, is enough to accurately position every second line in the energy diagrams from just relative values. The use of an additional empirical parameter is enough to also determine the individual pK_a values and redox potentials. Still, there are cases where even the normally most reliable DFT methods fail to be sufficiently accurate even for relative energies. In those cases even more empirical information is necessary at present. This area is probably the one in which most effort will be spent in the future for further improvements of the methods for treating mechanisms of redox-active enzymes.

AUTHOR INFORMATION

Corresponding Author

*E-mail: ps@organ.su.se. Phone: +46-8-16 26 16.

Notes

The authors declare no competing financial interest.

Biographies

Margareta R. A. Blomberg received her Ph.D. in the field of quantum chemistry at the Department of Physics, Stockholm University, in 1983. After a postdoctoral period at the IBM San Jose research laboratory with Bowen Liu, she returned to Per Siegbahn's group at Stockholm University. Most of her scientific work has been devoted to the elucidation of reaction mechanisms of transition-metal systems. In recent years her research has focused on biochemical systems, in particular redox-active metalloenzymes.

Tomasz Borowski received his Ph.D. (2003) at Jagiellonian University, Kraków, Poland, under the supervision of Ewa Broclawik. Between 2003 and 2006 he was a postdoctoral fellow with Per E. M. Siegbahn at Stockholm University. Since 2006 he has worked in the Jerzy Haber Institute of Catalysis and Surface Chemistry, Polish Academy of Sciences, in Kraków. His research interest focuses on catalytic mechanisms of metalloenzymes.

Fahmi Himo was born in 1973. He received his Ph.D. degree at Stockholm University in 2000. He then spent two years as a Wenner-Gren postdoctoral fellow at the Scripps Research Institute (with Prof. Louis Noodleman) and three years back in Sweden as a Wenner-Gren Fellow at the Royal Institute of Technology (KTH). From 2005 to 2009 he was an assistant professor at KTH before he moved to his current position at Stockholm University. He is the 2011 recipient of the Göran Gustafsson Prize in chemistry. His research interests lie in the fields of quantum chemical modeling of enzyme reactions and homogeneous catalysis.
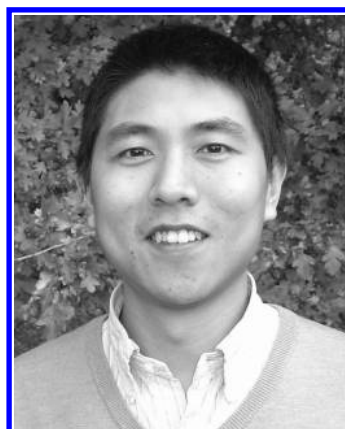
Rong-Zhen Liao was born in Hubei, China, in 1983. He received his B.Sc. degree at Beijing Normal University in 2005 and his Ph.D. degree at Stockholm University in 2010. He then spent two years as a postdoctoral fellow at the Max-Planck-Institut für Kohlenforschung in Mülheim an der Ruhr (with Prof. Walter Thiel). Currently, he is a postdoctoral researcher with Prof. Per Siegbahn at Stockholm University. His research interests focus on the modeling of enzyme catalysis and artificial water oxidation using quantum chemical methods.

Per E. M. Siegbahn was born in Stockholm, Sweden. He did his undergraduate studies at Uppsala University and received his Ph.D. degree at Stockholm University in 1973 (with Björn Roos). He was a postdoctoral fellow at the University of California, Berkeley (with Henry F. Schaefer, III), and at IBM, San Jose (with Bowen Liu). He returned to Stockholm and has remained ever since. His interests have varied over the years from the development of ab initio quantum chemical methods to applications on gas-phase reactions of small molecules, to models of heterogeneous catalysts, and to the present interest in mechanisms for redox-active enzymes.

REFERENCES

(1) Becke, A. D. *J. Chem. Phys.* **1993**, *98*, 5648−5652.

(2) Bauschlicher, C. W., Jr.; Ricca, A.; Partridge, H.; Langhoff, S. R. In *Recent Advances in Density Functional Methods, Part II*; Chong, D. P., Ed.; World Scientific Publishing Co.: Singapore, 1997; p 165.

(3) Siegbahn, P. E. M. Electronic Structure Calculations for Molecules Containing Transition Metals. In *Advances in Chemical Physics*; Prigogine, I., Rice, S. A., Eds.; J. Wiley: New York, 1996; Vol. *XCIII*, p 333.

(4) Siegbahn, P. E. M.; Crabtree, R. H. *J. Am. Chem. Soc.* **1997**, *119*, 3103.

(5) Warshel, A.; Levitt, M. *J. Mol. Biol.* **1976**, *103*, 227.

(6) Rothlisberger, U.; Carloni, P.; Doclo, K.; Parinello, M. *J. Biol. Inorg. Chem.* **2000**, *5*, 236.

(7) Mulholland, A. J.; Grant, G. H.; Richards, W. G. *Protein Eng.* **1993**, *6*, 133.

(8) Senn, H. M.; Thiel, W. *Top Curr. Chem.* **2007**, *268*, 173.

(9) Cramer, C. J.; Truhlar, D. G. *J. Comput.-Aided Mol. Des.* **1992**, *6*, 629.

(10) Tomasi, J.; Menucci, B.; Cammi, R. *Chem. Rev.* **2005**, *105*, 2999.

(11) Noodleman, L.; Lovell, T.; Han, W.-G.; Li, J.; Himo, F. *Chem. Rev.* **2004**, *104*, 459. Noodleman, L.; Han, W.-G. *J. Biol. Inorg. Chem.* **2006**, *11*, 674. Torres, R. A.; Lovell, T.; Noodleman, L.; Case, D. A. *J. Am. Chem. Soc.* **2003**, *125*, 1923.

(12) Siegbahn, P. E. M.; Blomberg, M. R. A. *Chem. Rev.* **2000**, *100*, 421.

(13) Siegbahn, P. E. M. *J. Comput. Chem.* **2001**, *22*, 1634.

(14) Warshel, A. *Computer Modeling of Chemical Reactions in Enzymes and Solutions*; Wiley: New York, 1991.

(15) Hughes, T. F.; Friesner, R. A. *J. Chem. Theory Comput.* **2012**, *8*, 442.

(16) Rod, T. H.; Ryde, U. *Phys. Rev. Lett.* **2005**, *94*, 138302.

(17) Stephens, P. J.; Jollie, D. R.; Warshel, A. *Chem. Rev.* **1996**, *96*, 2491.

(18) Siegbahn, P. E. M.; Blomberg, M. R. A. In *Computational Modeling for Homogeneous Catalysis and Biocatalysis*; Morokuma, K., Musaev, J., Eds.; Wiley-VCH: Weinheim, Germany, 2008; p 57.

(19) Blomberg, M. R. A.; Siegbahn, P. E. M. *J. Comput. Chem.* **2006**, *27*, 1373.

(20) Siegbahn, P. E. M.; Blomberg, M. R. A. *Dalton Trans.* **2009**, 5832.

(21) Siegbahn, P. E. M.; Blomberg, M. R. A.; Blomberg, M. L. *J. Phys. Chem. B* **2003**, *107*, 10946.

(22) Siegbahn, P. E. M. *Chem.—Eur. J.* **2008**, *27*, 8290.

(23) Siegbahn, P. E. M. *Acc. Chem. Res.* **2009**, *42*, 1871.

(24) Siegbahn, P. E. M. *Biochim. Biophys. Acta, Bioenerg.* **2013**, *1827*, 1003.

(25) Himo, F.; Siegbahn, P. E. M. *J. Biol. Inorg. Chem.* **2009**, *14*, 643.

(26) Siegbahn, P. E. M.; Himo, F. *Wiley Interdiscip. Rev.: Comput. Mol. Sci.* **2011**, *1*, 323.

(27) Pelmenschikov, V.; Blomberg, M. R. A.; Siegbahn, P. E. M. *J. Biol. Inorg. Chem.* **2002**, *7*, 284.

(28) Siegbahn, P. E. M.; Borowski, T. *Acc. Chem. Res.* **2006**, *39*, 729.

(29) Liao, R.-Z.; Thiel, W. *J. Phys. Chem. B* **2013**, *117*, 3954.

(30) Sevastik, R.; Himo, F. *Bioorg. Chem.* **2007**, *35*, 444.

(31) Hopmann, K. H.; Himo, F. *J. Chem. Theory Comput.* **2008**, *4*, 1129.

(32) Georgieva, P.; Himo, F. *J. Comput. Chem.* **2010**, *31*, 1707.

(33) Liao, R.-Z.; Yu, J.-G.; Himo, F. *J. Chem. Theory Comput.* **2011**, *7*, 1494.

(34) Velichkova, P.; Himo, F. *J. Phys. Chem. B* **2005**, *109*, 8216.

(35) Reiher, M.; Salomon, O.; Hess, B. A. *Theor. Chem. Acc.* **2001**, *107*, 48.

(36) Grimme, S. *J. Chem. Phys.* **2006**, *124*, 034108. Schwabe, T.; Grimme, S. *Phys. Chem. Chem. Phys.* **2007**, *9*, 3397.

(37) Siegbahn, P. E. M.; Blomberg, M. R. A.; Chen, S.-L. *J. Chem. Theory Comput.* **2010**, *6*, 2040.

(38) (a) Blomberg, M. R. A.; Siegbahn, P. E. M.; Styring, S.; Babcock, G. T.; Å kermark, B.; Korall, P. *J. Am. Chem. Soc.* **1997**, *119*, 8285. (b) Siegbahn, P. E. M.; Crabtree, R. H. *J. Am. Chem. Soc.* **1999**, *121*, 117. (c) Siegbahn, P. E. M. *Inorg. Chem.* **2000**, *39*, 2923. (d) Siegbahn, P. E. M. *Chem.—Eur. J.* **2006**, *12*, 9217. (e) Siegbahn, P. E. M. *ChemPhysChem* **2011**, *12*, 3274. (f) Brena, B.; Siegbahn, P. E. M.; Å gren, H. *J. Am. Chem. Soc.* **2012**, *134*, 17157. (g) Siegbahn, P. E. M. *J. Am. Chem. Soc.* **2009**, *131*, 18238. (h) Schinzel, S.; Schraut, J.; Arbuznikov, A. V.; Siegbahn, P. E. M.; Kaupp, M. *Chem.—Eur. J.* **2010**, *16*, 10424. (i) Siegbahn, P. E. M. *J. Am. Chem. Soc.* **2013**, *135*, 9442.

(39) Kok, B.; Forbush, B.; McGloin, M. *Photochem. Photobiol.* **1970**, *11*, 457.

(40) Yachandra, V. K.; Sauer, K.; Klein, M. P. *Chem. Rev.* **1996**, *96*, 2927.

(41) Ferreira, K. N.; Iverson, T. M.; Maghlaoui, K.; Barber, J.; Iwata, S. *Science* **2004**, *303*, 1831.

(42) Loll, B.; Kern, J.; Saenger, W.; Zouni, A.; Biesiadka, J. *Nature* **2005**, *438*, 1040−1044. Guskov, A.; Kern, J.; Gabdulkhakov, A.; Broser, M.; Zouni, A.; Saenger, W. *J. Nat. Struct. Biol.* **2009**, *16*, 334.

(43) Umena, Y.; Kawakami, K.; Shen, J.-R.; Kamiya, N. *Nature* **2011**, *473*, 55.

(44) (a) Ames, W.; Pantazis, D. A.; Krewald, V.; Cox, N.; Messinger, J.; Lubitz, W.; Neese, F. *J. Am. Chem. Soc.* **2011**, *133*, 19743. (b) Pantazis, D. A.; Orio, M.; Petrenko, T.; Zein, S.; Lubitz, W.; Messinger, J.; Neese, F. *Phys. Chem. Chem. Phys.* **2009**, *11*, 6788. (c) Cox, N.; Rapatskiy, L.; Su, J.-H.; Pantazis, D. A.; Sugiura, M.; Kulik, L.; Dorlet, P.; Rutherford, A. W.; Neese, F.; Boussac, A.; Lubitz, W.; Messinger, J. *J. Am. Chem. Soc.* **2011**, *133*, 3635.

(45) (a) Grundmeier, A.; Dau, H. *Biochim. Biophys. Acta, Bioenerg.* **2012**, *1817*, 88. (b) Dau, H.; Grundmeier, A.; Loja, P.; Haumann, M. *Philos. Trans. R. Soc., B* **2008**, *363*, 1237. (c) Dau, H.; Limberg, C.; Reier, T.; Risch, M.; Roggan, S.; Strasser, P. *ChemCatChem* **2010**, *2*, 724. (d) Iuzzolini, L.; Dittmer, J.; Dörner, W.; Meyer-Klaucke, W.; Dau, H. *Biochemistry* **1998**, *37*, 17112. (e) Haumann, M.; Liebisch, P.; Müller, C.; Barra, M.; Grabolle, M.; Dau, H. *Science* **2005**, *310*, 1019.

(46) Galstyan, A.; Robertazzi, A.; Knapp, E. W. *J. Am. Chem. Soc.* **2012**, *134*, 7442.

(47) Li, X.; Siegbahn, P. E. M. *J. Am. Chem. Soc.* **2013**, *135*, 13804.

(48) Rapatskiy, L.; Cox, N.; Savitsky, A.; Ames, W. M.; Sander, J.; Nowacyzk, M. M.; Rögner, M.; Boussac, A.; Neese, F.; Messinger, J.; Lubitz, W. *J. Am. Chem. Soc.* **2012**, *134*, 16619.

(49) Gatt, P.; Stranger, R.; Pace, R. J. *J. Photochem. Photobiol., B* **2011**, *104*, 80. Petrie, S.; Gatt, P.; Stranger, R.; Pace, R. J. *Phys. Chem. Chem. Phys.* **2012**, *14*, 11333.

(50) (a) Kusunoki, M. *Biochim. Biophys. Acta, Bioenerg.* **2007**, *1767*, 484. (b) Kusunoki, M. *J. Photochem. Photobiol., B* **2011**, *104*, 100.

(51) (a) Sproviero, E. M.; Newcomer, M. B.; Gascon, J. A.; Batista, E. R.; Brudvig, G. W.; Batista, V. S. *Photosynth. Res.* **2009**, *102*, 455. (b) Sproviero, E. M.; Gascon, J. A.; McEvoy, J. P.; Brudvig, G. W.; Batista, V. S. *J. Am. Chem. Soc.* **2008**, *130*, 3428. (c) Sproviero, E. M.; Gascon, J. A.; McEvoy, J. P.; Brudvig, G. W.; Batista, V. S. *J. Am. Chem. Soc.* **2008**, *130*, 6728. (d) Li, X.; Sproviero, E. M.; Ryde, U.; Batista, V. S.; Chen, G. *Int. J. Quantum Chem.* **2013**, *113*, 474. (e) Luber, S.; Rivalta, I.; Umena, Y.; Kawakami, K.; Shen, J.-R.; Kamiya, N.; Bruce, D.; Brudvig, G. W.; Batista, V. S. *Biochemistry* **2011**, *50*, 6308. (f) Rivalta, I.; Amin, M.; Luber, S.; Vassiliev, S.; Pokhrel, R.; Umena, Y.; Kawakami, K.; Shen, J.-R.; Kamiya, N.; Bruce, D.; Brudvig, G. W.; Gunner, M. R.; Batista, V. S. *Biochemistry* **2011**, *50*, 6312.

(52) Yano, J.; Kern, J.; Sauer, K.; Latimer, M. J.; Pushkar, Y.; Biesiadka, J.; Loll, B.; Saenger, W.; Messinger, J.; Zouni, A.; Yachandra, V. K. *Science* **2006**, *314*, 821.

(53) Sproviero, E. M.; Shinopoulos, K.; Gascon, J. A.; McEvoy, J. P.; Brudvig, G. W.; Batista, V. S. *Philos. Trans. R. Soc., B* **2008**, *363*, 1149.

(54) McConnell, I. L.; Grigoryants, V. M.; Scholes, C. P.; Myers, W. K.; Chen, P.-Y.; Whittaker, J. W.; Brudvig, G. W. *J. Am. Chem. Soc.* **2012**, *134*, 1504.

(55) Messinger, J.; Robblee, J. H.; Bergmann, U.; Fernandez, C.; Glatzel, P.; Visser, H.; Cinco, R. M.; McFarlane, K. L.; Bellacchio, E.; Pizarro, S. A.; Cramer, S. P.; Sauer, K.; Klein, M. P.; Yachandra, V. K. *J. Am. Chem. Soc.* **2001**, *123*, 7804.

(56) Diner, B. A. *Biochim. Biophys. Acta, Bioenerg.* **2001**, *1503*, 147.

(57) Rappaport, F.; Lavergne, J. *Biochim. Biophys. Acta, Bioenerg.* **2001**, *1503*, 246.

(58) Blomberg, M. R. A.; Siegbahn, P. E. M.; Babcock, G. T.; Wikström, M. *J. Am. Chem. Soc.* **2000**, *122*, 12848.

(59) Wirstam, M.; Blomberg, M. R. A.; Siegbahn, P. E. M. *J. Am. Chem. Soc.* **1999**, *121*, 10178.

(60) Shaik, S.; Kumar, D.; de Visser, S. P.; Altun, A.; Thiel, W. *Chem. Rev.* **2005**, *105*, 2279.

(61) Shaik, S.; Cohen, S.; Wang, Y.; Chen, H.; Kumar, D.; Thiel, W. *Chem. Rev.* **2010**, *110*, 949.

(62) Blomberg, M. R. A.; Siegbahn, P. E. M. *Biochim. Biophys. Acta, Bioenerg.* **2013**, *1827*, 826.

(63) Guallar, V.; Baik, M-H; Lippard, S. J.; Friesner, R. A. *Proc. Natl. Acad. Sci. U.S.A.* **2003**, *100*, 6998.

(64) Loew, G. H.; Harris, D. L. *Chem. Rev.* **2000**, *100*, 407.

(65) Rittle, J.; Green, M. T. *Science* **2010**, *330*, 933.

(66) Schlichting, I.; Berendzen, J.; Chu, K.; Stock, A. M.; Maves, S. A.; Benson, D. E.; Sweet, R. M.; Ringe, D.; Petsko, G. A.; Sligar, S. G. *Science* **2000**, *287*, 1615.

(67) Davydov, R.; Makris, T. M.; Kofman, V.; Werst, D. E.; Sligar, S. G.; Hoffman, B. M. *J. Am. Chem. Soc.* **2001**, *123*, 1403.

(68) Bach, R. D.; Dmitrenko, O. *J. Am. Chem. Soc.* **2006**, *128*, 1474.

(69) Wang, D.; Zheng, J.; Shaik, S.; Thiel, W. *J. Phys. Chem. B* **2008**, *112*, 5126.

(70) Harris, D.; Loew, G. H. *J. Am. Chem. Soc.* **1998**, *120*, 8941.

(71) Ogliaro, F.; de Visser, S. P.; Cohen, S.; Sharma, P. K.; Shaik, S. *J. Am. Chem. Soc.* **2002**, *124*, 2806.

(72) Kumar, D.; Hirao, H.; de Visser, S. P.; Zheng, J.; Wang, D.; Thiel, W.; Shaik, S. *J. Phys. Chem. B* **2005**, *109*, 19946.

(73) Zheng, J.; Wang, D.; Thiel, W.; Shaik, S. *J. Am. Chem. Soc.* **2006**, *128*, 13204.

(74) Bach, R. D. *J. Phys. Chem. A* **2010**, *114*, 9319.

(75) Groves, J. T.; McClusky, G. A. *J. Am. Chem. Soc.* **1976**, *98*, 859.

(76) Shaik, S.; Cohen, S.; de Visser, S. P.; Sharma, P. K.; Kumar, D.; Kozuch, S.; Oligaro, F.; Danovich, D. *Eur. J. Inorg. Chem.* **2004**, 207.

(77) Li, C.; Shaik, S. *RSC Adv.* **2013**, *3*, 2995.

(78) Lonsdale, R.; Harvey, J. N.; Mulholland, A. J. *J. Phys. Chem. Lett.* **2010**, *1*, 3232.

(79) Zurek, J.; Foloppe, N.; Harvey, J. N.; Mulholland, A. J. *Org. Biomol. Chem.* **2006**, *4*, 3931.

(80) Altun, A.; Guallar, V.; Friesner, R. A.; Shaik, S.; Thiel, W. *J. Am. Chem. Soc.* **2006**, *128*, 3924.

(81) Lonsdale, R.; Harvey, J. N.; Mulholland, A. J. *J. Chem. Theory Comput.* **2012**, *8*, 4637.

(82) de Visser, S. P.; Ogliaro, F.; Sharma, P. K.; Shaik, S. *Angew. Chem., Int. Ed.* **2002**, *41*, 1947.

(83) Cohen, S.; Kozuch, S.; Hazan, C.; Shaik, S. *J. Am. Chem. Soc.* **2006**, *128*, 11028.

(84) Kumar, D.; Karamzadeh, B.; Sastry, G. N.; de Visser, S. P. *J. Am. Chem. Soc.* **2010**, *132*, 7656.

(85) Bathelt, C.; Mulholland, A. J.; Harvey, J. N. *J. Phys. Chem. A* **2008**, *112*, 13149.

(86) Olah, J.; Mulholland, A. J.; Harvey, J. N. *Proc. Natl. Acad. Sci. U.S.A.* **2011**, *108*, 6050.

(87) Wikström, M. K. F. *Nature* **1977**, *266*, 271.

(88) Proshlyakov, D. A.; Pressler, M. A.; Babcock, G. T. *Proc. Natl. Acad. Sci. U.S.A.* **1998**, *95*, 8020.

(89) Karpefors, M.; Ädelroth, P.; Namslauer, A.; Zhen, Y.; Brzezinski, P. *Biochemistry* **2000**, *39*, 14664.

(90) Proshlyakov, D. A.; Pressler, M. A.; DeMaso, C.; Leykam, J. F.; DeWitt, D. L.; Babcock, G. T. *Science* **2000**, *290*, 1588.

(91) Qin, L.; Liu, J.; Mills, D. A.; Proshlyakov, D. A.; Hiser, C.; Ferguson-Miller, S. *Biochemistry* **2009**, *48*, 5121.

(92) Hansson, Ö.; Karlsson, B.; Vänngård, T.; Malmström, B. G. *EMBO J.* **1982**, *1*, 1295.

(93) Blomberg, M. R. A.; Siegbahn, P. E. M.; Wikström, M. *Inorg. Chem.* **2003**, *42*, 5231.

(94) Blomberg, M. R. A.; Siegbahn, P. E. M. *Biochim. Biophys. Acta, Bioenerg.* **2010**, *1797*, 129.

(95) Siegbahn, P. E. M.; Blomberg, M. R. A. *Chem. Rev.* **2010**, *110*, 7040.

(96) Brzezinski, P. *Trends Biochem. Sci.* **2004**, *29*, 380.

(97) Babcock, G. T.; Wikström, M. *Nature* **1992**, *356*, 301.

(98) Kaila, V. R. I.; Verkhovsky, M. I.; Wikström, M. *Chem. Rev.* **2010**, *110*, 7062.

(99) Kaukonen, M. *J. Phys. Chem. B* **2007**, *111*, 12543.

(100) Fee, J. A.; Case, D. A.; Noodleman, L. *J. Am. Chem. Soc.* **2008**, *130*, 15002.

(101) Blomberg, M. R. A.; Siegbahn, P. E. M. *Biochim. Biophys. Acta, Bioenerg.* **2012**, *1817*, 495.

(102) Siegbahn, P. E. M.; Blomberg, M. R. A. *Biochim. Biophys. Acta, Bioenerg.* **2007**, *1767*, 1143.

(103) Siegbahn, P. E. M.; Blomberg, M. R. A. *J. Phys. Chem. A* **2008**, *112*, 12772.

(104) Belevich, I.; Bloch, D. A.; Belevich, N.; Wikström, M.; Verkhovsky, M. I. *Proc. Natl. Acad. Sci. U.S.A.* **2007**, *104*, 2685.

(105) Blomberg, M. R. A.; Siegbahn, P. E. M. *Mol. Phys.* **2010**, *108*, 2733.

(106) Reimann, J.; Flock, U.; Lepp, H.; Honigmann, A.; Ädelroth, P. *Biochim. Biophys. Acta, Bioenerg.* **2007**, *1767*, 362.

(107) Hino, T.; Matsumoto, Y.; Nagano, S.; Sugimoto, H.; Fukumori, Y.; Murata, T.; Iwata, S.; Shiro, Y. *Science* **2010**, *330*, 1666.

(108) Blomberg, M. R. A.; Siegbahn, P. E. M. *Biochemistry* **2012**, *51*, 5173.

(109) Blomberg, L. M.; Blomberg, M. R. A.; Siegbahn, P. E. M. *J. Inorg. Biohem.* **2005**, *99*, 949.

(110) Strickland, N.; Harvey, J. N. *J. Phys. Chem. B* **2007**, *111*, 841.

(111) Radon, M.; Pierloot, K. *J. Phys. Chem. A* **2008**, *112*, 11824.

(112) Sundarajan, M.; Neese, F. *J. Chem. Theory Comput.* **2012**, *8*, 563.

(113) Copeland, D. M.; Soares, A. S.; West, A. H.; Richter-Addo, G. B. *J. Inorg. Biohem.* **2006**, *100*, 1413.

(114) Crane, B. R.; Arvai, A. S.; Ghosh, D. K.; Wu, C.; Getzoff, E. D.; Stuehr, D. J.; Tainer, J. A. *Science* **1998**, *279*, 2121.

(115) Stoll, S.; Jahromy, Y. N.; Woodward, J. J.; Ozarowski, A.; Marletta, M. A.; Britt, R. D. *J. Am. Chem. Soc.* **2010**, *132*, 11812.

(116) de Visser, S. P.; Tan, L. S. *J. Am. Chem. Soc.* **2008**, *130*, 12961.

(117) de Visser, S. P. *Biochem. Soc. Trans.* **2009**, *37*, 373.

(118) Cho, K.-B.; Carvajal, M. A.; Shaik, S. *J. Phys. Chem. B* **2009**, *113*, 336.

(119) Woodward, J. J.; Chang, M. M.; Martin, N. I.; Marletta, M. A. *J. Am. Chem. Soc.* **2009**, *131*, 297.

(120) Robinet, J. J.; Cho, K.-B.; Gauld, J. W. *J. Am. Chem. Soc.* **2008**, *130*, 3328.

(121) Radoul, M.; Bykov, D.; Rinaldo, S.; Cutruzzola, F.; Neese, F.; Goldfarb, D. *J. Am. Chem. Soc.* **2011**, *133*, 3043.

(122) Einsle, O.; Stach, P.; Messerschmidt, A.; Simon, J.; Kroger, A.; Huber, R.; Kroneck, P. M. *J. Biol. Chem.* **2000**, *275*, 39608.

(123) Bykov, D.; Neese, F. *J. Biol. Inorg. Chem.* **2011**, *16*, 417.

(124) Bykov, D.; Neese, F. *J. Biol. Inorg. Chem.* **2012**, *17*, 741.

(125) Hegg, E. L.; Que, L., Jr. *Eur. J. Biochem.* **1997**, *250*, 625.

(126) Que, L. *Nat. Struct. Biol.* **2000**, *7*, 182.

(127) Loeb, K. E.; Westre, T. E.; Kappock, T. J.; Mitić, N.; Glasfeld, E.; Caradonna, J. P.; Hedman, B.; Hodgson, K. O.; Solomon, E. I. *J. Am. Chem. Soc.* **1997**, *119*, 1901.

(128) Kemsley, J. N.; Mitić, N.; Zaleski, K. L.; Caradonna, J. P.; Solomon, E. I. *J. Am. Chem. Soc.* **1999**, *121*, 1528.

(129) Bassan, A.; Blomberg, M. R. A.; Siegbahn, P. E. M. *Chem.—Eur. J.* **2003**, *9*, 106.

(130) Bassan, A.; Blomberg, M. R. A.; Siegbahn, P. E. M. *Chem.—Eur. J.* **2003**, *9*, 4055.

(131) Bassan, A.; Blomberg, M. R.; Borowski, T.; Siegbahn, P. E. *J. Inorg. Biochem.* **2006**, *100*, 727.

(132) Lundberg, M.; Borowski, T. *Coord. Chem. Rev.* **2013**, *257*, 277.

(133) Hausinger, R. P. *Crit. Rev. Biochem. Mol.* **2004**, *39*, 21.

(134) Flashman, E.; Schofield, C. J. *Nat. Chem. Biol.* **2007**, *3*, 86.

(135) Tsukada, Y.-i.; Fang, J.; Erdjument-Bromage, H.; Warren, M. E.; Borchers, C. H.; Tempst, P.; Zhang, Y. *Nature* **2005**, *439*, 811.

(136) Klose, R. J.; Yamane, K.; Bae, Y.; Zhang, D.; Erdjument-Bromage, H.; Tempst, P.; Wong, J.; Zhang, Y. *Nature* **2006**, *442*, 312.

(137) Cloos, P. A. C.; Christensen, J.; Agger, K.; Maiolica, A.; Rappsilber, J.; Antal, T.; Hansen, K. H.; Helin, K. *Nature* **2006**, *442*, 307.

(138) Falnes, P. Ø; Johansen, R. F.; Seeberg, E. *Nature* **2002**, *419*, 178.

(139) Kershaw, N. J.; Caines, M. E. C.; Sleeman, M. C.; Schofield, C. J. *Chem. Commun.* **2005**, 4251.

(140) Hewitson, K. S. *J. Biol. Chem.* **2002**, *277*, 26351.

(141) Hanauske-Abel, H.; Günzler, V. *J. Theor. Biol.* **1982**, *94*, 421.

(142) Schofield, C. J.; Andersson, I.; Valegård, K.; van Scheltinga, A. C. T.; Lloyd, M. D.; Hara, T.; Ramaswamy, S.; Perrakis, A.; Thompson, A.; Lee, H.-J.; et al. *Nature* **1998**, *394*, 805.

(143) Lloyd, M. D.; Lee, H.-J.; Harlos, K.; Zhang, Z.-H.; Baldwin, J. E.; Schofield, C. J.; Charnock, J. M.; Garner, C.; Hara, T.; Terwisscha van Scheltinga, A. C.; et al. *J. Mol. Biol.* **1999**, *287*, 943.

(144) Harlos, K.; Schofield, C. J.; Zhang, Z.; Ren, J.; Stammers, D. K.; Baldwin, J. E. *Nat. Struct. Biol.* **2000**, *7*, 127.

(145) Pavel, E. G.; Zhou, J.; Busby, R. W.; Gunsior, M.; Townsend, C. A.; Solomon, E. I. *J. Am. Chem. Soc.* **1998**, *120*, 743.

(146) Zhou, J.; Kelly, W. L.; Bachmann, B. O.; Gunsior, M.; Townsend, C. A.; Solomon, E. I. *J. Am. Chem. Soc.* **2001**, *123*, 7388.

(147) Price, J. C.; Barr, E. W.; Tirupati, B.; Bollinger, J. M., Jr.; Krebs, C. *Biochemistry* **2003**, *42*, 7497.

(148) Proshlyakov, D. A.; Henshaw, T. F.; Monterosso, G. R.; Ryle, M. J.; Hausinger, R. P. *J. Am. Chem. Soc.* **2004**, *126*, 1022.

(149) Price, J. C.; Barr, E. W.; Hoffart, L. M.; Krebs, C.; Bollinger, J. M. *Biochemistry* **2005**, *44*, 8138.

(150) Galonić, D. P.; Barr, E. W.; Walsh, C. T.; Bollinger, J. M., Jr.; Krebs, C. *Nat. Chem. Biol.* **2007**, *3*, 113.

(151) Matthews, M. L.; Krest, C. M.; Barr, E. W.; Vaillancourt, F. d. r. H.; Walsh, C. T.; Green, M. T.; Krebs, C.; Bollinger, J. M. *Biochemistry* **2009**, *48*, 4331.

(152) Krebs, C.; GalonićFujimori, D.; Walsh, C. T.; Bollinger, J. M. *Acc. Chem. Res.* **2007**, *40*, 484.

(153) Zhang, Z.; Ren, J.-s.; Harlos, K.; McKinnon, C. H.; Clifton, I. J.; Schofield, C. J. *FEBS Lett.* **2002**, *517*, 7.

(154) Ye, S.; Price, J. C.; Barr, E. W.; Green, M. T.; Bollinger, J. M., Jr.; Krebs, C.; Neese, F. *J. Am. Chem. Soc.* **2010**, *132*, 4739.

(155) Diebold, A. R.; Brown-Marshall, C. D.; Neidig, M. L.; Brownlee, J. M.; Moran, G. R.; Solomon, E. I. *J. Am. Chem. Soc.* **2011**, *133*, 18148.

(156) Borowski, T.; Bassan, A.; Siegbahn, P. E. M. *Chem.—Eur. J.* **2004**, *10*, 1031.

(157) Borowski, T.; Bassan, A.; Siegbahn, P. E. M. *Biochemistry* **2004**, *43*, 12331.

(158) Topol, I. A.; Nemukhin, A. V.; Salnikow, K.; Cachau, R. E.; Abashkin, Y. G.; Kasprzak, K. S.; Burt, S. K. *J. Phys. Chem. A* **2006**, *110*, 4223.

(159) de Visser, S. P. *Chem. Commun.* **2007**, 171.

(160) Ye, S.; Riplinger, C.; Hansen, A.; Krebs, C.; Bollinger, J. M.; Neese, F. *Chem.—Eur. J.* **2012**, *18*, 6555.

(161) Wirstam, M.; Siegbahn, P. E. M. *J. Am. Chem. Soc.* **2000**, *122*, 8539.

(162) Lundberg, M.; Siegbahn, P. E. M.; Morokuma, K. *Biochemistry* **2008**, *47*, 1031.

(163) Lundberg, M.; Morokuma, K. *J. Phys. Chem. B* **2007**, *111*, 9380.

(164) Lundberg, M.; Kawatsu, T.; Vreven, T.; Frisch, M. J.; Morokuma, K. *J. Chem. Theory Comput.* **2009**, *5*, 222.

(165) Kawatsu, T.; Lundberg, M.; Morokuma, K. *J. Chem. Theory Comput.* **2011**, *7*, 390.

(166) Auldridge, M. E.; McCarty, D. R.; Klee, H. J. *Curr. Opin. Plant Biol.* **2006**, *9*, 315.

(167) Stahl, W.; Sies, H. *Biochim. Biophys. Acta, Mol. Basis Dis.* **2005**, *1740*, 101.

(168) von Lintig, J.; Hessel, S.; Isken, A.; Kiefer, C.; Lampert, J. M.; Voolstra, O.; Vogt, K. *Biochim. Biophys. Acta, Mol. Basis Dis.* **2005**, *1740*, 122.

(169) Kloer, D. P.; Ruch, S.; Al-Babili, S.; Beyer, P.; Schulz, G. E. *Science* **2005**, *308*, 267.

(170) Borowski, T.; Blomberg, M. R.; Siegbahn, P. E. *Chem.—Eur. J.* **2008**, *14*, 2264.

(171) Pirrung, M. C. *Acc. Chem. Res.* **1999**, *32*, 711.

(172) Rocklin, A. M.; Tierney, D. L.; Kofman, V.; Brunhuber, N. M.; Hoffman, B. M.; Christoffersen, R. E.; Reich, N. O.; Lipscomb, J. D.; Que, L., Jr. *Proc. Natl. Acad. Sci. U.S.A.* **1999**, *96*, 7905.

(173) Rocklin, A. M.; Kato, K.; Liu, H.-W.; Que, L.; Lipscomb, J. D. *J. Biol. Inorg. Chem.* **2004**, *9*, 171.

(174) Tierney, D. L.; Rocklin, A. M.; Lipscomb, J. D.; Que, L., Jr; Hoffman, B. M. *J. Am. Chem. Soc.* **2005**, *127*, 7005.

(175) Zhang, Z.; Ren, J.-S.; Clifton, I. J.; Schofield, C. J. *Chem. Biol.* **2004**, *11*, 1383.

(176) Bassan, A.; Borowski, T.; Schofield, C. J.; Siegbahn, P. E. M. *Chem.—Eur. J.* **2006**, *12*, 8835.

(177) Hirao, H.; Morokuma, K. *J. Am. Chem. Soc.* **2010**, *132*, 17901.

(178) Hirao, H.; Morokuma, K. *J. Am. Chem. Soc.* **2011**, *133*, 14550.

(179) Milaczewska, A.; Broclawik, E.; Borowski, T. *Chem.—Eur. J.* **2013**, *19*, 771.

(180) Aluri, S.; de Visser, S. P. *J. Am. Chem. Soc.* **2007**, *129*, 14846.

(181) de Visser, S. P.; Straganz, G. D. *J. Phys. Chem. A* **2009**, *113*, 1835.

(182) Kumar, D.; Thiel, W.; de Visser, S. P. *J. Am. Chem. Soc.* **2011**, *133*, 3869.

(183) Kovaleva, E. G.; Neibergall, M. B.; Chakrabarty, S.; Lipscomb, J. D. *Acc. Chem. Res.* **2007**, *40*, 475.

(184) Davis, M. I.; Wasinger, E. C.; Decker, A.; Pau, M. Y. M.; Vaillancourt, F. H.; Bolin, J. T.; Eltis, L. D.; Hedman, B.; Hodgson, K. O.; Solomon, E. I. *J. Am. Chem. Soc.* **2003**, *125*, 11214.

(185) Siegbahn, P. E. M.; Haeffner, F. *J. Am. Chem. Soc.* **2004**, *126*, 8919.

(186) Christian, G. J.; Ye, S.; Neese, F. *Chem. Sci.* **2012**, *3*, 1600.

(187) Georgiev, V.; Borowski, T.; Siegbahn, P. E. M. *J. Biol. Inorg. Chem.* **2006**, *11*, 571.

(188) Georgiev, V.; Borowski, T.; Blomberg, M. R. A.; Siegbahn, P. E. M. *J. Biol. Inorg. Chem.* **2008**, *13*, 929.

(189) Borowski, T.; Georgiev, V.; Siegbahn, P. E. M. *J. Mol. Model.* **2010**, *16*, 1673.

(190) Borowski, T.; Wójcik, A.; Milaczewska, A.; Georgiev, V.; Blomberg, M. R. A.; Siegbahn, P. E. M. *J. Biol. Inorg. Chem.* **2012**, *17*, 881.

(191) Mbughuni, M. M.; Chakrabarti, M.; Hayden, J. A.; Bominaar, E. L.; Hendrich, M. P.; Munck, E.; Lipscomb, J. D. *Proc. Natl. Acad. Sci. U.S.A.* **2010**, *107*, 16788.

(192) Xin, M.; Bugg, T. D. H. *J. Am. Chem. Soc.* **2008**, *130*, 10422.

(193) Kovaleva, E. G.; Lipscomb, J. D. *Science* **2007**, *316*, 453.

(194) Kovaleva, E. G.; Lipscomb, J. D. *Biochemistry* **2008**, *47*, 11168.

(195) Borowski, T.; Georgiev, V.; Siegbahn, P. E. M. *J. Am. Chem. Soc.* **2005**, *127*, 17303.

(196) Straganz, G. D.; Glieder, A.; Brecker, L.; Ribbons, D. W.; Steiner, W. *Biochem. J.* **2003**, *369*, 573.

(197) Diebold, A. R.; Straganz, G. D.; Solomon, E. I. *J. Am. Chem. Soc.* **2011**, *133*, 15979.

(198) Borowski, T.; Siegbahn, P. E. M. *J. Am. Chem. Soc.* **2006**, *128*, 12941.

(199) Pau, M. Y. M.; Davis, M. I.; Orville, A. M.; Lipscomb, J. D.; Solomon, E. I. *J. Am. Chem. Soc.* **2007**, *129*, 1944.

(200) Karlsson, A.; Parales, J. V.; Parales, R. E.; Gibson, D. T.; Eklund, H.; Ramaswamy, S. *Science* **2003**, *299*, 1039.

(201) Wolfe, M. D.; Parales, J. V.; Gibson, D. T.; Lipscomb, J. D. *J. Biol. Chem.* **2001**, *276*, 1945.

(202) Bassan, A.; Blomberg, M. R. A.; Siegbahn, P. E. M. *J. Biol. Inorg. Chem.* **2004**, *9*, 439.

(203) Rosenzweig, A. C.; Nordlund, P.; Takahara, P. M.; Frederick, C. A.; Lippard, S. J. *J. Chem. Biol.* **1995**, *2*, 409.

(204) Baik, M.-H.; Newcomb, M.; Friesner, R. A.; Lippard, S. *Chem. Rev.* **2003**, *103*, 2385.

(205) Himo, F.; Siegbahn, P. E. M. *Chem. Rev.* **2003**, *103*, 2421.

(206) Basch, H.; Mogi, K.; Musaev, D. G.; Morokuma, K. *J. Am. Chem. Soc.* **1999**, *121*, 7249.

(207) Liu, K. E.; Johnson, C. C.; Newcomb, M.; Lippard, S. J. *J. Am. Chem. Soc.* **1993**, *115*, 939.

(208) Siegbahn, P. E. M. *J. Biol. Inorg. Chem.* **2001**, *6*, 27.

(209) Guallar, V.; Gherman, B. F.; Miller, W. H.; Lippard, S. J.; Friesner, R. A. *J. Am. Chem. Soc.* **2002**, *124*, 3377.

(210) Torrent, M.; Musaev, D. G.; Basch, H.; Morokuma, K. *J. Comput. Chem.* **2002**, *23*, 59.

(211) Friesner, R. A.; Baik, M.; Gherman, B. F.; Guallar, V.; Wirstam, M.; Murphy, R. B.; Lippard, S. J. *Coord. Chem. Rev.* **2003**, *238–239*, 267.

(212) Lovell, T.; Himo, F.; Han, W.; Noodleman, L. *Coord. Chem. Rev.* **2003**, *238–239*, 211. Noodleman, L.; Lovell, T.; Han, W.; Himo, F. *Chem. Rev.* **2004**, *104*, 459.

(213) Tinberg, C. E.; Lippard, S. J. *Acc. Chem. Res.* **2011**, *44*, 280.

(214) (a) Yoshizawa, K.; Shiota, Y. *J. Am. Chem. Soc.* **2006**, *128*, 9873. (b) Shiota, Y.; Yoshizawa, K. *Inorg. Chem.* **2009**, *48*, 838.

(215) Chen, P. P.-Y; Chan, S. I. *J. Inorg. Biochem.* **2006**, *100*, 801.

(216) (a) Culpepper, M. A.; Rosenzweig, A. C. *Crit. Rev. Biochem. Mol. Biol.* **2012**, *47*, 483. (b) Balasubramanian, R.; Rosenzweig, A. C. *Acc. Chem. Res.* **2007**, *40*, 573.

(217) Siegbahn, P. E. M. *Q. Rev. Biophys.* **2003**, *36*, 91.

(218) Uhlin, U.; Eklund, H. *Nature* **1994**, *370*, 533.

(219) Nordlund, P.; Eklund, H. *J. Mol. Biol.* **1993**, *232*, 123.

(220) Ehrenberg, A.; Reichard, P. *J. Biol. Chem.* **1972**, *247*, 3485.

(221) Siegbahn, P. E. M. *Chem. Phys. Lett.* **2002**, *351*, 311.

(222) Siegbahn, P. E. M.; Eriksson, L.; Himo, F.; Pavlov, M. *J. Phys. Chem.* **1998**, *102*, 10622.

(223) (a) Stubbe, J.; Nocera, D. G.; Yee, C. S.; Chang, M. C. Y. *Chem. Rev.* **2003**, *98*, 2167. (b) Seyedsayamdost, M. R.; Xie, J.; Chan, C. T. Y.; Schultz, P. G.; Stubbe, J. *J. Am. Chem. Soc.* **2007**, *129*, 15060.

(224) (a) Siegbahn, P. E. M. *J. Am. Chem. Soc.* **1998**, *120*, 8417. (b) Pelmenschikov, V.; Cho, K.-B.; Siegbahn, P. E. M. *J. Comput. Chem.* **2004**, *25*, 311. (c) Cho, K.-B.; Pelmenschikov, V.; Gräslund, A.; Siegbahn, P. E. M. *J. Phys. Chem. B* **2004**, *108*, 2056.

(225) Marcus, R. A. *Annu. Rev. Phys. Chem.* **1964**, *15*, 155.

(226) Jiang, W.; Yun, D.; Saleh, L.; Barr, E. W.; Xing, G.; Hoffart, L. M.; Maslak, M. A.; Krebs, C.; Bollinger, J. M. *Science* **2007**, *316*, 1188.

(227) (a) Roos, K.; Siegbahn, P. E. M. *Biochemistry* **2009**, *48*, 1878. (b) Roos, K.; Siegbahn, P. E. M. *J. Biol. Inorg. Chem.* **2011**, *16*, 533. (c) Roos, K.; Siegbahn, P. E. M. *J. Biol. Inorg. Chem.* **2012**, *17*, 363.

(228) (a) Willing, A.; Follman, H.; Auling, G. *Eur. J. Biochem.* **1988**, *170*, 603. (b) Abbouini, B.; Oehlmann, W.; Stolle, P.; Pierik, A. J.; Auling, G. *Free Radical Res.* **2009**, *43*, 943.

(229) Cotruvo, J. A.; Stubbe, J. *Biochemistry* **2010**, *49*, 1297.

(230) Minnihan, E. C.; Nocera, D. G.; Stubbe, J. *Acc. Chem. Res.* **2013**, *46*, 2524.

(231) Klinman, J. P. *Chem. Rev.* **1996**, *96*, 2541.

(232) Johnson, B. J.; Cohen, J.; Welford, R. W.; Pearson, A. R.; Schulten, K.; Klinman, J. P.; Wilmot, C. M. *J. Biol. Chem.* **2007**, *282*, 17767.

(233) Klinman, J. P.; Mu, D. *Annu. Rev. Biochem.* **1994**, *63*, 299.

(234) Liu, Y.; Mukherjee, A.; Nahumi, N.; Ozbil, M.; Brown, D.; Angeles-Boza, A. M.; Dooley, D. M.; Prabhakar, R.; Roth, J. P. *J. Phys. Chem. B* **2013**, *117*, 218.

(235) Dooley, D. M. *J. Biol. Inorg. Chem.* **1999**, *94*, 1.

(236) Prabhakar, R.; Siegbahn, P. E. M. *J. Am. Chem. Soc.* **2004**, *126*, 3996.

(237) (a) Whittaker, J. W. *Arch. Biochem. Biophys.* **2005**, *433*, 227. (b) Whittaker, J. W. *Chem. Rev.* **2003**, *103*, 2347.

(238) Himo, F.; Eriksson, L. A.; Maseras, F.; Siegbahn, P. E. M. *J. Am. Chem. Soc.* **2000**, *122*, 8031.

(239) (a) Himo, F.; Babcock, G. T.; Eriksson, L. A. *Chem. Phys. Lett.* **1999**, *313*, 374. (b) Wise, E. W.; Pate, J. B.; Wheeler, R. A. *J. Phys. Chem. B* **1999**, *103*, 4772. (c) Himo, F.; Eriksson, L. A.; Blomberg, M. R. A.; Siegbahn, P. E. M. *Int. J. Quantum Chem.* **2000**, *76*, 714. (d) Engström, M.; Himo, F.; Ågren, H. *Chem. Phys. Lett.* **2000**, *319*, 191. (e) Himo, F.; Noodleman, L.; Blomberg, M. R. A.; Siegbahn, P. E. M. *J. Phys. Chem. A.* **2002**, *168*, 8757.

(240) Ellis, M. J.; Dodd, F. E.; Sawers, G.; Eady, R. R.; Hasnain, S. S. *J. Mol. Biol.* **2003**, *328*, 429.

(241) de Marothy, S. A.; Blomberg, M. R. A.; Siegbahn, P. E. M. *J. Comput. Chem.* **2007**, *28*, 528.

(242) Siegbahn, P. E. M. *Inorg. Chem.* **2004**, *43*, 5944.

(243) Volbeda, A.; Hol, W. G. *J. Mol. Biol.* **1989**, *209*, 249.

(244) Magnus, K. A.; Hazes, B.; Ton-That, H.; Bonaventura, C.; Bonaventura, J.; Hol, W. G. *J. Proteins* **1994**, *19*, 302.

(245) Klabunde, T.; Eicken, C.; Saccettini, J. C.; Krebs, B. *Nat. Struct. Biol.* **1998**, *5*, 1084.

(246) Matoba, Y.; Kumagai, T.; Yamamoto, A.; Yoshitsu, H.; Sugiyama, M. *J. Biol. Chem.* **2006**, *281*, 8981.

(247) (a) Siegbahn, P. E. M. *J. Biol. Inorg. Chem.* **2003**, *8*, 567. (b) Siegbahn, P. E. M.; Borowski, T. *Faraday Symp. Chem. Soc.* **2011**, *148*, 109.

(248) (a) Siegbahn, P. E. M. *J. Biol. Inorg. Chem.* **2004**, *9*, 577. (b) Güell, M.; Siegbahn, P. E. M. *J. Biol. Inorg. Chem.* **2007**, *12*, 1251.

(249) Solomon, E. I.; Sundaram, U. M.; Machonkin, T. E. *Chem. Rev.* **1996**, *96*, 2563.

(250) Halcrow, M. A.; Knowles, P. F.; Phillips, S. E. V. In *Handbook on Metalloproteins*; Bertini, I., Sigel, H., Eds.; Marcel Dekker: New York, 2001; Chapter 15, p 709.

(251) Inoue, T.; Shiota, Y.; Yoshizawa, K. *J. Am. Chem. Soc.* **2009**, *130*, 16890.

(252) Solomon, E. I.; Sundaram, U. M.; Machonkin, T. E. *Chem. Rev.* **1996**, *96*, 2563.

(253) (a) Rulíšek, L.; Solomon, E. I.; Ryde, U. *Inorg. Chem.* **2005**, *44*, 5612. (b) Chalupsky, J.; Neese, F.; Solomon, E. I.; Ryde, U.; Rulíšek, L. *Inorg. Chem.* **2006**, *45*, 11051. (c) Ryde, U.; Hsiao, Y.-W.; Rulíšek, L.; Solomon, E. I. *J. Am. Chem. Soc.* **2007**, *129*, 726. (d) Zhekova, H.; Seth, M.; Ziegler, T. *J. Chem. Theory Comput.* **2011**, *7*, 1858. (e) Vancoillie, S.; Chalupsky, J.; Ryde, U.; Solomon, E. I.; Pierloot, K.; Neese, F.; Rulíšek, L. *J. Phys. Chem. B* **2010**, *114*, 7692. (f) Yoon, J.; Solomon, E. I. *J. Am. Chem. Soc.* **2007**, *129*, 13127. (g) Srnec, M.; Ryde, U.; Rulíšek, L. *Faraday Discuss.* **2011**, *148*, 41. (h) Hu, L.; Farrokhnia, M.; Heimdal, J.; Shleev, S.; Rulíšek, L.; Ryde, U. *J. Phys. Chem. B* **2011**, *115*, 13111.

(254) Gorelsky, S. I.; Ghosh, S.; Solomon, E. I. *J. Am. Chem. Soc.* **2006**, *128*, 278.

(255) Ertem, M. Z.; Cramer, C. J.; Himo, F.; Siegbahn, P. E. M. *J. Biol. Inorg. Chem.* **2012**, *17*, 687.

(256) Rulíšek, L.; Ryde, U. *Coord. Chem. Rev.* **2013**, *257*, 445.

(257) For a recent review on N2OR, see: Pauleta, S. R.; Dell'Acqua, S.; Moura, I. *Coord. Chem. Rev.* **2013**, *257*, 332.

(258) (a) Prudencio, M.; Pereira, A. S.; Tavares, P.; Besson, S.; Cabrito, I.; Brown, K.; Samyn, B.; Devreese, B.; Van Beeumen, J.; Rusnak, F.; Fauque, G.; Moura, J. J. G.; Tegoni, M.; Cambillau, C.; Moura, I. *Biochemistry* **2000**, *39*, 3899. (b) Brown, K.; Tegoni, M.; Prudencio, M.; Pereira, A. S.; Besson, S.; Moura, J. J.; Moura, I.; Cambillau, C. *Nat.*

3655

dx.doi.org/10.1021/cr400388t | *Chem. Rev.* 2014, 114, 3601–3658

Struct. Mol. Biol. **2000**, *7*, 191. (c) Brown, K.; Djinovic-Carugo, K.; Haltia, T.; Cabrito, I.; Saraste, M.; Moura, J. G.; Moura, I.; Tegoni, M.; Cambillau, C. *J. Biol. Chem.* **2000**, *275*, 41133. (d) Rasmussen, T.; Berks, B. C.; Sanders-Loehr, J.; Dooley, D. M.; Zumft, W. G.; Thomson, A. J. *Biochemistry* **2000**, *39*, 12753. (e) Haltia, T.; Brown, K.; Tegoni, M.; Cambillau, C.; Saraste, M.; Mattila, K.; Djinovic-Carugo, K. *Biochem. J.* **2003**, *369*, 77.

(259) (a) Ghosh, S.; Gorelsky, S. I.; Chen, P.; Cabrito, I.; Moura, J. J. G.; Moura, I.; Solomon, E. I. *J. Am. Chem. Soc.* **2003**, *125*, 15708. (b) Chan, J. M.; Bollinger, J. A.; Grewell, C. L.; Dooley, D. M. *J. Am. Chem. Soc.* **2004**, *126*, 3030.

(260) Bar-Nahum, I.; Gupta, A. K.; Huber, S. M.; Ertem, M. Z.; Cramer, C. J.; Tolman, W. B. *J. Am. Chem. Soc.* **2009**, *131*, 2812.

(261) (a) Pomowski, A.; Zumft, W. G.; Kroneck, P. M. H.; Einsle, O. *Nature* **2011**, *477*, 234. (b) Wüst, A.; Schneider, L.; Pomowski, A.; Zumft, W. G.; Kroneck, P. M. H.; Einsle, O. *Biol. Chem.* **2012**, *393*, 1067.

(262) Przbyla, A. E.; Robbins, J.; Menon, N.; Peck, H. D., Jr. *FEMS Microbiol. Rev.* **1992**, *88*, 109.

(263) Nicolet, Y.; Lemon, B. J.; Fontecilla-Camps, J. C.; Peters, J. W. *Trends Biochem. Sci.* **2000**, *25*, 138.

(264) Lyon, E. J.; Shima, S.; Buurman, G.; Chowdhuri, S.; Batschauer, A.; Steinbach, K.; Thauer, R. K. *Eur. J. Biochem.* **2004**, *271*, 195.

(265) Fontecilla-Camps, J. C.; Volbeda, A.; Cavazza, C.; Nicolet, Y. *Chem. Rev.* **2007**, *107*, 4273.

(266) De Lacey, A. L.; Fernandez, V. M.; Rousset, M.; Cammack, R. *Chem. Rev.* **2007**, *107*, 4304.

(267) Lubitz, W.; Reijerse, E.; van Gastel, M. *Chem. Rev.* **2007**, *107*, 4331.

(268) Siegbahn, P. E. M.; Tye, J. W.; Hall, M. B. *Chem. Rev.* **2007**, *107*, 4414.

(269) Bruschi, M.; Zampella, G.; Greco, Y.; Bertini, L.; Fantucci, P.; De Gioia, L. In *Computational Inorganic and Bioinorganic Chemistry*; Solomon, E. I., King, B., Scott, R., Eds.; John Wiley and Sons, Ltd.: Chichester, England, 2009.

(270) Volbeda, A.; Martin, L.; Cavazza, C.; Matho, M.; Faber, B.; Roseboom, W.; Albracht, S.; Garcin, E.; Rousset, M.; Fontecilla-Camps, J. J. *Biol. Inorg. Chem.* **2005**, *10*, 239.

(271) Armstrong, F. A.; Albracht, S. P. J. *J. Philos. Trans. R. Soc., A* **2005**, *363*, 937.

(272) Kurkin, S.; George, S. J.; Thorneley, R. N. F.; Albracht, S. P. J. *Biochemistry* **2004**, *43*, 6820.

(273) Roberts, L. M.; Lindahl, P. A. *J. Am. Chem. Soc.* **1995**, *117*, 2565.

(274) (a) Niu, S. Q.; Thomson, L. M.; Hall, M. B. *J. Am. Chem. Soc.* **1999**, *121*, 4000. (b) Pardo, A.; de Lacey, A.; Fernandez, V. M.; Fan, Y.; Hall, M. B. *J. Biol. Inorg. Chem.* **2006**, *11*, 286.

(275) Nilsson Lill, S. O.; Siegbahn, P. E. M. *Biochemistry* **2009**, *48*, 1056.

(276) Ogata, H.; Hirota, S.; Nakahara, A.; Komori, H.; Shibata, N.; Kato, T.; Kano, K.; Higuchi, Y. *Structure* **2005**, *13*, 1635.

(277) Jayapal, P.; Sundararajan, M.; Hillier, I. H.; Burton, N. A. *Phys. Chem. Chem. Phys.* **2006**, *8*, 4086.

(278) Siegbahn, P. E. M. *C. R. Chim.* **2007**, *10*, 766.

(279) Goris, T.; Wait, A. F.; Saggu, M.; Fritsch, J.; Heidary, N.; Stein, M.; Zebger, I.; Lendzian, F.; Armstrong, F. A.; Friedrich, B.; Lenz, O. *Nat. Chem. Biol.* **2011**, *7*, 310.

(280) Mouesca, J. M.; Fontecilla-Camps, J. C.; Amara, P. *Angew. Chem., Int. Ed.* **2013**, *52*, 2002.

(281) Pandelia, M.-E.; Bykov, D.; Izsak, R.; Infossi, P.; Giudici-Orticoni, M.-T.; Bill, E.; Neese, F.; Lubitz, W. *Proc. Natl. Acad. Sci. U.S.A.* **2013**, 485.

(282) Nicolet, Y.; Piras, C.; Legrand, P.; Hatchikian, C. E.; Fontecilla-Camps, J. C. *Structure* **1999**, *7*, 13.

(283) Peters, J. W.; Lanzilotta, W. N.; Lemon, B. J.; Seefeldt, L. C. *Science* **1998**, *282*, 1853.

(284) Fan, H.-J.; Hall, M. B. *J. Am. Chem. Soc.* **2001**, *123*, 3828.

(285) Zampella, G.; Greco, C.; Fantucci, P.; De Gioia, L. *Inorg. Chem.* **2006**, *45*, 4109.

(286) Georgiadis, M. M.; Komiya, H.; Chakrabarti, P.; Woo, D.; Kornuc, J. J.; Rees, D. C. *Science* **1992**, *257*, 1653.

(287) Einsle, O.; Tezcan, F. A.; Andrade, S. L. A.; Schmid, B.; Yoshida, M.; Howard, J. B.; Rees, D. C. *Science* **2002**, *297*, 1696.

(288) Lancaster, K. M.; Roemelt, M.; Ettenhuber, P.; Hu, Y.; Ribbe, M. W.; Neese, F.; Bergmann, U.; De Beer, S. *Science* **2011**, *334*, 974.

(289) Spatzal, T.; Aksoyoglu, M.; Zhang, L. M.; Andrade, S. L. A.; Schleicher, E.; Weber, S.; Rees, D. C.; Einsle, O. *Science* **2011**, *334*, 940.

(290) Seefeldt, L. C.; Hoffman, B. M.; Dean, R. D. *Annu. Rev. Biochem.* **2009**, *78*, 701.

(291) Tuzcek, F. In *Computational Inorganic and Bioinorganic Chemistry*; Solomon, E. I., Scott, R. A., King, R. B., Eds.; Wiley: New York, 2009; p 287.

(292) Ertl, G. *Angew. Chem., Int. Ed.* **2008**, *47*, 3524.

(293) Honkala, K.; Hellman, A.; Remediakis, I. N.; Logadottir, A.; Carlsson, A.; Dahl, S.; Christensen, C. H.; Nørskov, J. K. *Science* **2005**, *307*, 555.

(294) (a) Sandala, G. M.; Noodleman, L. *Methods Mol. Biol.* **2011**, *49*, 293. (b) Ed. Ribbe, M. W.; Springer; Lovell, T.; Li, J.; Case, D. A.; Noodleman, L. *J. Biol. Inorg. Chem.* **2002**, *7*, 735. (c) Lovell, T.; Li, J.; Liu, T.; Case, D. A.; Noodleman, L. *J. Am. Chem. Soc.* **2001**, *123*, 12392. (d) Lovell, T.; Liu, T.; Case, D. A.; Noodleman, L. *J. Am. Chem. Soc.* **2003**, *125*, 8377.

(295) (a) Dance, I. *Inorg. Chem.* **2011**, *50*, 178. (b) Dance, I. *Dalton Trans.* **2011**, *40*, 6480. (c) Dance, I. *Dalton Trans.* **2011**, *40*, 5516. (d) Dance, I. *Dalton Trans.* **2010**, *39*, 2972. (e) Dance, I. *Dalton Trans.* **2008**, 5977.

(296) Schimpfl, J.; Petrilli, H. M.; Blöchl, P. E. *J. Am. Chem. Soc.* **2003**, *125*, 15772. Kästner, J.; Blöchl, P. E. *J. Am. Chem. Soc.* **2007**, *129*, 2998.

(297) Hinnemann, B.; Nørskov, J. K. *J. Am. Chem. Soc.* **2004**, *126*, 3920.

(298) Huniar, U.; Ahlrichs, R.; Coucouvanis, D. *J. Am. Chem. Soc.* **2004**, *126*, 2588.

(299) Harris, T. V.; Szilagyi, R. K. *Inorg. Chem.* **2011**, *50*, 4811.

(300) Yan, L.; Pelmenschikov, V.; Dapper, C. H.; Scott, A. D.; Newton, W. E.; Cramer, S. P. *Chemistry* **2012**, *18*, 16349.

(301) (a) Thauer, R. K. *Microbiol.* **1998**, *144*, 2377. (b) Ermler, U.; Grabarse, W.; Shima, S.; Goubeaud, M.; Thauer, R. K. *Science* **1997**, *278*, 1457. (c) Ebner, S.; Jaun, B.; Goenrich, M.; Thauer, R. K.; Harmer, J. *J. Am. Chem. Soc.* **2010**, *132*, 567. (d) Scheller, S.; Goenrich, M.; Boecher, R.; Thauer, R. K.; Jaun, B. *Nature* **2010**, *465*, 606. (e) Scheller, S.; Goenrich, M.; Mayr, S.; Thauer, R. K.; Jaun, B. *Angew. Chem., Int. Ed.* **2010**, *49*, 8112.

(302) (a) Ragsdale, S. W. *J. Biol. Chem.* **2009**, *284*, 18571. (b) Dey, M.; Telser, J.; Kunnz, R. C.; Lees, N. S.; Ragsdale, S. W.; Hoffmann, B. M. *J. Am. Chem. Soc.* **2007**, *129*, 11030.

(303) (a) Pelmenschikov, V.; Blomberg, M. R. A.; Siegbahn, P. E. M.; Crabtree, R. H. *J. Am. Chem. Soc.* **2002**, *124*, 4039. (b) Chen, S.-L.; Pelmenschikov, V.; Blomberg, M. R. A.; Siegbahn, P. E. M. *J. Am. Chem. Soc.* **2009**, *131*, 9912. (c) Chen, S.-L.; Blomberg, M. R. A.; Siegbahn, P. E. M. *Chem.—Eur. J.* **2012**, *18*, 6309.

(304) Brunold, T. C.; Conrad, K. S.; Liptak, M. D.; Park, K. *Coord. Chem. Rev.* **2009**, *253*, 779.

(305) (a) Andruniow, T.; Zgierski, M. Z.; Kozlowski, P. M. *J. Am. Chem. Soc.* **2001**, *123*, 2679. (b) Dölker, N.; Maseras, F.; Lledó s, A. *J. Phys. Chem. B* **2001**, *105*, 7564. (c) Jensen, K. P.; Ryde, U. *J. Mol. Struct.: THEOCHEM* **2002**, *585*, 239. (d) Dölker, N.; Maseras, F.; Lledó s, A. *J. Phys. Chem. B* **2003**, *107*, 306. (e) Jensen, K. P.; Ryde, U. *J. Phys. Chem. A* **2003**, *107*, 7539. (f) Kozlowski, P. M.; Zgierski, M. Z. *J. Phys. Chem. B* **2004**, *108*, 14163. (g) Dölker, N.; Maseras, F.; Siegbahn, P. E. M. *Chem. Phys. Lett.* **2004**, *386*, 174. (h) Rovira, C.; Biarnes, X.; Kunc, K. *Inorg. Chem.* **2004**, *43*, 6628. (i) Dölker, N.; Morreale, A.; Maseras, F. *J. Biol. Inorg. Chem.* **2005**, *10*, 509. (j) Kozlowski, P. M.; Kuta, J.; Galezowski, W. *J. Phys. Chem. B* **2007**, *111*, 7638. (k) Galezowski, W.; Kuta, J.; Kozlowski, P. M. *J. Phys. Chem. B* **2008**, *112*, 3177. (l) Kozlowski, P. M.; Kumar, M.; Piecuch, P.; Li, W.; Bauman, N. P.; Hansen, J. A.; Lodowski, P.; Jaworska, M. *J. Chem. Theory Comput.* **2012**, *8*, 1870. (m) Govender, P. P.; Navizet, I.; Perry, C. B.; Marques, H. M. *J. Phys. Chem. A* **2013**, *117*, 3057.

(306) Chen, S.-L.; Blomberg, M. R. A.; Siegbahn, P. E. M. *J. Phys. Chem. B* **2011**, *115*, 4066.

(307) Hirao, H. *J. Phys. Chem. A* **2011**, *115*, 9308.

(308) Jensen, K. P.; Ryde, U. *Coord. Chem. Rev.* **2009**, *253*, 769.

(309) Reitzer, R.; Gruber, K.; Jogl, G.; Wagner, U. G.; Bothe, H.; Buckel, W.; Kratky, C. *Structure* **1999**, *7*, 891.

(310) Gruber, K.; Reitzer, R.; Kratky, C. *Angew. Chem., Int. Ed.* **2011**, *40*, 3377.

(311) Jensen, K. P.; Ryde, U. *J. Am. Chem. Soc.* **2005**, *127*, 9117.

(312) Sharma, P. K.; Chu, Z. T.; Olsson, M. H. M.; Warshel, A. *Proc. Natl. Acad. Sci. U.S.A.* **2007**, *104*, 9661.

(313) (a) Kwiecien, R. A.; Khavrutskii, I. V.; Musaev, D. G.; Morokuma, K.; Banerjee, R.; Paneth, P. *J. Am. Chem. Soc.* **2006**, *128*, 1287. (b) Li, X.; Chung, L. W.; Paneth, P.; Morokuma, K. *J. Am. Chem. Soc.* **2009**, *131*, 5115.

(314) Bucher, D.; Sandala, G. M.; Durbeej, B.; Radom, L.; Smith, D. M. *J. Am. Chem. Soc.* **2012**, *134*, 1591.

(315) Pang, J.; Li, X.; Morokuma, K.; Scrutton, N. S.; Sutcliffe, M. J. *J. Am. Chem. Soc.* **2012**, *134*, 2367.

(316) Jensen, K. P.; Ryde, U. *J. Am. Chem. Soc.* **2003**, *125*, 13970.

(317) Alfonso-Prieto, M.; Biarné s, X.; Kumar, M.; Rovira, C.; Kozlowski, P. M. *J. Phys. Chem. B* **2010**, *114*, 12965.

(318) Kozlowski, P. M.; Kamachi, T.; Kumar, M.; Yoshizawa, K. *J. Biol. Inorg. Chem.* **2012**, *17*, 611.

(319) Dybala-Defratyka, A.; Paneth, P. *J. Inorg. Biochem.* **2001**, *86*, 681.

(320) Kozlowski, P. M.; Kamachi, T.; Toraya, T.; Yoshizawa, K. *Angew. Chem., Int. Ed.* **2007**, *46*, 980.

(321) Durbeej, Bo.; Sandala, G. M.; Buncher, D.; Smith, D. M.; Radom, L. *Chem.—Eur. J.* **2009**, *15*, 8578.

(322) Johnson, M. K.; Rees, D. C.; Adams, M. W. W. *Chem. Rev.* **1996**, *96*, 2817.

(323) Rosner, B. M.; Schink, B. *J. Bacteriol.* **1995**, *177*, 5767.

(324) Seiffert, G. B.; Ullmann, G. M.; Messerschmidt, A.; Schink, B.; Kroneck, P. M. H.; Einsle, O. *Proc. Natl. Acad. Sci. U.S.A.* **2007**, *104*, 3073.

(325) ten Brink, F.; Schink, B.; Kroneck, P. M. H. *J. Bacteriol.* **2011**, *193*, 1229.

(326) Liao, R.-Z.; Yu, J.-G.; Himo, F. *Proc. Natl. Acad. Sci. U.S.A.* **2010**, *107*, 22523.

(327) Liao, R.-Z.; Thiel, W. *J. Chem. Theory Comput.* **2012**, *8*, 3793.

(328) Liu, Y.-F.; Liao, R.-Z.; Ding, W.-J.; Yu, J.-G.; Liu, R.-Z. *J. Biol. Inorg. Chem.* **2011**, *16*, 745.

(329) Antony, S.; Bayse, C. A. *Organometallics* **2009**, *28*, 4938.

(330) Vincent, M. A.; Hillier, I. H.; Periyasamy, G.; Burton, N. A. *Dalton Trans.* **2010**, *39*, 3816.

(331) Liao, R.-Z.; Himo, F. *ACS Catal.* **2011**, *1*, 937.

(332) Roy, R.; Mukund, S.; Schut, G. J.; Dunn, D. M.; Weiss, R.; Adams, M. W. W. *J. Bacteriol.* **1999**, *181*, 1171.

(333) Hu, Y.; Faham, S.; Roy, R.; Adams, M. W. W.; Rees, D. C. *J. Mol. Biol.* **1999**, *286*, 899.

(334) Liao, R.-Z.; Yu, J.-G.; Himo, F. *J. Inorg. Biochem.* **2011**, *105*, 927.

(335) Stewart, L. J.; Bailey, S.; Bennett, B.; Charnock, J. M.; Garner, C. D.; McAlpine, A. S. *J. Mol. Biol.* **2000**, *299*, 593.

(336) Buc, J.; Santini, C. L.; Giordani, R.; Czjzek, M.; Wu, L. F.; Giordano, G. *Mol. Microbiol.* **1999**, *32*, 159.

(337) Bertram, P. A.; Schmitz, R. A.; Linder, D.; Thauer, R. K. *Arch. Microbiol.* **1994**, *161*, 220.

(338) Boll, M.; Schink, B.; Messerschmidt, A.; Kroneck, P. M. H. *Biol. Chem.* **2005**, *386*, 999.

(339) Sevcenco, A. M; Bevers, L. E.; Pinkse, M. W. H.; Krijger, G. C.; Wolterbeek, H. T.; Verhaert, P. D. E. M.; Hagen, W. R.; Hagedoorn, P. L. *J. Bacteriol.* **2010**, *192*, 4143.

(340) Liao, R.-Z. *J. Biol. Inorg. Chem.* **2013**, *18*, 175.

(341) For selected recent examples of quantum chemical studies of mononuclear zinc enzymes, see: (a) Smith, C. R; Smith, G. K.; Yang, Z.; Xu, D.; Guo, H. *Theor. Chem. Acc.* **2011**, *128*, 83. (b) Amata, O.; Marino, T.; Russo, N.; Toscano, M. *J. Am. Chem. Soc.* **2011**, *133*, 17824. (c) Chen, S.-L.; Li, Z.-S.; Fang, W.-H. *J. Inorg. Biochem.* **2012**, *111*, 70. (d) Zhang, C.; Liu, X.; Xue, Y. *Comput. Theor. Chem.* **2012**, *980*, 85. (e) Wong, K.-Y.; Gao, J. *FEBS J.* **2011**, *278*, 2579.

(342) For a recent review, see: Wu, R.; Cao, Z.; Zhang, Y. *Prog. Chem.* **2012**, *24*, 1175.

(343) (a) Chen, S.-L.; Fang, W.-H.; Himo, F. *J. Phys. Chem. B* **2007**, *111*, 1253. (b) Chen, S.-L.; Fang, W.-H.; Himo, F. *Theor. Chem. Acc.* **2008**, *120*, 515. (c) Kim, J.; Tsai, P.-C.; Chen, S.-L.; Himo, F.; Almo, S. C.; Raushel, F. M. *Biochemistry* **2008**, *47*, 9497. (d) Wong, K. Y.; Gao, J. *Biochemistry* **2007**, *46*, 13352. (e) Zhang, X.; Wu, R. B.; Song, L. C.; Lin, Y. C.; Lin, M. H.; Cao, Z. X.; Wu, W.; Mo, Y. R. *J. Comput. Chem.* **2009**, *30*, 2388. (f) López-Canut, V.; Ruiz-Pernía, J. J.; Castillo, R.; Moliner, V.; Tunon, I. *Chem.—Eur. J.* **2012**, *18*, 9612.

(344) Liao, R.-Z.; Yu, J.-G.; Himo, F. *Eur. J. Inorg. Chem.* **2009**, 2967.

(345) (a) Chen, S.-L.; Marino, T.; Fang, W.-H.; Russo, N.; Himo, F. *J. Phys. Chem. B* **2008**, *112*, 2494. (b) Schürer, G.; Lanig, H.; Clark, T. *Biochemistry* **2004**, *43*, 5414.

(346) Liao, R.-Z.; Yu, J.-G.; Raushel, F. M.; Himo, F. *Chem.—Eur. J.* **2008**, *14*, 4287.

(347) Liao, R.-Z.; Yu, J.-G.; Himo, F. *J. Inorg. Biochem.* **2010**, *104*, 37.

(348) Chen, S.-L.; Fang, W.-H.; Himo, F. *J. Inorg. Biochem.* **2009**, *103*, 274.

(349) Liao, R.-Z.; Yu, J.-G.; Himo, F. *Inorg. Chem.* **2009**, *48*, 1442.

(350) (a) Borosky, G. L.; Lin, S. *J. Chem. Inf. Model.* **2011**, *51*, 2538. (b) López-Canut, V.; Roca, M.; Bertrán, J.; Moliner, V.; Tunon, I. *J. Am. Chem. Soc.* **2011**, *133*, 12050. (c) López-Canut, V.; Martí, S.; Bertrán, J.; Moliner, V.; Tunon, I. *J. Phys. Chem. B* **2009**, *113*, 7816. (d) Hou, G.; Cui, Q. *J. Am. Chem. Soc.* **2012**, *134*, 229.

(351) (a) Xu, D.; Guo, H.; Cui, Q. *J. Am. Chem. Soc.* **2007**, *129*, 10814. (b) Peraro, M. D.; Vila, A. J.; Carloni, P.; Klein, M. L. *J. Am. Chem. Soc.* **2007**, *129*, 2808. (c) Park, H.; Brothers, E. N.; Merz, K. M., Jr. *J. Am. Chem. Soc.* **2005**, *127*, 4232. (d) Peraro, M. D.; Llarrull, L. I.; Rothlisberger, U.; Vila, A. J.; Carloni, P. *J. Am. Chem. Soc.* **2004**, *126*, 12661. (e) Valdez, C. E.; Alexandrova, A. N. *J. Phys. Chem. B* **2012**, *116*, 10649.

(352) Klusák, V.; Bainka, C.; Plechanovová, A.; Mleochová, P.; Konvalinka, J.; Rulíšek, L.; Lubkowski, J. *Biochemistry* **2009**, *48*, 4126.

(353) Alberto, M. E.; Leopoldini, M.; Russo, N. *Inorg. Chem.* **2011**, *50*, 3394.

(354) López-Canut, V.; Roca, M.; Bertrán, J.; Moliner, V.; Tunon, I. *J. Am. Chem. Soc.* **2010**, *132*, 6995.

(355) Leopoldini, M.; Russo, N.; Toscano, M. *J. Am. Chem. Soc.* **2007**, *129*, 7776.

(356) (a) Aubert, S. D.; Li, Y.; Raushel, F. M. *Biochemistry* **2004**, *43*, 5707. (b) Jackson, C. J.; Foo, J. L.; Kim, H. K.; Carr, P. D.; Liu, J. W.; Salem, G.; Ollis, D. L. *J. Mol. Biol.* **2008**, *375*, 1189.

(357) Weston, J. *Chem. Rev.* **2005**, *105*, 2151.

(358) Bigley, A. N.; Raushel, F. M. *Biochim. Biophys. Acta, Proteins Proteomics* **2013**, *1834*, 443.

(359) Benning, M. M.; Shim, H.; Raushel, F. M.; Holden, H. M. *Biochemistry* **2001**, *40*, 2712.

(360) Hough, E.; Hansen, L. K.; Birknes, B.; Jynge, K.; Hansen, S.; Hordvik, A.; Little, C.; Dodson, E.; Derewenda, Z. *Nature* **1989**, *338*, 357.

(361) Romier, C.; Dominguez, R.; Lahm, A.; Dahl, O.; Suck, D. *Proteins* **1998**, *32*, 414.

(362) Hosfield, D. J.; Guan, Y.; Haas, B. J.; Cunningham, R. P.; Tainer, J. A. *Cell* **1999**, *98*, 397.

(363) Liao, R.-Z.; Yu, J.-G.; Himo, F. *J. Phys. Chem. B* **2010**, *114*, 2533.

(364) Liao, R.-Z.; Yu, J.-G.; Himo, F. *Inorg. Chem.* **2010**, *49*, 6883.

(365) Ivanov, I.; Tainer, J. A.; McCammon, J. A. *Proc. Natl. Acad. Sci. U.S.A.* **2007**, *104*, 1465.

(366) Hergenrother, P. J.; Martin, S. F. *Top. Curr. Chem.* **2001**, *211*, 131.

(367) Thrige, D. D.; Buur, J. R. B.; Jorgensen, S. F. *Biopolymers* **1997**, *42*, 319.

(368) Sundell, S.; Hansen, S.; Hough, E. *Protein Eng.* **1994**, *7*, 571.

(369) Tan, C. A.; Roberts, M. F. *Biochemistry* **1998**, *37*, 4275.

(370) Hille, R. *Chem. Rev.* **1996**, *96*, 2757.

(371) Kisker, C.; Schindelin, H.; Rees, D. C. *Annu. Rev. Biochem.* **1997**, *66*, 233.

(372) (a) Leopoldini, M.; Russo, N.; Toscano, M.; Dulak, M.; Wesolowski, T. A. *Chem.—Eur. J.* **2006**, *12*, 2532. (b) Hofmann, M. *J. Biol. Inorg. Chem.* **2007**, *12*, 989. (c) Pal, K.; Sarkar, S. *Eur. J. Inorg. Chem.*

2008, 5338. (d) Hofmann, M. *J. Biol. Inorg. Chem.* **2009**, *4*, 1023. (e) Cerqueira, N. M. F. S. A.; González, P. J.; Brondino, C. D.; Romão, M. J.; Romão, C. C.; Moura, I.; Moura, J. J. G. *J. Comput. Chem.* **2009**, *30*, 2446. (f) Xie, H.; Cao, Z. *Organometallics* **2010**, *29*, 436. (g) Silaghi-Dumitrescu, R.; Mich, M.; Matyas, C.; Cooper, C. E. *Nitric Oxide* **2012**, *26*, 27.

(373) (a) Thomson, L. M.; Hall, M. B. *J. Am. Chem. Soc.* **2001**, *123*, 3995. (b) Thapper, A.; Deeth, R. J.; Nordlander, E. *Inorg. Chem.* **2002**, *41*, 6695. (c) Mohr, M.; McNamara, J. P.; Wang, H.; Rajeev, S. A.; Ge, J.; Morgado, C. A.; Hillier, I. H. *Faraday Discuss.* **2003**, *124*, 413. (d) Kaupp, M. *Angew. Chem., Int. Ed.* **2004**, *43*, 546. (e) McNamara, J. P.; Mohr, M.; Hillier, I. H. *Mol. Phys.* **2005**, *103*, 3465. (f) McNamara, J. P.; Hillier, I. H.; Bhachu, T. S.; Garner, C. D. *Dalton Trans.* **2005**, 3572. (g) McNamara, J. P.; Joule, J. A.; Hillier, I. H.; Garner, C. D. *Chem. Commun.* **2005**, 177. (h) Hofmann, M. *J. Mol. Struct.: THEOCHEM* **2006**, *773*, 59. (i) Hofmann, M. *Inorg. Chem.* **2008**, *47*, 5546. (j) Hernandez-Marin, E.; Ziegler, T. *Can. J. Chem.* **2010**, *88*, 683. (k) Tenderholt, A. L.; Hodgson, K. O.; Hedman, B.; Holm, R. H.; Solomon, E. I. *Inorg. Chem.* **2012**, *51*, 3436. (l) Li, J.-L.; Mata, R. A.; Ryde, U. *J. Chem. Theory Comput.* **2013**, *9*, 1799.

(374) (a) Pal, K.; Chaundhury, P. K.; Sarkar, S. *Chem.—Asian J.* **2007**, *2*, 956. (b) Hernandez-Marin, E.; Ziegler, T. *Inorg. Chem.* **2009**, *48*, 1323.

(375) (a) Szaleniec, M.; Borowski, T.; Schühle, K.; Witko, M.; Heider, J. *J. Am. Chem. Soc.* **2010**, *132*, 6014. (b) Szaleniec, M.; Salwinski, A.; Borowski, T.; Heider, J.; Witko, M. *Int. J. Quantum Chem.* **2012**, *112*, 1990.

(376) (a) Bray, M. R.; Deeth, R. J. *J. Chem. Soc., Dalton Trans.* **1997**, 1267. (b) Voityuk, A. A.; Albert, K.; Romão, M. J.; Huber, R.; Rösch, N. *Inorg. Chem.* **1998**, *37*, 176. (c) Zhang, X.-H.; Wu, Y.-D. *Inorg. Chem.* **2005**, *44*, 1466. (d) Amano, T.; Ochi, N.; Sato, H.; Sakaki, S. *J. Am. Chem. Soc.* **2007**, *129*, 8131. (e) Metz, S.; Wang, D.; Thiel, W. *J. Am. Chem. Soc.* **2009**, *131*, 4628. (f) Dieterich, J. M.; Werner, H.-J.; Mata, R. A.; Metz, S.; Thiel, W. *J. Chem. Phys.* **2010**, *132*, 035101.

(377) (a) Bayse, C. A. *Dalton Trans.* **2009**, 2306. (b) Metz, S.; Thiel, W. *J. Am. Chem. Soc.* **2009**, *131*, 14885. (c) Metz, S.; Thiel, W. *J. Phys. Chem. B* **2010**, *114*, 1506.

(378) (a) Leopoldini, M.; Chiodo, S. G.; Toscano, M.; Russo, N. *Chem.—Eur. J.* **2008**, *14*, 8674. (b) Mota, C. S.; Rivas, M. G.; Brondino, C. D.; Moura, I.; Moura, J. J. G.; González, P. J.; Cerqueira, N. M. F. S. A. *J. Biol. Inorg. Chem.* **2011**, *16*, 1255. (c) Tiberti, M.; Papaleo, E.; Russo, N.; De Gioia, L.; Zampella, G. *Inorg. Chem.* **2012**, *51*, 8331.

(379) Metz, S.; Thiel, W. *Coord. Chem. Rev.* **2011**, *255*, 1085.

(380) Dias, J. M.; Than, M. E.; Humm, A.; Huber, R.; Bourenkov, G. P.; Bartunik, H. D.; Bursakov, S.; Calvete, J.; Caldeira, J.; Carneiro, C.; Moura, J. J. G.; Moura, I.; Romão, M. J. *Structure* **1999**, *7*, 65.

(381) Najmudin, S.; Gonzalez, P. J.; Trincao, J.; Coelho, C.; Mukhopadhyay, A.; Cerqueira, N. M. F. S. A.; Romão, C. C.; Moura, I.; Moura, J. J. G.; Brondino, C. D.; Romão, M. J. *J. Biol. Inorg. Chem.* **2008**, *13*, 737.

(382) Okamoto, K.; Eger, B. T.; Nishino, T.; Kondo, S.; Pai, E. F.; Nishino, T. *J. Biol. Chem.* **2003**, *278*, 1848.

(383) Huber, R.; Hof, P.; Duarte, R. O.; Moura, J. J. G.; Moura, I.; Liu, M. Y.; LeGall, J.; Hille, R.; Archer, M.; Romão, M. J. *Proc. Natl. Acad. Sci. U.S.A.* **1996**, *93*, 8846.

(384) Yamaguchi, Y.; Matsumura, T.; Ichida, K.; Okamoto, K.; Nishino, T. *J. Biochem.* **2007**, *141*, 513.

(385) Massey, V.; Edmondson, D. *J. Biol. Chem.* **1970**, *245*, 6595.